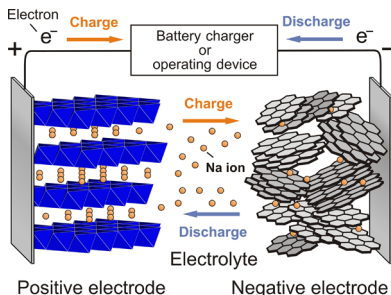


## Research Development on Sodium-Ion Batteries

Naoaki Yabuuchi,<sup>†,‡,§</sup> Kei Kubota,<sup>†,‡</sup> Mouad Dahbi,<sup>†,‡</sup> and Shinichi Komaba\*,<sup>†,‡</sup>

<sup>†</sup>Department of Applied Chemistry, Tokyo University of Science, 1-3 Kagurazaka, Shinjuku, Tokyo 162-8061, Japan

<sup>‡</sup>Elements Strategy Initiative for Catalysts and Batteries (ESICB), Kyoto University, Katsura, Kyoto 615-8520, Japan



Sodium-ion batteries

### CONTENTS

1. Introduction
2. Why Are Sodium Ions Important as Charge Carriers for Energy Storage?
3. Positive Electrode Materials
  - 3.1. Layered Oxides
    - 3.1.1. Classification of Layered Structures
    - 3.1.2. Iron- and Manganese-Based Layered Oxides
    - 3.1.3. Other 3d Transition-Metal Oxides with Layered Structures
    - 3.1.4. Binary/Ternary Metal Oxides with Layered Structures
  - 3.2. Other Oxides as Na Insertion Host
    - 3.2.1. Iron-Based Oxides
    - 3.2.2. Manganese-Based Oxides
    - 3.2.3. Vanadium-Based Oxides
    - 3.2.4. Oxides of 4d Transition Metals
  - 3.3. Polyanionic Compounds
    - 3.3.1. Phosphates with Fe(II) and Mn(II)
    - 3.3.2. Pyrophosphates with Fe(II) and Mn(II)
    - 3.3.3. Fluorophosphates, Carbophosphates, and Fluorosulfates with Fe(II) and Mn (II)
    - 3.3.4. Polyanionic Compounds with Other Transition Metals
  - 3.4. Miscellaneous Na Insertion Materials as Positive Electrode Materials
4. Negative Electrode Materials
  - 4.1. Carbon-Based Electrode Materials
    - 4.1.1. Na Insertion into Hard Carbon
    - 4.1.2. Electrolyte and Additive for Na Cells
    - 4.1.3. Binders
    - 4.1.4. Solid Electrolyte Interphase
  - 4.2. Ti-Based Compounds as Negative Electrode Materials
    - 4.2.1. Titanium Oxides and Titanates
    - 4.2.2. Titanium Phosphates

### 4.3. Na Alloys and Other Sodiable Compounds as Negative Electrodes

AF

#### 4.3.1. Background of Na Alloys and Compounds

AF

#### 4.3.2. Tin and Antimony as Alloy Electrode Materials

AG

#### 4.3.3. Phosphorus-Based Materials

AI

### 5. Organic Compounds as Electrode Materials

AK

### 6. Future Outlook of NIBs

AL

### 7. Conclusions

AN

### Author Information

AN

#### Corresponding Author

AN

#### Present Address

AN

#### Notes

AO

#### Biographies

AO

#### Acknowledgments

AO

#### References

AO

## 1. INTRODUCTION

Rechargeable lithium batteries that are so-called a Li-ion battery, LIB, consisting of two lithium insertion electrodes and lithium-ion conducting electrolyte, free from lithium metal, have become successful and sophisticated energy storage devices since the first commercialization of lithium-ion batteries, carbon//LiCoO<sub>2</sub> cell, in 1991. LIBs were originally developed as a high-energy power source for portable electronic devices, and their energy is typically limited to less than 100 Wh as a single battery pack. Cobalt/nickel-based layered materials are often used as positive electrodes for the high-energy but small-sized batteries. LIBs with electric motors are now used as an alternative power source for combustion engines with a fuel tank; (plug-in hybrid) electric vehicles equipped with large-scale LIBs as power sources have been introduced to the automotive market, which could reduce the energy dependence on fossil fuels for a transportation system in the future. The energy of a battery module is increased to 5000–20 000 Wh for (plug-in hybrid) electric vehicles (EVs). To reduce the battery cost, high-energy cobalt-based materials as positive electrodes cannot be used for large-scale application. In addition, recently, the demand for advanced energy storage technology is rapidly emerging throughout the world. A large-scale energy storage system for the grid is necessary to utilize electrical energy with high efficiency and for peak shift operation.<sup>1</sup> Indeed, some battery companies have already developed LIBs with megawatt hour (MWh) scale and plan to

Special Issue: 2014 Batteries

Received: April 4, 2014



begin a demonstration test for electrical energy storage (EES). Such MWh-class batteries are also probably used to store electricity generated from solar cells and wind turbines as green and renewable energy resources.

Although LIBs potentially provide a solution to meet these tough challenges to realize sustainable energy development through the increasing market for electric vehicles and an emerging market for EES, we must reconsider the feasibility of lithium,<sup>2</sup> which is certainly the inherent element in LIBs. Lithium is widely distributed in the Earth's crust but is not regarded as an abundant element. The relative abundance of lithium in the Earth's crust is limited to be only 20 ppm as shown in Figure 1.<sup>3</sup> Indeed, the materials cost (the price of

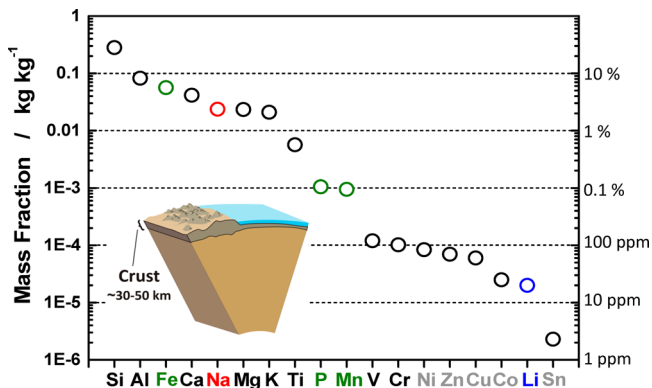


Figure 1. Elemental abundance in the Earth's crust. Data derived from ref 3.

$\text{Li}_2\text{CO}_3$ ) was steeply increased during the first decade of this century.<sup>4</sup> Moreover, lithium resources are unevenly distributed (mainly in South America); therefore, production of LIBs depends on the import of lithium from South America. In contrast to lithium, sodium resources are unlimited everywhere, and sodium is one of the most abundant elements in the Earth's crust. The infinite sodium resources are also found in the ocean. Additionally, sodium is the second-lightest and -smallest alkali metal next to lithium as shown in Table 1. On the basis of material abundance and standard electrode potential, rechargeable sodium batteries (or Na-ion battery, NIB, if we follow the terminology of LIB) are the ideal alternative to LIBs.<sup>4–6</sup>

NIBs are operable at ambient temperature, and metallic sodium is not used as the negative electrode, which is different

from commercialized high-temperature sodium-based technology, e.g.,  $\text{Na}/\text{S}$ <sup>7</sup> and  $\text{Na}/\text{NiCl}_2$ <sup>8</sup> batteries. These batteries utilize alumina-based solid (ceramic) electrolyte, and high-temperature operation ( $\sim 300^\circ\text{C}$ ) is required for maintaining the electrodes in the liquid state to ensure good contact with the solid-electrolyte. Since molten sodium and sulfur are used as active materials at such high temperature, safety issues of these batteries have not been completely satisfied for consumer appliances. In contrast, NIBs consist of sodium insertion materials with aprotic solvent as electrolyte and, therefore, are free from metallic sodium unless there are unfavorable reactions (e.g., overcharge) causing the failure in batteries. Structures, components, systems, and charge storage mechanisms of NIBs are essentially the same except that lithium ions are replaced with sodium ions as shown in Figure 2a.<sup>5</sup> A NIB consists of two sodium insertion materials, positive and negative electrodes, which are electronically separated by electrolyte (in general, electrolyte salts dissolved in aprotic polar solvents) as a pure ionic conductor. The battery performance depends on battery components selected, and many different NIBs for different purposes can be assembled.

Historically, studies of  $\text{Li}^+/\text{Na}^+$  ions as charge carriers for electrochemical energy storage at ambient temperature started before 1980. Electrochemical lithium insertion into  $\text{TiS}_2$  and its application for energy storage devices were first proposed in 1970s.<sup>9,10</sup> Immediately after this report, electrochemical and highly reversible sodium insertion into  $\text{TiS}_2$  at room temperature was also demonstrated in 1980.<sup>11</sup> The electrode performance of lithium cobalt oxide,  $\text{LiCoO}_2$ , which is a lithium-containing layered oxide and is still widely used as high-energy positive electrode materials in LIB, was first reported in 1980.<sup>12</sup> Similarly, the electrochemical properties of sodium-containing layered oxides,  $\text{Na}_x\text{CoO}_2$ , were also reported.<sup>13</sup> The early history of sodium insertion materials was reviewed in the literature published in 1982.<sup>14,15</sup> Nevertheless, in the past three decades, significant research efforts have been conducted only for LIBs, and studies on sodium insertion materials for energy storage once almost disappeared.

This big rush of Li battery research after 1980 could originate from the fact that available energy density was believed to be much higher for the Li system compared with the Na system. Figure 3 compares typical charge/discharge curves of Li/ $\text{LiCoO}_2$  and Na/ $\text{NaCoO}_2$  cells. Since an ionic radius of cobalt is relatively fairly small (0.54 Å) compared with those of both

Table 1. Comparison of Physical Properties for “Lithium” and “Sodium” as Charge Carriers for Rechargeable Batteries<sup>a</sup>

	$\text{Li}^+$	$\text{Na}^+$	$\text{K}^+$	$\text{Mg}^{2+}$
relative atomic mass	6.94	23.00	39.10	24.31
mass-to-electron ratio	6.94	23.00	39.10	12.16
Shannon's ionic radii/Å	0.76	1.02	1.38	0.72
$E^\circ$ (vs SHE)/V	-3.04	-2.71	-2.93	-1.55
melting point/°C	180.5	97.7	63.4	650.0
theoretical capacity of metal electrodes/mAh g⁻¹	3861	1166	685	2205
theoretical capacity of metal electrodes/mAh cm⁻³	2062	1131	591	3837
theoretical capacity of $\text{ACoO}_2$ /mAh g⁻¹	274	235	206	260 as $\text{Mg}_{0.5}\text{CoO}_2$
theoretical capacity of $\text{ACoO}_2$ /mAh cm⁻³	1378	1193		
molar conductivity in $\text{AClO}_4/\text{PC/S}$ cm² mol⁻¹	6.54	7.16		
desolvation energy in PC/kJ mol⁻¹	218.0	157.3		572.3
coordination preference	octahedral and tetrahedral	octahedral and prismatic		octahedral and tetrahedral

<sup>a</sup>Some sets of data are also compared for potassium and magnesium. Data for ionic radii derived from ref 34; data for molar conductivity from ref 35 and data for desolvation energy from ref 30.

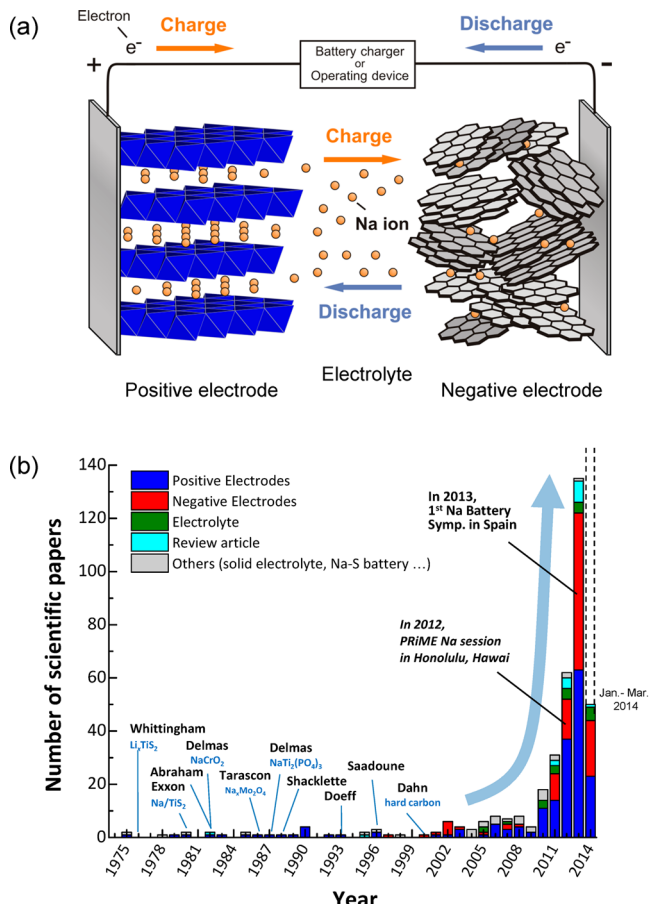


**Figure 2.** (a) Schematic illustration of Na-ion batteries, and (b) a number of publications, related to the sodium for energy storage devices, published in the past three decades. Data was derived from ref 26. The number in 2014 is limited to the articles published from January to March.

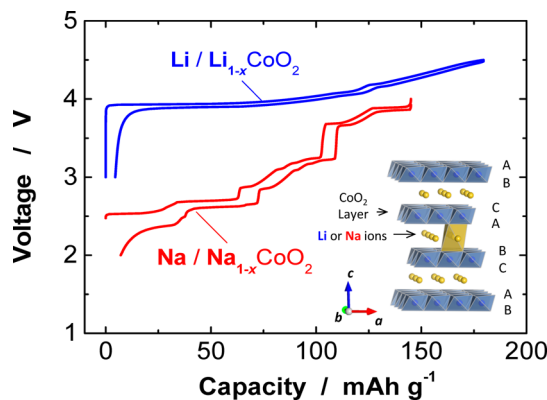


**Figure 3.** Comparison of charge/discharge curves of Li/LiCoO<sub>2</sub> and Na/NaCoO<sub>2</sub> cells. Schematic illustration of Li(Na)CoO<sub>2</sub> is also shown. Data of Li/LiCoO<sub>2</sub> cell derived from ref 12. Data of Na/NaCoO<sub>2</sub> cell derived from ref 13.

lithium (0.76 Å) and sodium (1.02 Å) ions as shown in Table 2, layered materials with both Li and Na are easily prepared. Although both samples have the same crystal lattice built up by sheets of edge-sharing CoO<sub>6</sub> octahedra, the operating voltage of LiCoO<sub>2</sub> for the region at the end of discharge (start of charge) is >1.0 V higher than that of NaCoO<sub>2</sub>. When both cells are charged to >100 mAh g<sup>-1</sup>, the difference in voltage is decreased

**Table 2. Comparison of Abundance in the Earth's Crust and Ionic Radii for Li<sup>+</sup>, Na<sup>+</sup>, and 3d Transition-Metal Elements (Ti<sup>3+</sup>–Ni<sup>3+</sup>) Used as Electrode Materials for Rechargeable Batteries<sup>a</sup>**

element	material abundance (ppm)	Shannon's ionic radii (Å)
Li <sup>+</sup>	20	0.76
Na <sup>+</sup>	23 600	1.02
Ti <sup>3+</sup>	5600	0.67
V <sup>3+</sup>	120	0.64
Cr <sup>3+</sup>	102	0.615
Fe <sup>3+</sup>	56 300	0.645 (high spin)
Mn <sup>3+</sup>	950	0.645 (high spin)
Co <sup>3+</sup>	25	0.545 (low spin)
Ni <sup>3+</sup>	84	0.6 (high spin)

<sup>a</sup>Data for elemental abundance in the Earth's crust derived from ref 3 and data for ionic radii from ref 34.

to approximately 0.4 V, which is similar to the difference in the standard electrochemical potential for Li (3.04 V) and Na (2.71 V) as shown in Table 1. The reduction of voltage becomes more significant as Na content in the structure increases. As a result, the available energy density is much lower for the Na system when the same chemistry (redox species and host crystal structures) with the Li system is used as the comparison between LiCoO<sub>2</sub> and NaCoO<sub>2</sub> in Figure 3. This fact also suggests that the different chemistry from the Li system is needed to overcome the problem of low energy density for NIBs.

The important second reason was the absence of suitable negative electrodes for a long period of time. In the mid 1980s, carbonaceous materials have been found to be promising candidates for Li insertion (intercalation) hosts, which are currently widely utilized as negative electrode materials for LIBs, e.g., disordered carbons<sup>16,17</sup> and graphite.<sup>18–20</sup> Research interest of LIBs is further accelerated by the finding of graphite, which delivers high reversible capacity (theoretically 372 mAh g<sup>-1</sup>) with a low and flat operating potential of 0.1–0.2 V vs Li/Li<sup>+</sup>. Unfortunately, graphite cannot be used as an insertion host of sodium ions.<sup>21,22</sup> Only a few studies were available as potential negative electrode materials for NIBs before 1990s, for instance, Na–Pb alloy<sup>23,24</sup> and disordered carbon.<sup>22</sup> However, it was clear that the energy density as a battery system was inferior to that of LIBs with graphite as negative electrode materials.

As the first turning point in the research for NIBs, Stevens and Dahn were reported in 2000 that a high reversible capacity of 300 mAh g<sup>-1</sup>, close to that for lithium insertion in graphitic carbon, has been demonstrated with hard carbon in a Na cell even though its cyclability was insufficient for battery applications at that time. Hard carbon is now extensively studied as a potential candidates as a negative electrode material for NIBs. As the second important discovery, Okada and co-workers reported that NaFeO<sub>2</sub> is electrochemically active in Na cells based on the Fe<sup>3+</sup>/Fe<sup>4+</sup> redox couple.<sup>25</sup> This discovery may correspond to the finding of LiCoO<sub>2</sub>, which is still used as the most important electrode material for high-energy LIBs, in 1980.<sup>12</sup> The Fe<sup>3+</sup>/Fe<sup>4+</sup> redox is unique chemistry for the Na system and never reported as active for LiFeO<sub>2</sub> in the Li system. Utilization of the Fe<sup>3+</sup>/Fe<sup>4+</sup> redox is an important subject to realize the high-energy and cost-effective NIBs in the future. Now, research interest for sodium ions is completely attractively changed on the basis of these important findings

and because of the increasing worldwide demand for EVs and EES with large-scale batteries.

In this review, recent research progress on NIBs is reviewed. In the past few years, many different sodium insertion materials have been found (and revisited) by many different research groups. In fact, the number of publications on NIBs has drastically increased in recent years after 2010, as shown in Figure 2b. Negative electrode materials have been also newly found in the past few years. The important difference is noticed in the chemistry between Li and Na in aprotic polar solvents. For instance, surface passivation processes are clearly different in both systems. The design of better electrolyte and suitable interphase for the Na system is quite important to realize long cycle life.

Recently, review articles related to NIBs also have been published by different groups.<sup>4,6,27,28</sup> Our review provides detailed and comprehensive research progress for sodium-ion battery technology in the past three decades. The similarity and difference between Li and Na systems for different electrode materials, including crystallography, kinetics (solid-state ionic diffusion and desolvation process), and thermodynamics of Li-ion and Na-ion chemistry, including the passivation process in aprotic polar solvent etc., are also summarized. Moreover, the possibility and difficulty of NIBs are also shown in this review, from which we further discuss whether or not NIBs will be the competitive and attractive battery system for a LiCoO<sub>2</sub>/graphite system as the most widely used high-energy 4 V-class LIBs.

## 2. WHY ARE SODIUM IONS IMPORTANT AS CHARGE CARRIERS FOR ENERGY STORAGE?

The material's abundance is a simple and clear reason as to why sodium ions are attractive as charge carriers for rechargeable batteries. A decrease in the theoretical gravimetric and volumetric reversible capacity is also a clear disadvantage when compared between Li and Na metal electrodes as shown in Table 1. The electrochemical equivalent of Na<sup>+</sup>/Na is more than three times heavier than that of Li<sup>+</sup>/Li. However, the difference in the theoretical reversible capacity becomes smaller when compared for LiCoO<sub>2</sub> and NaCoO<sub>2</sub> as layered oxides with the same crystal structure. When one-electron redox of the cobalt ion (Co<sup>3+</sup>/Co<sup>4+</sup> redox) is assumed to occur, the theoretical capacity is calculated to be 274 and 235 mAh g<sup>-1</sup> for LiCoO<sub>2</sub> and NaCoO<sub>2</sub>, respectively. As a result, reversible capacity is reduced by only 14%. The sacrifice is found in the voltage difference as shown in Figure 3. This problem can be potentially solved if the material's innovation is realized in the future, and current research progress to overcome this problem is shown in this review. Similarly, the volumetric capacity of Li metal is much larger than that of Na metal because of the large difference in the molar volume of Li and Na metals (21.3 Å<sup>3</sup> per Li atom and 39.3 Å<sup>3</sup> per Na atom; ΔV = 18 Å<sup>3</sup>). The difference in the volumetric capacity becomes much smaller when compared for LiCoO<sub>2</sub> and NaCoO<sub>2</sub> because the difference in the molar volume for LiCoO<sub>2</sub> and NaCoO<sub>2</sub> is small (32.3 Å<sup>3</sup> per LiCoO<sub>2</sub> and 37.3 Å<sup>3</sup> per NaCoO<sub>2</sub>; ΔV = 5 Å<sup>3</sup>). If the final target is to realize the battery technology based on the sodium ions, not metal, the energy sacrifice can be potentially reduced, and therefore, NIBs are expected to be the competitive battery system for LIBs.

Additionally, sodium ions as relatively large ions offer the possibility to increase the flexibility of materials design. The size gap of ionic radii for Na<sup>+</sup> and Me<sup>3+</sup> is large, and therefore,

layered oxides with different stacking manners from many different 3d transition metals (Sc–Ni) are easily prepared as shown in a later section. In addition to the oxides, a wide variety of crystal structures is known for polyanionic compounds and the structural chemistry of the Na system is much more complicated in comparison to the Li system. Moreover, many natural minerals containing sodium ions are known, and crystallographic information is recorded in the database. Many materials with different crystal structures are easily prepared under thermodynamic equilibrium conditions. Indeed, so far, many sodium-containing compounds have been prepared and used as precursors to obtain new lithium insertion materials by Na<sup>+</sup>/Li<sup>+</sup> ion exchange.<sup>29</sup>

Another merit from larger ionic radii is found to be a weak solvation energy in polar solvents, which has been evidenced by systematic and theoretical studies on Li<sup>+</sup>, Na<sup>+</sup>, and Mg<sup>2+</sup> together with different aprotic polar solvents.<sup>30</sup> Since the desolvation energy highly influences the kinetics of alkali-ion insertion processes at the electrolyte interface,<sup>31,32</sup> the relatively low energy for desolvation is an important finding to design high-power batteries. Small lithium ions have a relatively high charge density around ions when compared with sodium ions as the same monovalent ions. Lithium ions are, therefore, energetically stabilized by accepting/sharing more electrons from/with the solvated polar molecules, namely, Li<sup>+</sup> is classified as a relatively strong Lewis acid. As a result, a relatively large energy for the desolvation process is required for Li<sup>+</sup> compared with Na<sup>+</sup> (Table 1).<sup>30</sup> Similarly, results of first-principles calculation suggest that the activation energy of Na<sup>+</sup> diffusion is relatively small for NaCoO<sub>2</sub> when compared with LiCoO<sub>2</sub>.<sup>33</sup> Since the ionic radius of magnesium ions (Mg<sup>2+</sup>) as a divalent ion is similar to that of lithium ions as a monovalent ion (Li<sup>+</sup> 0.76 Å and Mg<sup>2+</sup> 0.72 Å at 6-coordinated site<sup>34</sup>), the surface charge density of Mg<sup>2+</sup> ions is also significantly increased (strong Lewis acid). This fact indicates that Mg<sup>2+</sup> ions are stabilized by the further electron donation from polar molecules, resulting in the high desolvation energy when similar aprotic polar solvents, e.g., alkyl/alkylene carbonate, are used as the electrolyte. It is also expected that potassium ions (K<sup>+</sup>) have a further smaller desolvation energy compared with the Li and Na systems in aprotic solvents. However, further energy sacrifice is also unavoidable for the potassium system due to heavy atomic weight.

Lastly, the high ion conductivity of Na<sup>+</sup>-based electrolyte is also beneficial to increase the battery performance compared to Li<sup>+</sup> electrolyte.<sup>35</sup> A comparative study of the molar conductivity of NaClO<sub>4</sub> and LiClO<sub>4</sub> has revealed a relatively low viscosity of NaClO<sub>4</sub> solutions with aprotic solvents, and conductivity is also high (10–20%) in comparison to LiClO<sub>4</sub> solutions. These facts also probably originate from the size difference between Na and Li in relation to the solvation energy and solvated states of ions in aprotic polar solvents.

## 3. POSITIVE ELECTRODE MATERIALS

### 3.1. Layered Oxides

Since 2010, many publications have appeared in relation to the electrode materials as the sodium insertion host in Figure 2b. The positive electrode materials, especially for the layered oxides, are the most extensively studied topic in the research of NIBs. Early contributions to layered oxides for the sodium system have been made mostly by Delmas, Hagenmuller, and co-workers in the early 1980s.<sup>15</sup> LiMeO<sub>2</sub> (Me = 3d transition

metals) is typically inactive or has a tendency to undergo unfavorable and irreversible phase transitions by the lithium extraction, except  $\text{Co}^{3+}$  and  $\text{Ni}^{3+}$ , which are fairly small-sized cations when compared to  $\text{Li}^+$ . In contrast, from Ti to Ni as 3d transition metals, all elements with layered structures are highly active as sodium insertion host. In this section, sodium-containing layered oxides ( $\text{Na}_x\text{MeO}_2$  as a general formula) are reviewed including the early studies.

**3.1.1. Classification of Layered Structures.** The most common layered structures are built up of a sheet of edge-sharing  $\text{MeO}_6$  octahedra. Polymorphisms appear when the sheets of edge-sharing  $\text{MeO}_6$  octahedra are stacked with different orientations along the  $c$ -axis direction. Sodium-based layered materials can be categorized into two main groups using the classification proposed by Delmas et al.<sup>36</sup> O3 type or P2 type, in which the sodium ions are accommodated at octahedral and prismatic sites, respectively, as shown in Figure 4.

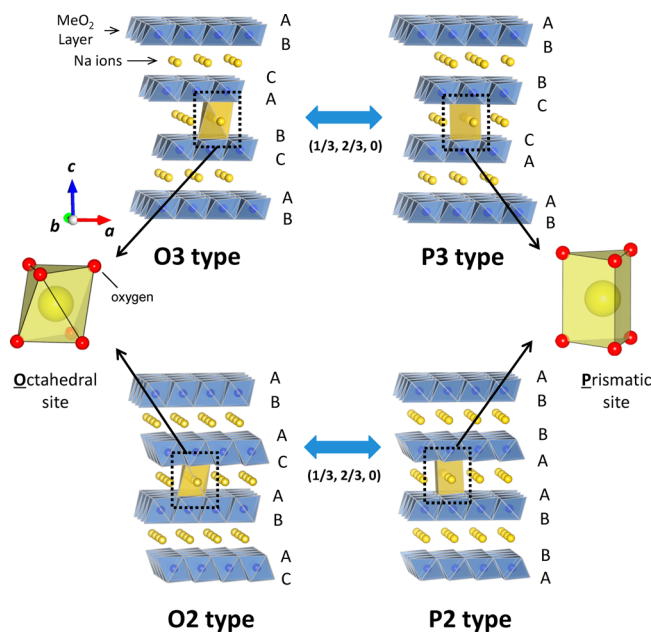


Figure 4. Classification of Na–Me–O layered materials with sheets of edge-sharing  $\text{MeO}_6$  octahedra and phase transition processes induced by sodium extraction. See text for more details.

Schematic illustrations of crystal structures used in this review were drawn using the program VESTA.<sup>37</sup> O3-type  $\text{NaMeO}_2$  consists of a cubic close-packed (ccp) oxygen array in which sodium and 3d transition-metal ions are accommodated at distinct octahedral sites because the ionic radius of sodium ions (1.02 Å) is much larger than those of 3d transition-metal ions with a trivalent state (<0.7 Å).<sup>34</sup> O3-type layered phases are classified as one of the cation-ordered rock-salt superstructure oxides.<sup>38</sup> Edge-shared  $\text{NaO}_6$  and  $\text{MeO}_6$  octahedra order into alternate layers perpendicular to [111], forming the  $\text{NaO}_2$  and  $\text{MeO}_2$  slabs, respectively. As a layered structure,  $\text{NaMeO}_2$  is composed of crystallographically “three” different  $\text{MeO}_2$  layers (AB, CA, and BC layers in Figure 4, and the layered stacking manner of  $\text{MeO}_2$  is isostructural with that of  $\text{CdCl}_2$ ) to describe the unit cell, and sodium ions are accommodated at the “octahedral” (O) sites between  $\text{MeO}_2$  layers. The structure is, therefore, classified as an O3-type layered structure. The structure is also classified as a 3R phase with a space group of  $\bar{R}\bar{3}m$ . P2-type  $\text{Na}_x\text{MeO}_2$  also consists of “two”  $\text{MeO}_2$  layers (AB

and BA layers). However, the sodium environment is different from the O3 type. Since the size of sodium ions is much larger than that of lithium ions, sodium ions can be also located at trigonal “prismatic” (P) sites. When a sodium off-stoichiometry condition (typically  $0.6 < x < 0.7$  in  $\text{Na}_x\text{MeO}_2$ ) is applied to materials synthesis, the P2-type phase is empirically known to be structurally stabilized. The P2-type layered structure is also often classified as a 2H phase with a space group of  $P6_3/mmc$ . Moreover, a prime symbol (') is added to the abbreviation when the crystal lattice contains in-plane distortion, such as O'3-type  $\text{NaMnO}_2$  with a monoclinic lattice (space group  $C2/m$ )<sup>39</sup> and P'2-type  $\text{Na}_x\text{MnO}_2$  with a orthorhombic lattice (space group  $Cmcm$ ).<sup>40</sup>

Sodium extraction from O3- and P2-type phases generally induces phase transitions. Sodium ions in the O3-type phase are originally stabilized at edge-shared octahedral sites with  $\text{MeO}_6$  octahedra. Na ions at prismatic sites become energetically stable when sodium ions are partly extracted from the O3-type phase, associated with formation of vacancies, similar to the P2-type phase. Formation of prismatic sites is achieved by the gliding of  $\text{MeO}_2$  slabs without breaking Me–O bonds.<sup>13,36</sup> As a result, oxygen packing changes from “AB CA BC” to “AB BC CA”, and this phase is classified as a P3-type phase as shown in Figure 4. It is also possible to directly crystallize this P3-type phase by solid-state reaction without electrochemical sodium extraction in Na cells in some cases. For instance, P3- and P2-type  $\text{Na}_{2/3}[\text{Ni}_{1/3}\text{Mn}_{2/3}]\text{O}_2$  are known as low- and high-temperature phases, respectively.<sup>41</sup> The phase transition from P3/O3- to P2-type phase is, however, impossible in Na cells because its phase transition is only achieved by breaking/reforming Me–O bonds and is therefore required for higher temperature environment.

Instead, the P2 phase changes into an O2-type phase in Na cells (Figure 4). Since large prismatic sites in the P2-type phase are energetically stabilized by large sodium ions,  $\text{MeO}_2$  slabs move (glide) to form octahedral sites after extraction of sodium ions<sup>42,43</sup> (and also by  $\text{Na}^+/\text{Li}^+$  ion exchange<sup>44</sup>). Such  $\text{MeO}_2$  gliding leads to formation of a new phase with a unique oxygen packing, “AB AC AB” (Figure 4). This phase contains crystallographically two different  $\text{MeO}_2$  layers with AB and AC oxygen arrangements. Vacancies left in between AB and AC layers are octahedral sites, that is, the O2-type phase. Both O3- and O2-type phases have close-packed oxygen arrays. In the O3-type phase with the ccp array (ABC-type oxygen arrangement),  $\text{NaO}_2$  layers share only edges with  $\text{MeO}_2$  layers on both sides. In contrast, the O2-type phase is locally composed of ABA-type and ACA-type (Figure 4) oxygen arrangements, namely, local structures are classified as a hexagonal close-packed (hcp) oxygen array. On the basis of oxygen packing, the O2-type structure is classified as an intergrowth structure between ccp and hcp arrays. Note that two glide vectors of  $\text{MeO}_2$  slabs,  $(1/3, 2/3, z)$  and  $(2/3, 1/3, z)$ , exist to form the O2 phase. This fact often induces formation of stacking faults after sodium extraction from the P2 phase.<sup>42</sup> Although only a few studies on the P2–O2 phase transition in Na cells have been reported so far,<sup>42,43</sup> several reports on the P2–O2 phase transitions by  $\text{Na}^+/\text{Li}^+$  ion exchange, including formation of a variety of stacking faults, are available in the literature.<sup>41,44–49</sup> Additionally, stacking faults and/or intergrowth between P2 and P3 phases are also reported for manganese-based materials, highly dependent on the materials synthesis conditions.<sup>50,51</sup>

### 3.1.2. Iron- and Manganese-Based Layered Oxides.

LIBs are now widely used for (plug-in hybrid) electric vehicles.

Since cutting the cost of the battery module is a key issue to reduce the total cost of electric vehicles, a choice of electrode materials is also limited by the cost of materials. Although the available energy density is inevitably lower when compared with that of cobalt/nickel-based layered materials used for small-sized batteries, spinel-type  $\text{LiMn}_2\text{O}_4$ <sup>52–55</sup> is often used in present large-scale batteries used for electric vehicles. Manganese-based materials, more preferably iron-based materials, are used because the elemental abundance in the Earth's crust (Figure 1) is relatively high (and therefore low cost). Iron- and manganese-based electrode materials as the sodium insertion host, therefore, provide great advantages in application for large-scale batteries, especially electrical energy storage (EES) systems.

**3.1.2.1. O3-Type  $\text{NaFeO}_2$ .**  $\alpha\text{-NaFeO}_2$  is known as a typical example of a O3-type layered structure and easily prepared by conventional solid-state reaction.<sup>56</sup> In contrast, there are no reports of direct synthesis of  $\text{LiFeO}_2$  with O3-type layered structures by solid-state reaction. Since the ionic radii of  $\text{Li}^+$  and  $\text{Fe}^{3+}$  are similar to each other (Table 2), a cation-disordered rock-salt phase is easily obtained by solid-state reaction at higher temperatures. Although a single phase of  $\text{LiFeO}_2$  was successfully obtained by hydrothermal treatment at 230 °C with concentrated KOH aqueous solution, thus synthesized  $\text{LiFeO}_2$  was electrochemically inactive in Li cells.<sup>57</sup> Instead, triphylite-type  $\text{LiFePO}_4$  was extensively studied as iron-based positive electrode materials for LIBs.<sup>58</sup> Electrochemical reversibility of sodium extraction/insertion processes for a single phase of O3-type  $\text{NaFeO}_2$  is shown in Figure 5a. Electrochemical Na extraction from  $\text{NaFeO}_2$  in nonaqueous Li/

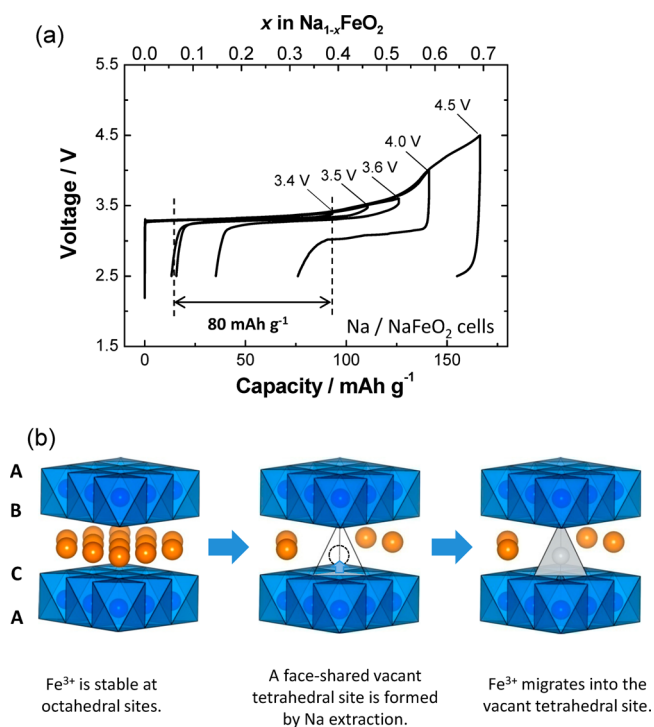
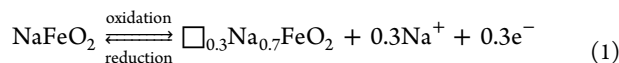


**Figure 5.** (a) Galvanostatic charge/discharge curves of  $\text{Na}/\text{NaFeO}_2$  cell. (b) Proposed mechanism of the iron migration process on sodium extraction. (a) Reprinted from ref 61 with permission of The Electrochemical Society of Japan. Copyright 2012. (b) Reprinted from ref 62 with permission from IOP Publishing. Copyright National Institute for Materials Science (NIMS). CC BY-NC-SA.

$\text{NaFeO}_2$  cell was first demonstrated by Takeda and co-workers.<sup>59</sup> Reversible charge and discharge processes for a  $\text{Na}/\text{NaFeO}_2$  cell were first reported by Okada and co-workers as mentioned above.<sup>25,60</sup> Reversibility in electrode materials is significantly influenced by cutoff conditions upon the charge (sodium extraction) process as shown in Figure 5. Although charging capacity, corresponding to amounts of sodium ions extracted from the crystal lattice, increases as a function of cutoff voltage, reversible capacity obviously decreases when charged beyond 3.5 V. Excellent reversibility with small polarization is observed with a cutoff voltage of 3.4 V. Reversible capacity observed reaches 80  $\text{mAh g}^{-1}$ , indicating that approximately 0.3 mol of Na is reversibly extracted from  $\text{NaFeO}_2$  and inserted into the  $\text{Na}_{0.7}\text{FeO}_2$  host structures. Such deterioration of the electrode properties beyond 3.5 V originates from the irreversible phase transition as suggested by ex-situ X-ray diffraction (XRD)<sup>61</sup> and X-ray absorption spectroscopy (XAS).<sup>62</sup> These facts suggest that part of the  $\text{Fe}^{3+}$  ions could migrate into the neighboring tetrahedral sites as shown in Figure 5b. When sodium ions are extracted from the crystal lattice, vacancies are created at face-shared tetrahedral sites with  $\text{FeO}_6$  octahedra. Since trivalent iron ions are energetically stabilized at tetrahedral sites, iron ions easily migrate to the face-shared sites, similar to  $\text{LiCo}_x\text{Fe}_{1-x}\text{O}_2$ .<sup>63</sup> Solid-state diffusion of sodium ions is easily disturbed by the iron at tetrahedral sites, leading to degradation of electrode properties. As a result, a reversible range of  $\text{Na}_x\text{FeO}_2$  is limited to be narrow. This reversible process in the Na cell is expressed as follows



where the open square denotes the vacant sites created in the structure. The energy density available as electrode material is also limited to be small ( $300 \text{ mWh g}^{-1}$  vs Na). Although its reversible range is narrow, quite small polarization between charge/discharge processes with submicrometer-sized particles is the attractive character as shown in Figure 6. Additionally, the thermal stability of  $\text{Na}_{0.58}\text{FeO}_2$  was reported to be better than that of  $\text{Li}_{0.50}\text{CoO}_2$  in aprotic solvents.<sup>60</sup> The rate capability of  $\text{Na}_x\text{FeO}_2$  in Na cells is also shown in Figure 7a. The cell can deliver >50% of discharge capacity at 1 C rate (the C rate is defined as the current that delivers a nominal capacity in 1 h, and the nominal capacity here is defined by one-electron redox of iron, i.e., 241  $\text{mA g}^{-1}$ ). Another major drawback of  $\text{NaFeO}_2$  as electrode material is  $\text{Na}^+/\text{H}^+$  ion exchange when  $\text{NaFeO}_2$  is in contact with water.<sup>64</sup>  $\text{NaFeO}_2$  changes into  $\text{FeOOH}$  and  $\text{NaOH}$  ( $\text{Na}_2\text{CO}_3$  and/or  $\text{NaHCO}_3$  by uptake of  $\text{CO}_2$ ). Such  $\text{Na}^+/\text{H}^+$  ion exchange is generally observed in O3-type  $\text{NaMeO}_2$ .

**3.1.2.2. O'3-Type  $\text{NaMnO}_2$  and P2-Type  $\text{Na}_x\text{MnO}_2$ .** O'3-type  $\text{NaMnO}_2$  with a monoclinic lattice (space group  $C2/m$ )<sup>39</sup> and P'2-type  $\text{Na}_x\text{MnO}_2$  with a orthorhombic lattice (space group  $Cmcm$ )<sup>40</sup> are prepared as thermodynamically stable polymorphs of layered Na–Mn oxides. Nondistorted P2- $\text{Na}_x\text{MnO}_2$  with a hexagonal lattice (space group  $P6_3/mmc$ ) is also obtained by controlling the synthesis conditions.<sup>40</sup> Herein, layered Na–Mn oxides are only described, and the structural complexity of Na–Mn oxides will be further discussed in a later section. Electrochemical reversibility of Na extraction/insertion from/into O'3-type  $\text{NaMnO}_2$  was first reported in 1985.<sup>39</sup> A very narrow reversible range ( $x < 0.2$  in  $\text{Na}_{1-x}\text{MnO}_2$ ) was, however, reported in this original publication. The electro-

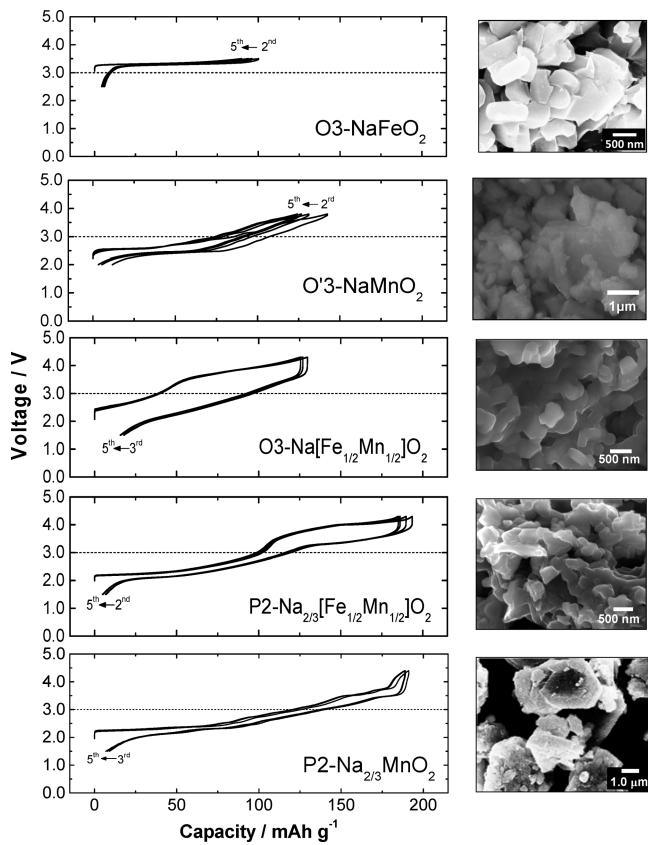


**Figure 6.** Comparison of galvanostatic charge/discharge curves of layered  $\text{Na}_x\text{MeO}_2$  samples with different structures. Morphology of particles for each sample is also compared (right). Data of O3-NaMnO<sub>2</sub> and P2-Na<sub>x</sub>MnO<sub>2</sub> derived from ref 36, data of NaFeO<sub>2</sub> from ref 61, and data of O3-Na[Fe<sub>1/2</sub>Mn<sub>1/2</sub>]O<sub>2</sub> and P2-Na<sub>x</sub>[Fe<sub>1/2</sub>Mn<sub>1/2</sub>]O<sub>2</sub> from ref 51.

chemical properties of O'3-type NaMnO<sub>2</sub> were revisited in 2011,<sup>65</sup> and it was found that O'3-type  $\text{Na}_{1-x}\text{MnO}_2$  shows a much wider reversible range ( $x < 0.8$ ). Although this reversible range is much wider than that of  $\text{Na}_{1-x}\text{FeO}_2$ , cyclability in the Na cell is insufficient as an electrode material. A large reversible capacity rapidly declines by subsequent electrochemical cycles. Selected charge/discharge curves of O'3-type NaMnO<sub>2</sub> are shown in Figure 6. The Na/NaMnO<sub>2</sub> cell delivers 120–130 mAh/g of reversible capacity (approximately 50% of Na ions are extracted/inserted) with small polarization. The operating voltage of  $\text{Na}_{1-x}\text{MnO}_2$  is relatively lower than that of  $\text{Na}_{1-x}\text{FeO}_2$  as shown in Figure 6.

The electrode performance of P2-Na<sub>x</sub>MnO<sub>2</sub> was also examined in some early studies.<sup>39,66</sup> Its reversible domain for Na extraction/insertion is wider than that of O'3-Na<sub>1-x</sub>MnO<sub>2</sub>. Over 150 mAh g<sup>-1</sup> of reversible capacity in the Na cell was reported in the early study.<sup>66</sup> The reversible limit is highly increased,  $\Delta x < 0.8$  in P2-Na<sub>x</sub>MnO<sub>2</sub> when the battery grade (high-purity with <20 ppm of water) electrolyte solution is used.<sup>67</sup> Approximately 190 mAh g<sup>-1</sup> of reversible capacity with good capacity retention is obtained as shown in Figure 6. The electrode performance of P2-Na<sub>x</sub>MnO<sub>2</sub> is much better than that of O'3-Na<sub>1-x</sub>MnO<sub>2</sub>. While in-plane conduction of electrons/holes in MnO<sub>2</sub> layers must be essentially the same for both polymorphs, the difference is expected to originate from in-plane Na-ion conduction manners between MnO<sub>2</sub> layers. Schematic illustrations of in-plane Na-ion conduction

in different phases are compared in Figure 8. For the O3-type layered system, since direct hopping from one octahedral site to an adjacent octahedral site requires high activation energy to overcome barriers, sodium ions migrate through interstitial tetrahedral sites (similar to O3-type  $\text{Li}_x\text{CoO}_2$ <sup>68</sup>), which are face-shared sites with  $\text{MoO}_6$  octahedra in  $\text{MoO}_2$  layers. According to the results of first-principles calculations, a diffusion barrier of sodium ions (vacancies) in a O3-type layered framework structure is relatively small (180 meV for O3-type  $\text{Na}_x\text{CoO}_2$ ).<sup>33</sup> The diffusion barrier of sodium ions is expected to be slightly smaller than that of Li in O3-type  $\text{Li}_x\text{CoO}_2$  (205 meV).<sup>33</sup> In contrast to the O3-type layered system, since the P2-type layered framework has an open path for Na ions, a lower diffusion barrier than that of the O3-type phase is probably expected. Sodium ions migrate from one prismatic site to adjacent sites through open square bottlenecks surrounded by four oxide ions (and thus a smaller repulsive interaction from oxide ions is expected<sup>69</sup>) because of no interstitial tetrahedral sites dissimilar to the O3 structure. Indeed, a higher ionic conductivity of the P2-type layered material than that of O3-type layered materials is observed when similar sodium/vacancy chemical compositions are formed.<sup>69</sup> Note that O3–P3 and P2–O2 phase transition could alter the mechanism of in-plane Na-ion diffusion. For instance, according to the first-principles calculation, the activation energy of Na-ion diffusion in P2-type  $\text{Na}_x[\text{Ni}_{1/3}\text{Mn}_{2/3}]\text{O}_2$  ( $2/3 > x > 1/3$ ) significantly increases (>100 meV) in O2-type  $\text{Na}_x[\text{Ni}_{1/3}\text{Mn}_{2/3}]\text{O}_2$  ( $1/3 > x > 0$ )<sup>70</sup> even though the P2–O2 phase transition is unavoidable for  $\text{Na}_x[\text{Ni}_{1/3}\text{Mn}_{2/3}]\text{O}_2$  in Na cells. On the other hand, O3-type  $\text{Na}_x[\text{Fe}_{1/2}\text{Co}_{1/2}]\text{O}_2$  shows excellent rate capability in Na cells, which could originate from the faster ion conduction for the P3 phase formed by the O3–P3 phase transition on the desodiation process.<sup>71</sup> Note that the local environment of Na ions at prismatic sites and diffusion pathway in the P2 and P3 phases are different as shown in Figure 8. It is expected, therefore, that the mobility of Na ions in both phases could be different. Although a NMR study on P2 and P3  $\text{Na}_x\text{CoO}_2$  suggested that the mobility of Na ions in both phases is clearly different on the NMR time scale,<sup>72</sup> the difference in Na-ion mobility as the electrode materials is not known so far. Further systematic studies on the diffusion process of Na ions in these different phases are necessary.

**3.1.2.3. O3-Type  $\text{Na}[\text{Fe}_{1/2}\text{Mn}_{1/2}]\text{O}_2$  and P2-Type  $\text{Na}_x[\text{Fe}_{1/2}\text{Mn}_{1/2}]\text{O}_2$ .** The electrode performance of P2-Na<sub>x</sub>MnO<sub>2</sub> is promising based on the reversible capacity as shown in the previous section. The average operating voltage with a Mn<sup>3+</sup>/Mn<sup>4+</sup> redox couple is, however, limited to less than 3 V vs metallic Na. The average operating voltage of O3-NaFeO<sub>2</sub> with a Fe<sup>3+</sup>/Fe<sup>4+</sup> redox couple is much higher (3.2–3.3 V) than that of P2 Na<sub>x</sub>MnO<sub>2</sub>, even though the reversible range is narrower associated with irreversible iron migration. From these pieces of experimental evidence, P2-type Na<sub>x</sub>FeO<sub>2</sub> is predictably considered to be a possible candidate as high-capacity and high-energy electrode materials. All of our trials, however, failed because Fe<sup>4+</sup> cannot be stabilized in the oxide–ion framework under ambient conditions.<sup>73</sup> Therefore, manganese ions have been partly substituted for iron to stabilize the P2-type phase, and finally, we succeeded in the synthesis of P2-type Fe-based layered oxide,  $\text{Na}_{2/3}[\text{Fe}_{1/2}\text{Mn}_{1/2}]\text{O}_2$ .<sup>51</sup> P2-Na<sub>2/3</sub>[Fe<sub>1/2</sub>Mn<sub>1/2</sub>]O<sub>2</sub> can be easily prepared by solid-state reaction of Na<sub>2</sub>O<sub>2</sub> (or Na<sub>2</sub>CO<sub>3</sub>), Fe<sub>2</sub>O<sub>3</sub>, and Mn<sub>2</sub>O<sub>3</sub> at 900 °C for 12 h.<sup>51</sup> The electrode performance of P2-type Na<sub>2/3</sub>[Fe<sub>1/2</sub>Mn<sub>1/2</sub>]O<sub>2</sub> in the

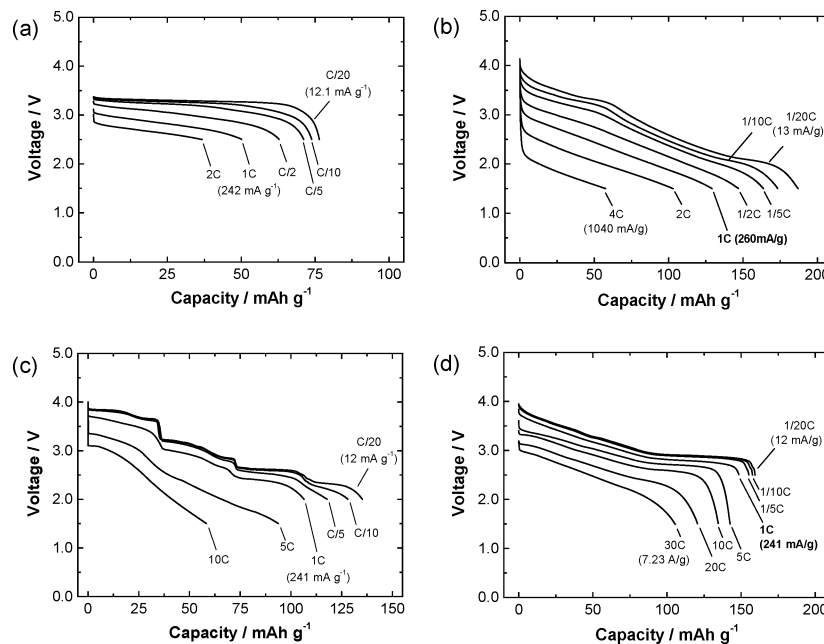


**Figure 7.** Comparison of the rate capability of (a)  $\text{Na}/\text{NaFeO}_2$ , (b)  $\text{Na}/\text{Na}_{2/3}[\text{Fe}_{1/2}\text{Mn}_{1/2}] \text{O}_2$ , (c)  $\text{Na}/\text{Na}_{2/3}\text{CoO}_2$ , and (d)  $\text{Na}/\text{Na}[\text{Fe}_{1/2}\text{Co}_{1/2}] \text{O}_2$  cells.  $\text{Na}/\text{NaFeO}_2$  cell was charged (oxidized) to 3.4 V at a rate of  $12.1 \text{ mA g}^{-1}$  and then discharged (reduced) to 2.5 V at from 1/20 ( $12.1 \text{ mA g}^{-1}$ ) to 2 C ( $484 \text{ mA g}^{-1}$ ) rates. Sample loading of  $\text{NaFeO}_2$  electrode used was  $1.3 \text{ mg cm}^{-2}$ .  $\text{Na}/\text{Na}_{2/3}[\text{Fe}_{1/2}\text{Mn}_{1/2}] \text{O}_2$  cell was charged to 4.2 V at a rate of  $13 \text{ mA g}^{-1}$  and then discharged to 1.5 V at different rates from 1/20 ( $13 \text{ mA g}^{-1}$ ) to 4 C ( $1040 \text{ mA g}^{-1}$ ). Sample loading on Al foil was  $8.4 \text{ mg cm}^{-2}$ , which is much heavier than that of the  $\text{NaFeO}_2$  electrode.  $\text{Na}/\text{Na}_{2/3}\text{CoO}_2$  and  $\text{Na}/\text{Na}[\text{Fe}_{1/2}\text{Co}_{1/2}] \text{O}_2$  cells were charged to 4.0 V at a rate of  $12 \text{ mA g}^{-1}$  and then discharged at different rates; from 1/20 ( $12 \text{ mA g}^{-1}$ ) to 30 C ( $7260 \text{ mA g}^{-1}$ ). Sample loading of  $\text{Na}_{2/3}\text{CoO}_2$  and  $\text{Na}/\text{Na}[\text{Fe}_{1/2}\text{Co}_{1/2}] \text{O}_2$  on Al foil was  $2.2$  and  $2.4 \text{ mg cm}^{-2}$ , respectively, as the active material. (a, c, and d) Reprinted with permission from ref 71. Copyright 2013 Elsevier. (b) Reprinted by permission from Macmillan Publishers Ltd.: (Nature Materials) (ref 51), copyright 2012.

voltage range of 1.5–4.2 V is also shown in Figure 6.  $\text{P2-Na}_{2/3}[\text{Fe}_{1/2}\text{Mn}_{1/2}] \text{O}_2$  delivers large reversible capacity, similar to  $\text{P2-Na}_x\text{MnO}_2$ , in the Na cell. The reversible capacity (reversible range) of  $\text{P2-Na}_{2/3}[\text{Fe}_{1/2}\text{Mn}_{1/2}] \text{O}_2$  is much higher (wider) than that of  $\text{O3-NaFeO}_2$ . The rate capability of  $\text{P2-Na}_{2/3}[\text{Fe}_{1/2}\text{Mn}_{1/2}] \text{O}_2$  is also better than that of  $\text{O3-NaFeO}_2$  as compared in Figure 7. Additionally, the operating voltage is also increased in comparison to  $\text{P2-Na}_x\text{MnO}_2$ , which will be discussed in a later section.

$\text{O3}$ -type  $\text{Na}[\text{Fe}_{1/2}\text{Mn}_{1/2}] \text{O}_2$  can be also prepared by changing the ratio of sodium/(iron and manganese).<sup>51</sup> The electrode performance of  $\text{O3-Na}[\text{Fe}_{1/2}\text{Mn}_{1/2}] \text{O}_2$  in the Na cell is shown in Figure 6. Large polarization (>1 V) between oxidation (charge) and reduction (discharge) processes is observed when the Na cell is cycled in the voltage range of 1.5–4.2 V. In comparison with the O3 phase, the P2 phase clearly shows larger reversible capacity. Since the P2 and O3 phases have similar particle morphology (Figure 6), the kinetic limitation related to the diffusion length is not responsible for the difference in performance. Research interest for the Na–Fe–Mn system as a high-capacity electrode material is rapidly increasing, and now the electrode performance for P2- and O3- $\text{Na}_x[\text{Fe}_y\text{Mn}_{1-y}] \text{O}_2$  with different chemical compositions is also reported in the literature.<sup>74–76</sup>

Charge compensation mechanisms on the sodium extraction process were further analyzed by XAS. XANES spectra of  $\text{P2-Na}_x[\text{Fe}_{1/2}\text{Mn}_{1/2}] \text{O}_2$  at the iron K-edge are shown in Figure 9a. When  $\text{Na}_x[\text{Fe}_{1/2}\text{Mn}_{1/2}] \text{O}_2$  is oxidized from 3.8 to 4.2 V, the shift in the iron K-edge absorption spectrum is obviously found in the higher energy region. The shift could be due to complicated situations, including the changes in the local structures, for example, sodium extraction from the iron face-

shared sites and phase transitions.<sup>51</sup> Therefore, EXAFS spectra during sodium extraction were further analyzed. The change in the radial distribution around iron during oxidation to 4.2 V is shown in Figure 9b. The radial distribution around iron is not affected by oxidation to 3.8 V, and the interatomic distance of Fe–O remains unchanged (2.00 Å for the as-prepared and 1.99 Å for the 3.8 V charged state). The Fe–O local environment is markedly changed after oxidation to 4.2 V. The intensity for both the first and the second coordination shells, Fe–O and Fe–Fe(Mn), is reduced, indicating the distortion around Fe. The distortion also influences the neighboring manganese ions.<sup>51</sup> The interatomic distance of Fe–O is clearly shortened after oxidation to 4.2 V (1.90(1) Å). A large Debye–Waller factor indicates the distortion by a noncooperative Jahn–Teller effect of high-spin  $\text{Fe}^{4+}$  ( $t_{2g}^3 e_g^1$ ). Mössbauer spectroscopy further supports the oxidation of  $\text{Fe}^{3+}$  to  $\text{Fe}^{4+}$ , as shown in Figure 9c. Oxidation of  $\text{Fe}^{3+}$  was also reported for  $\text{O3-NaFeO}_2$  by Mössbauer spectroscopy.<sup>25,60</sup> The results indicate that  $\text{Fe}^{3+}$  in  $\text{P2-Na}_x[\text{Fe}_{1/2}\text{Mn}_{1/2}] \text{O}_2$  is electrochemically active in the sodium system based on the  $\text{Fe}^{3+}/\text{Fe}^{4+}$  redox. Note that  $\text{O3-LiFeO}_2$  is never electrochemically active on the basis of the  $\text{Fe}^{3+}/\text{Fe}^{4+}$  redox,<sup>57</sup> or the reaction seems to be dominated by the oxygen removal process at the solid/electrolyte interface. Indeed, nanometer-sized O3-type  $\text{LiFeO}_2$  is electrochemically active associated with the  $\text{Fe}^{2+}/\text{Fe}^{3+}$  redox.<sup>77</sup> As the  $\text{Fe}^{3+}$  3d orbital is strongly hybridized with the oxygen 2p orbital in the Li system, oxygen removal is favorable rather than oxidation to  $\text{Fe}^{4+}$ , similarly to the  $\text{Li}_2\text{MnO}_3$  system. In general, the sodium system shows a lower redox potential when compared with the lithium system as shown in Figure 3. Sodium ions are strongly ionized when compared with lithium ions, resulting in the lower covalency with oxygen. Iron and oxygen gain more (net)

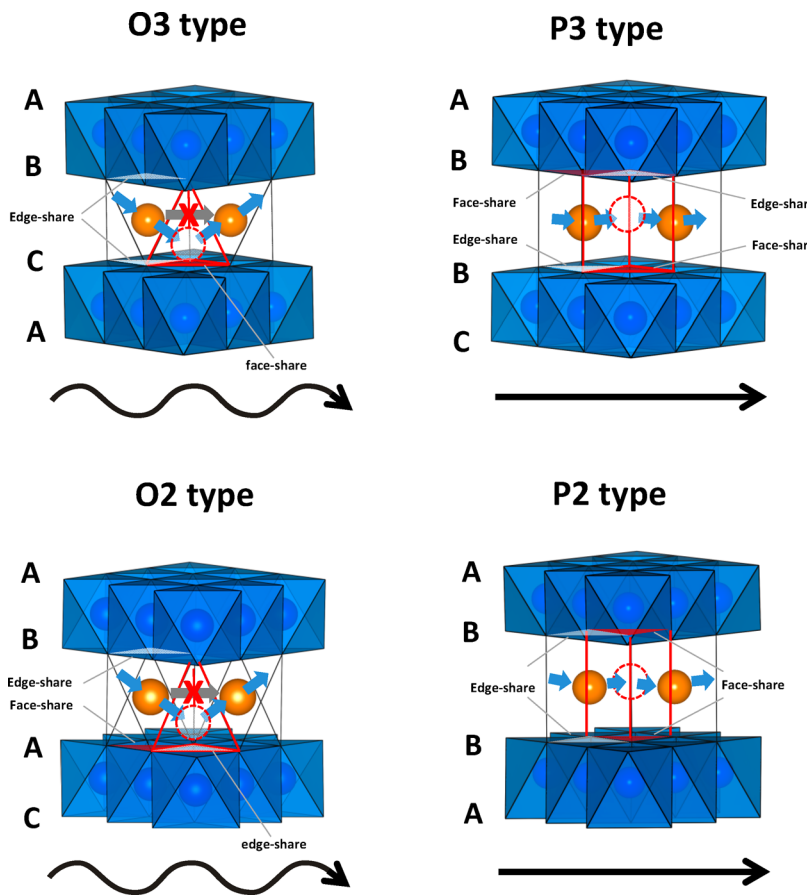


**Figure 8.** Na migration paths in different layered structures. See text for more details.

electrons when compared with the lithium system. As a result, the electrochemical potential of the  $\text{Fe}^{3+}/\text{Fe}^{4+}$  redox is relatively low compared with the lithium system. Thus, the  $\text{Fe}^{3+}/\text{Fe}^{4+}$  redox in  $\text{P2-Na}_x[\text{Fe}_{1/2}\text{Mn}_{1/2}]_{\text{O}2}$  could be accessible without oxygen loss and used as an electrode material with a relatively high operating voltage in the Na system.

As described above, the available reversible capacity of  $\text{P2-Na}_x[\text{Fe}_{1/2}\text{Mn}_{1/2}]_{\text{O}2}$  reaches  $190 \text{ mAh g}^{-1}$  with an average voltage of  $2.75 \text{ V}$  versus sodium metal. The energy density is estimated to be  $520 \text{ mWh g}^{-1}$  vs Na, which is comparable to that of  $\text{LiFePO}_4$  (about  $530 \text{ mWh g}^{-1}$  versus Li) and slightly higher than that of  $\text{LiMn}_2\text{O}_4$  (about  $450 \text{ mWh g}^{-1}$ ). The density of  $\text{P2-Na}_x[\text{Fe}_{1/2}\text{Mn}_{1/2}]_{\text{O}2}$  estimated from XRD is  $4.1 \text{ g cm}^{-3}$ , which is higher than that of  $\text{LiFePO}_4$  ( $3.6 \text{ g cm}^{-3}$ ), and the submicrometer-sized primary particles are electrochemically active without carbon coating. In addition, the feature of stepwise voltage change observed for  $\text{P2-O'3-Na}_x\text{MnO}_2$  is not observed for  $\text{P2-Na}_x[\text{Fe}_{1/2}\text{Mn}_{1/2}]_{\text{O}2}$  (Figure 6). The appearance of voltage plateaus is closely correlated with in-plane sodium/vacancy ordering (presumably coupled with charge ordering in  $\text{MnO}_2$  layers). Stabilization of the Na/vacancy ordering also results in biphasic reactions (two phases with, generally, different unit cell volume coexist in the single particle, namely, first-order phase transitions) in the region of voltage plateaus. Rate capability in the electrode materials could be restricted because of the phase boundary movement for two-phase regions.<sup>71</sup> Partial Fe substitution for Mn effectively reduces the tendency for in-plane sodium/vacancy ordering. These characters are highly beneficial to increase the energy

and power density of the electrode materials in the sodium batteries.

Although the P2-type Na–Fe–Mn system is a promising candidate as a high-capacity positive electrode material for NIBs, three major drawbacks are known for electrode materials: (1) a large volume change (11.3% shrinkage after charge to  $4.2 \text{ V}$ ) during electrochemical cycles, (2) its hygroscopic character, which restricts sample handling in moist air (as-prepared  $\text{P2-Na}_{2/3}[\text{Fe}_{1/2}\text{Mn}_{1/2}]_{\text{O}2}$  is somewhat oxidized by water, forming  $\text{P2-Na}_{1/2}[\text{Fe}_{1/2}\text{Mn}_{1/2}]_{\text{O}2}$  and  $\text{NaOH}$ , and it is also reported that water molecules can be intercalated into P2 phases<sup>80</sup>), and (3) the sodium deficiency in the as-prepared sample which limits the charge capacity in a full-cell configuration, unless an additional source of sodium ions is added. In the first discharge process, the sodium ions in part inserted beyond the starting composition of  $x = 2/3$  in  $\text{Na}_x[\text{Fe}_{1/2}\text{Mn}_{1/2}]_{\text{O}2}$ . The excess amount of sodium is estimated to be  $0.2$  ( $\sim 50 \text{ mAh g}^{-1}$ ), forming the  $\text{P}'2-\text{Na}_{0.86}[\text{Fe}_{1/2}\text{Mn}_{1/2}]_{\text{O}2}$  in the fully discharged state.<sup>51</sup> It is difficult to directly prepare this sodium-rich phase because this phase is metastable. Compensation for the deficient sodium ions is, therefore, needed to use the full capacity of  $\text{P2-Na}_x[\text{Fe}_{1/2}\text{Mn}_{1/2}]_{\text{O}2}$  for NIBs. One idea to compensate for the sodium ions is addition of sacrificial salts. For instance,  $\text{NaN}_3$  electrochemically decomposes into sodium ion and  $\text{N}_2$  gas, and this reaction is irreversible. Mixing of  $\text{P2-Na}_{2/3}[\text{Fe}_{1/2}\text{Mn}_{1/2}]_{\text{O}2}$  with  $\text{NaN}_3$ , therefore, increases the initial charge capacity and thus effectively compensates for the sodium deficiency for the P2 phase in the initial state.<sup>81</sup> Further optimization is needed to overcome these disadvantages of the

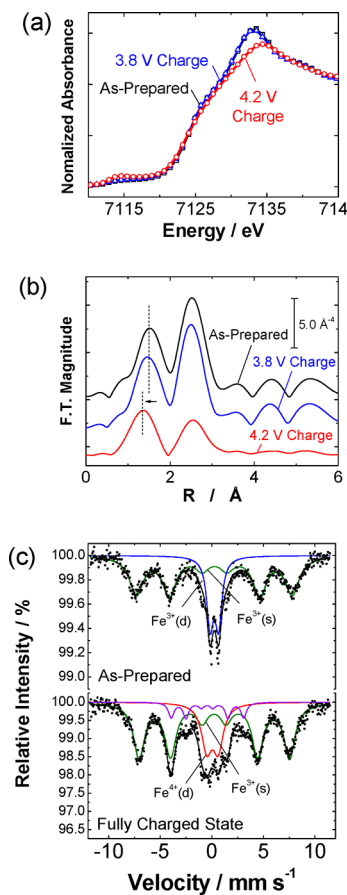


**Figure 9.** XAS analysis of the P2-type  $\text{Na}_x[\text{Fe}_{1/2}\text{Mn}_{1/2}]\text{O}_2$  samples charged to 3.8 and 4.2 V: iron K-edge XANES (a) and radial distribution of the iron ion (b). (c) Comparison of the Mössbauer spectra of the as-prepared sample and the fully charged state. Observed spectra are shown as black dots, and deconvoluted spectra by a curve-fitting procedure are shown as colored lines. Here *s* and *d* represent sextet and doublet, respectively. The purple curve corresponds to the sextet component. This minor sextet component can be assigned to neither  $\text{Fe}^{3+}$  nor  $\text{Fe}^{4+}$ . Instead, this component could be potentially assigned into  $\text{Fe}^{5+}$  because of the lower isomer shift.  $\text{Fe}^{5+}$  probably originates from the charge disproportionation of  $\text{Fe}^{4+}$  ( $\text{Fe}^{4+} \rightarrow \text{Fe}^{5+} + \text{Fe}^{3+}$ ) as reported in refs 78 and 79. Reprinted by permission from Macmillan Publishers Ltd.: (*Nature Materials*) (ref 51), copyright 2012.

electrode materials and to realize large-scale and high-energy NIBs in the future.

**3.1.3. Other 3d Transition-Metal Oxides with Layered Structures.** **3.1.3.1. O3-, P3-, and P2-Type  $\text{Na}_x\text{CoO}_2$ .** Layered  $\text{Na}_x\text{CoO}_2$  is known as the oldest layered oxide studied as the sodium insertion host.<sup>13</sup> Similar to manganese, both O3- and P2-type layered phases are easily prepared and both samples show high reversibility as an electrode material. In addition, the P3-type  $\text{Na}_x\text{CoO}_2$  ( $x \approx 0.62$ ) can be prepared as a low-temperature phase (with monoclinic distortion at room temperature).<sup>82</sup> The first NIBs were demonstrated with P2- and P3-type  $\text{Na}_x\text{CoO}_2$  as positive electrode materials and a composite of poly(*p*-phenylene) and  $\text{Na}_x\text{Pb}$  as the negative electrode in 1988.<sup>83</sup> Research interest for layered  $\text{Na}_x\text{CoO}_2$  in the past decade has been mainly focused on the thermoelectric properties<sup>84,85</sup> and superconductivity for the hydrate phase.<sup>86</sup> Figure 10 compares the charge/discharge curves of O3-, P2-, and P3-type  $\text{Na}_x\text{CoO}_2$  in Na cells. Many voltage plateaus

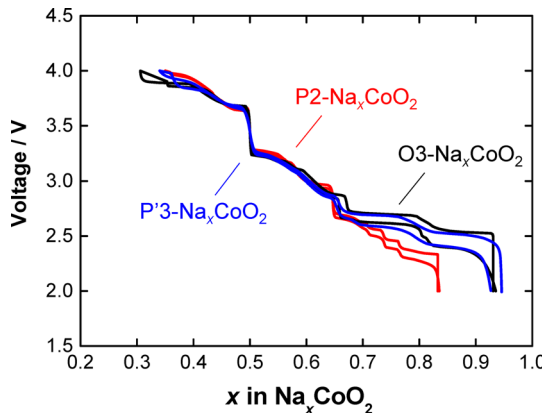


**Figure 10.** Comparison of typical charge/discharge curves of Na cells with layered polymorphs: O3-, P'3-, and P2-type  $\text{Na}_x\text{CoO}_2$ . Similar profiles are observed for three polymorphs except the region with high sodium content ( $x > 0.7$ ). Data derived from ref 13 and 82.

similarly appear for  $\text{Na}_x\text{CoO}_2$  phases regardless of the difference in stacking sequence of  $\text{CoO}_2$  layers. Large reversible capacities of  $140 \text{ mAh g}^{-1}$  for O3,  $130 \text{ mAh g}^{-1}$  for P3, and  $120 \text{ mAh g}^{-1}$  for P2 phases are observed. The biphasic behavior with several sets of plateaus is a characteristic feature of  $\text{Na}_x\text{CoO}_2$ . This character is clearly different from  $\text{Li}_x\text{CoO}_2$  as shown in Figure 3. Although a monoclinic phase transition is observed for  $\text{Li}_x\text{CoO}_2$  ( $x \approx 0.5$ ) with the presence of a short voltage plateau, it is easily noticed that  $\text{Na}_x\text{CoO}_2$  shows much more complicated phase transitions on sodiation/desodiation. Since similar charge ordering (electron–electron interaction) is expected for  $\text{Na}_x\text{CoO}_2$  and  $\text{Li}_x\text{CoO}_2$ , the sodium ions would be responsible for the difference in the phase transitions with biphasic behavior. A relatively large repulsive interaction for large and highly ionized  $\text{Na}^+$  is expected compared with  $\text{Li}^+$ . Detailed studies on sodium-ion ordering have been published so far, especially for P2-type  $\text{Na}_x\text{CoO}_2$ . A phase diagram of P2-type  $\text{Na}_x\text{CoO}_2$  in relation to the  $\text{Na}^+$  content and ordering has been predicted by first-principles calculation<sup>87</sup> and experimentally studied by in-situ XRD coupled with an electrochemical method.<sup>88</sup> Typical examples of in-plane  $\text{Na}^+$  ordering are compared in Figure 11. Crystallographic sites for  $\text{Na}^+$  are different for the O3 and P2 phases. For the O3 phase, only octahedral sites, which share three edges with  $\text{CoO}_6$  octahedra, exist between  $\text{CoO}_2$  layers, whereas for the P2 phase, two distinct prismatic sites are present, i.e., edge shared (prism A (e-e) in Figure 11b) and face shared (prism B (f-f) in Figure 11b) prismatic sites with the  $\text{CoO}_6$  octahedra. The complication for in-plane Na ordering arises from two different repulsive interactions, sodium–sodium and sodium–cobalt interaction for the P2 phase. Clustering of  $\text{Na}^+$  for P2-type  $\text{Na}_{2/3}\text{CoO}_2$  at edge-shared sites was predicted by first-principles calculation<sup>87,89</sup> and experimentally evidenced.<sup>82,88,90</sup> Part of the sodium ions are also located at the face-shared sites as shown in Figure 11, suggesting that the in-plane sodium–sodium interaction can be highly influential in comparison to the sodium–cobalt interaction at the face-shared sites. This speculation is further supported by the observation of sodium ordering in P2-type  $\text{Na}_{0.5}\text{CoO}_2$ .<sup>88,91</sup> Only one-half of the sodium ions are located at the edge-shared sites, and the rest of them are found to be at the face-shared sites in the case of the P2-type structure as shown in Figure 11e. The sodium ions are uniformly distributed in the two-dimensional triangle (pris-

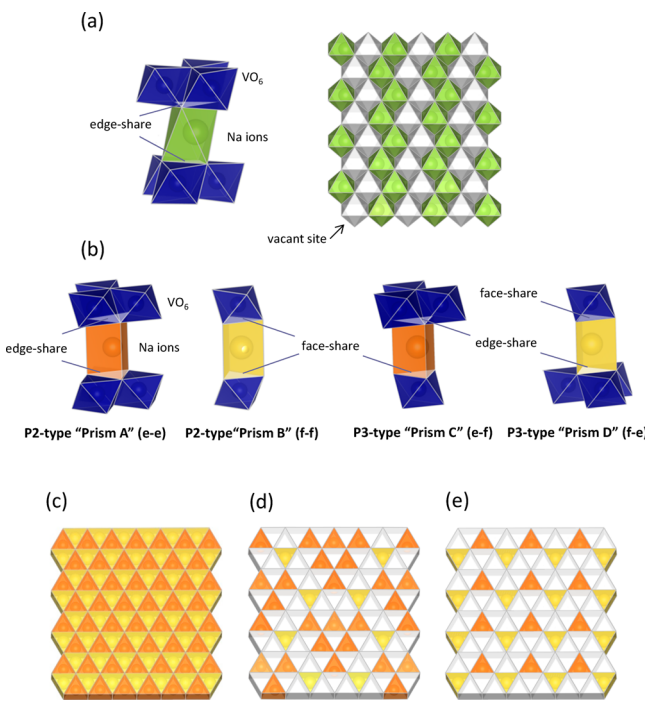


**Figure 11.** Schematic illustrations of sodium/vacancy ordering: (a) sodium/vacancy ordering observed for O'3-Na<sub>0.5</sub>VO<sub>2</sub>, (b) four different prismatic sites in P2- and P3-type layered structures, (c) full occupation of prismatic sites in P2 and P3 phases (a hypothetical model), and sodium/vacancy ordering observed for (d) P2-Na<sub>2/3</sub>CoO<sub>2</sub> and (e) P'2-Na<sub>1/2</sub>CrO<sub>2</sub>, P'2-Na<sub>1/2</sub>VO<sub>2</sub>, and P'3-Na<sub>1/2</sub>CrO<sub>2</sub>. (a) Data derived from ref 114, (d) data from ref 90, and (e) data from ref 91.

matic) lattice, probably to minimize the in-plane repulsive interaction.

Note that the voltage profile, operating voltage, and phase transition behavior for three different layered polymorphs, O3, P3, and P2, are very similar as seen in Figure 10. It is very difficult to distinguish the kind of phases only from the voltage profiles in the figure. Recently, the electrochemical properties of three Li<sub>x</sub>CoO<sub>2</sub> polymorphs, O2, O3, and O4, have been also reported.<sup>49,92</sup> Some differences for the phase transition behavior and voltage profiles for the Li system have been found, and the phase transition associated with Li ordering is more evidenced for the O2 phase. For the O3-type Na<sub>x</sub>CoO<sub>2</sub>, the O3–P3 phase transition occurs when a small amount of Na ions is extracted. P3 phase has two prismatic sites (prism C (e-f) and prism D (f-e) in Figure 11b), but both are crystallographically identical sites. The ordering of Na<sup>+</sup> in the P3 and P2 phases is expected to be very similar as discussed in the former section, and therefore, three different polymorphs show very similar voltage profiles with the biphasic reaction. A difference in the voltage profile is observed for a high sodium content region ( $x > 0.8$  for Na<sub>x</sub>CoO<sub>2</sub>). In this region, the O3 phase is energetically stabilized, resulting in the difference in the phase transition and Na<sup>+</sup> ordering for the P2- and O3-phases. Among the three polymorphs of Na<sub>x</sub>CoO<sub>2</sub>, the O3 phase experimentally shows wider reversible range when compared with the P2 phase, probably because of the difference in the kinetics in the high sodium content region. The trend is clearly reversed compared with the Na–Fe–Mn system. Further systematic studies are needed to explain the origins of these differences in layered polymorphs with different elements.

Xia and Dahn recently reported the thermal stability of P2-type Na<sub>x</sub>CoO<sub>2</sub> by accelerating the rate calorimetry.<sup>93</sup> In addition to the reaction with aprotic solvents, Na<sub>x</sub>CoO<sub>2</sub> reacts with the electrolyte salt (NaPF<sub>6</sub>), leading to formation of NaCoF<sub>3</sub>. Such chemistry has not been found in Li<sub>x</sub>CoO<sub>2</sub>.<sup>94</sup> From these results they proposed that proper selection of electrolyte salts is also an important factor to design safe batteries without such unfavorable reaction.

**3.1.3.2. O3-Type NaCrO<sub>2</sub> and O'3-Type NaNiO<sub>2</sub>.** The electrode performance of O3-type NaCrO<sub>2</sub> and O'3-type NaNiO<sub>2</sub> was first reported in 1982, and both samples show the complicated phase transition on sodium extraction.<sup>95</sup> The reversibility of the Na extraction/reinsertion process was revisited in 2009 and reported to be that approximately 50% of sodium ions can be reversibly extracted from NaCrO<sub>2</sub> with small polarization based on the Cr<sup>3+</sup>/Cr<sup>4+</sup> redox as shown in Figure 12.<sup>96,97</sup> A voltage plateau at nearly 3.0 V vs Na metal is

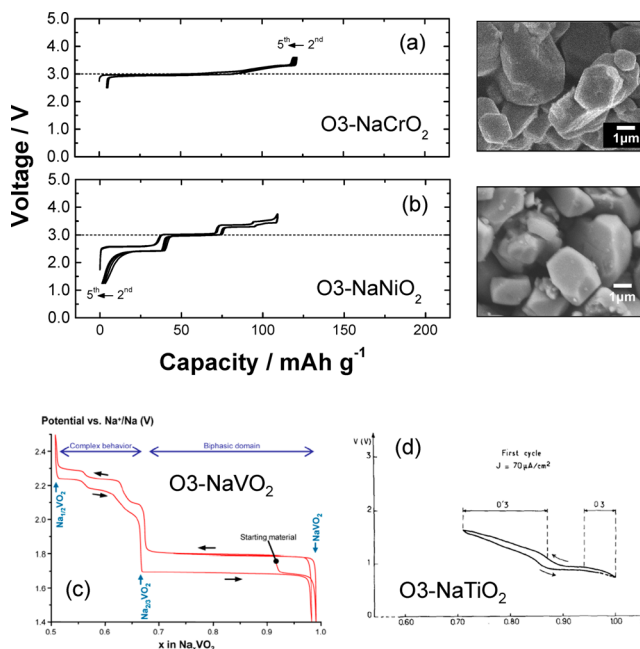


**Figure 12.** Comparison of galvanostatic charge/discharge curves of layered O3-type Na<sub>x</sub>MeO<sub>2</sub> (Me = Cr, Ni, V, and Ti) samples. Morphology of particles for O3-type Na<sub>x</sub>MeO<sub>2</sub> (Me = Cr and Ni) is also compared. Data of NaCrO<sub>2</sub> (a) and NaNiO<sub>2</sub> (b) derived from refs 96 and 95, respectively. Data of NaVO<sub>2</sub> (c). Reprinted with permission from ref 114. Copyright 2012 American Chemical Society. Data of NaTiO<sub>2</sub> (d) Reprinted with permission from ref 116. Copyright 1983 Springer.

observed in the high sodium content region, and the voltage shifts up gradually to 3.3 V. An additional plateau at 3.6 V appears near  $x \approx 0.5$  in Na<sub>1-x</sub>CrO<sub>2</sub>. Further sodium extraction beyond 50% results in the loss of reversibility because of the irreversible phase transition similar to NaFeO<sub>2</sub>.<sup>97</sup> The reversible range is slightly wider than that of NaFeO<sub>2</sub> (less than 40%). Although a Li counterpart, LiCrO<sub>2</sub>, also crystallizes into the layered structure, reversibility as electrode materials is quite low.<sup>96,99</sup> For the Li system, Cr<sup>3+</sup> is oxidized into Cr<sup>6+</sup> and small Cr<sup>6+</sup> migrates into and stabilized at the tetrahedral sites in the lithium layers.<sup>100</sup> Small Cr<sup>6+</sup> is expected to be difficult to migrate into the relatively large tetrahedral sites in Na layers, and instead of formation of Cr<sup>6+</sup>, Cr<sup>4+</sup> could be energetically stabilized in Na<sub>x</sub>CrO<sub>2</sub>.<sup>96</sup> Additionally, O3-type NaCrO<sub>2</sub>

translates into the P3 phase by sodium extraction,<sup>101</sup> and migration of Cr is an unlikely consequence because of no tetrahedral site in the Na layer when the P3 phase is formed.  $\text{Na}_{0.5}\text{CrO}_2$  has a monoclinic lattice, namely, P'3-type  $\text{Na}_{0.5}\text{CrO}_2$ . The monoclinic phase is stabilized coupled with in-plane  $\text{Na}^+$  ordering. Although the local site environment for P3 and P2 phases is different as discussed above, the in-plane  $\text{Na}^+$  ordering manner for P'3-type  $\text{Na}_{0.5}\text{CrO}_2$  is essentially identical to that observed for P2- $\text{Na}_{0.5}\text{CoO}_2$  in Figure 11.<sup>98</sup>

An important finding of O3- $\text{NaCrO}_2$  as an electrode material is the thermal stability. A study on the thermal stability of  $\text{Na}_{0.5}\text{CrO}_2$  by accelerating rate calorimetry has revealed that  $\text{Na}_{0.5}\text{CrO}_2$  is surprisingly more stable than  $\text{Li}_x\text{FePO}_4$  as one of the most thermally stable electrode materials in the Li system.<sup>102</sup> The electrode performance of O3- $\text{NaCrO}_2$  at elevated temperature (80 °C) has been recently reported in pure ionic liquid, alkali metal ions ( $\text{Na}^+$  and  $\text{K}^+$ ) as cations, and bis(fluorosulfonyl)amide (FSA) as an anion, and excellent cyclability and rate capability have been demonstrated.<sup>101,103</sup> No structural degradation and long cycle life at elevated temperature are a consistent result with the excellent thermal stability as an electrode material.

$\text{LiNiO}_2$  is also extensively studied as high-capacity positive electrode materials for LIBs. Synthesis of really stoichiometric  $\text{LiNiO}_2$  has never been achieved. Instead, an off-stoichiometric  $\text{Li}_{1-x}\text{Ni}_{1+x}\text{O}_2$  phase is more easily obtained with a trace of  $\text{Ni}^{2+}$  in the lithium site.<sup>104</sup> Moreover, the electrode performance is drastically deteriorated by the presence of  $\text{Ni}^{2+}$  in the lithium layers. In contrast, stoichiometric  $\text{NaNiO}_2$  can be prepared with a monoclinic distortion because of the presence of low-spin  $\text{Ni}^{3+}$  as Jahn–Teller ions, whereas even nearly stoichiometric  $\text{Li}_{1-x}\text{Ni}_{1+x}\text{O}_2$  ( $x \approx 0.02$ ) has a rhombohedral lattice, and only a local distortion is found by EXAFS analysis.<sup>105</sup> Similar to O3- $\text{NaCrO}_2$ , O'3- $\text{NaNiO}_2$  has been also revisited and its electrode performance is found in the literature.<sup>106</sup> Since  $\text{Ni}^{2+}$  cannot be located in Na sites for  $\text{NaNiO}_2$  because of the large size gap, good electrode performance is obtained as shown in Figure 12. Several voltage plateaus are observed similar to other layered phases. Reversibility is quite high when the cutoff voltage is limited to 3.7 V vs Na metal, and 50% of sodium ions is reversibly extracted/reinserted in the lattice. Although nearly all of the Na ions are electrochemically extracted by charge to 4.5 V vs Na metal, reversibility as an electrode material is deteriorated.<sup>106</sup> The O'3–P'3 phase transition depending on the sodium content in  $\text{Na}_{1-x}\text{NiO}_2$  was also reported.<sup>95,106</sup>

**3.1.3. O3- and P2-Type  $\text{Na}_x\text{VO}_2$  and O3-Type  $\text{NaTiO}_2$ .** The electrochemical properties and changes in the crystal structure for  $\text{LiVO}_2$  as an electrode material were first reported in 1980s. The original layered structure transforms into a cation-disordered rock-salt phase because of vanadium migration induced by lithium extraction,<sup>107</sup> leading to the inferior electrode performance. Recently,  $\text{LiVO}_2$  (Li/V off-stoichiometric samples) has been proposed as a negative electrode with low voltage, 0.3 V vs Li metal.  $\text{LiVO}_2$  is reduced by further insertion of Li to form  $\text{Li}_2\text{VO}_2$ ,<sup>108,109</sup> where 2 mol of lithium ions are accommodated between  $\text{VO}_2$  layers, namely, the T1-type phase as observed for  $\text{Li}_2\text{NiO}_2$ .<sup>110</sup> The electrochemical properties of  $\text{NaVO}_2$  in Na cells were not published before 2010. The electrode performance of O3- $\text{NaVO}_2$  was first reported by two individual research groups.<sup>111,112</sup> The electrochemical properties of P2- $\text{Na}_{0.7}\text{VO}_2$  in Na cells were also reported and compared with O3-type phase.<sup>112</sup> O3- $\text{NaVO}_2$  and P2- $\text{Na}_{0.7}\text{VO}_2$  delivers approximately 120 and 100 mAh g<sup>-1</sup>

of the reversible capacity, respectively. The operating voltage is located near 2 V vs Na, which would be slightly low as a positive electrode and relatively high as a negative electrode (Figure 12) for the aprotic electrolyte system (however, this system could be potentially used as the negative electrode for the aqueous electrolyte system discussed in a later section). Na extraction beyond  $x = 0.5$  in O3- $\text{Na}_{1-x}\text{VO}_2$  results in the deterioration of electrode performance,<sup>111</sup> similar to O3- $\text{Na}_{1-x}\text{CrO}_2$ . Although a relatively wider reversible range for the O3 phase was reported ( $0 \leq x \leq 0.5$  in  $\text{Na}_{1-x}\text{VO}_2$ ), slightly large hysteresis (0.2 V) was observed in the high sodium content region ( $0 \leq x \leq 1/3$ ). Such hysteresis was not observed in the P2 phase in Na cells.<sup>112</sup>

In-plane  $\text{Na}^+$  ordering in P2- $\text{Na}_{0.5}\text{VO}_2$ <sup>113</sup> and O'3- $\text{Na}_{0.5}\text{VO}_2$ <sup>114</sup> has been also studied. The  $\text{Na}^+$  ordering found in P2- $\text{Na}_{0.5}\text{VO}_2$  is essentially the same as that of P2- $\text{Na}_{0.5}\text{CoO}_2$  (Figure 11). Additionally, vanadium ions in P2- $\text{Na}_{0.5}\text{VO}_2$  form pseudotrimers with very short V–V distances (two at 2.58 Å and one at 2.69 Å).<sup>113</sup> Since the only edge-shared octahedral sites with  $\text{VO}_6$  octahedra are present in the O'3 phase, a cation ordering pattern for O'3- $\text{Na}_{0.5}\text{VO}_2$  is different from P2- $\text{Na}_{0.5}\text{VO}_2$ . Zigzag-type ordering at the octahedral sites (Figure 11a) has been experimentally evidenced for O'3- $\text{Na}_{0.5}\text{VO}_2$ , and this ordering has been proposed to be stabilized by coupling with formation of V–V dimers with a short distance of 2.64 Å.<sup>114</sup>

By comparing the V<sup>3+</sup> system, a few studies are found for the Ti<sup>3+</sup> system as an electrode material, and instead, the Ti<sup>4+</sup> system has been extensively studied as an electrode material, which will be discussed in the next section. Since the ionic radii of  $\text{Li}^+$  (0.76 Å) and  $\text{Ti}^{3+}$  (0.67 Å) are similar in size,  $\text{LiTiO}_2$  generally crystallizes into a cation-disordered rock-salt phase. However, according to the literature, there are non-cation-disordered polymorphs of  $\text{LiTiO}_2$ .<sup>115</sup> Although the electrode performance of  $\text{LiTiO}_2$  is not well known, the cation-disordered rock-salt phase could show insufficient performance in Li cells without preparation of nanoarchitected samples. The electrode performance of  $\text{NaTiO}_2$ , which has a strong reducing character, was found in the literature.<sup>116</sup> High reversibility with small polarization was reported when the voltage was limited to 1.6 V in the Na cell. The original O3 phase changes into the O'3 phase by sodium extraction with a relatively low operating voltage (0.8–1.6 V vs Na metal). A low operating voltage based on  $\text{Ti}^{3+}/\text{Ti}^{4+}$  redox is suitable for negative electrode materials as shown in a later section.

**3.1.4. Binary/Ternary Metal Oxides with Layered Structures.** **3.1.4.1. O3-Type Iron-Based Materials.** In the former section, the electrode performance of O3- $\text{NaFeO}_2$  with a narrow reversible range has been described. Recently, some iron-based layered materials have been also reported with a wider reversible range in comparison to O3- $\text{NaFeO}_2$ . In these materials, Ni, Mn, and Co ions are partly substituted for Fe ions.<sup>71,117–120</sup> Metal substitution effectively changes the electrochemical phase transition behavior for  $\text{NaFeO}_2$ . For the pure iron system, the crystal structure of  $\text{Na}_{0.5}\text{FeO}_2$  was reported as an O'3-type phase with monoclinic lattice distortion.<sup>59</sup> O3–P3 phase transition is not evidenced for  $\text{Na}_x\text{FeO}_2$ , and therefore, such iron migration to the adjacent face-shared tetrahedral sites is probably unavoidable. The O3–P3 phase transition in Na cells, however, is generally observed for the metal-substituted  $\text{Na}[\text{Fe}_{1-x}\text{Me}_x]\text{O}_2$  samples with relatively wide reversible range. Since iron migration to the large prismatic sites is expected to be unlikely, formation of the

P3 phase is expected to effectively extend reversible ranges as the electrode materials in Na cells. Stabilization of the P3 phase has been also theoretically predicted for  $\text{Na}_{0.5}\text{MeO}_2$  (Me = Ni, Mn, and Co).<sup>121</sup> Among layered materials with 3d transition-metal ions, the P3-type phase is significantly stabilized for  $\text{Na}_x\text{CoO}_2$ <sup>121</sup> and excellent electrode performance has been reported for  $\text{Na}[\text{Fe}_{1/2}\text{Co}_{1/2}]\text{O}_2$ <sup>71</sup> (Figure 13) and  $\text{Na}$

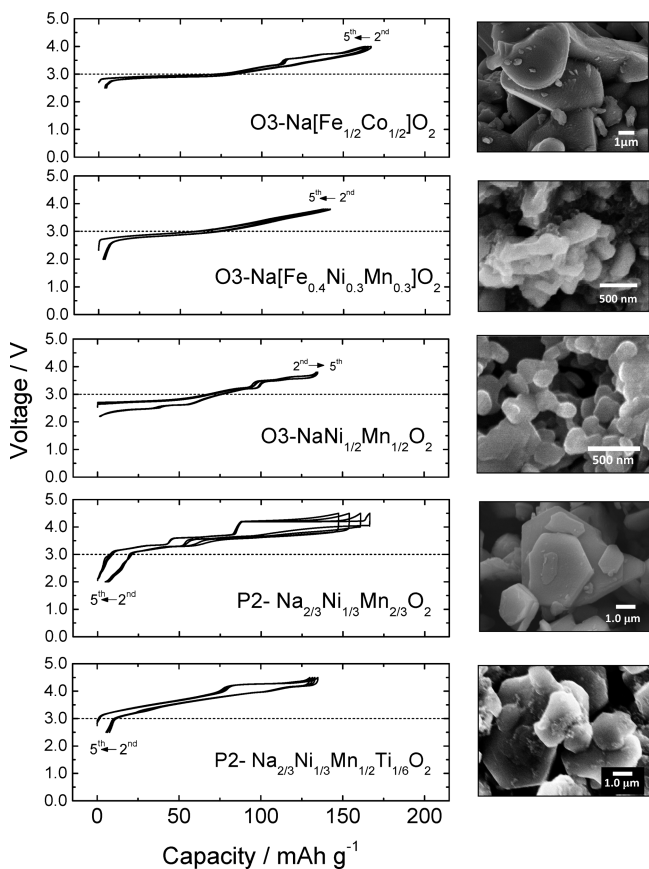


**Figure 13.** Comparison of galvanostatic charge/discharge curves of layered  $\text{Na}_x\text{MeO}_2$  samples with different structures. Morphology of particles for each sample is also compared (right). Data of O3- $\text{Na}[\text{Co}_{1/2}\text{Fe}_{1/2}]\text{O}_2$  derived from ref 71, O3- $\text{Na}[\text{Fe}_{0.4}\text{Ni}_{0.3}\text{Mn}_{0.3}]\text{O}_2$  from ref 117, O3- $\text{Na}[\text{Ni}_{1/2}\text{Mn}_{1/2}]\text{O}_2$  from ref 125, and P2- $\text{Na}_{2/3}[\text{Ni}_{1/3}\text{Mn}_{2/3}]\text{O}_2$  and P2- $\text{Na}_{2/3}[\text{Ni}_{1/3}\text{Mn}_{1/2}\text{Ti}_{1/6}]\text{O}_2$  from ref 131.

$[\text{Ni}_{1/3}\text{Co}_{1/3}\text{Fe}_{1/3}]\text{O}_2$ .<sup>119</sup> Micrometer-sized and dense O3- $\text{Na}[\text{Fe}_{1/2}\text{Co}_{1/2}]\text{O}_2$  surprisingly shows excellent rate capability, which is much better than that of O3- $\text{NaCoO}_2$ , as shown in Figure 7. Over 60% of reversible capacity is preserved at the 30 C rate ( $7.2 \text{ A g}^{-1}$ ) for O3- $\text{Na}[\text{Fe}_{1/2}\text{Co}_{1/2}]\text{O}_2$ , while such superior rate capability is not observed for O3- $\text{NaCoO}_2$ . It has been proposed that the excellent rate capability originates from the difference in the phase transition behavior related to formation of the P3 phase.<sup>71</sup> From a stepwise voltage profile observed for O3- $\text{Na}_x\text{CoO}_2$ , limited rate capability is expected because the phase boundary movement for two-phase regions is required. Additionally, the tendency of Na/vacancy ordering could energetically stabilize the sodium ions at the prismatic sites, probably leading to the relatively slow kinetics for solid-state diffusion of  $\text{Na}^+$ . Although some voltage plateaus are still observed for  $\text{Na}[\text{Fe}_{1/2}\text{Co}_{1/2}]\text{O}_2$ , structural analysis revealed that a two-phase region for  $\text{Na}[\text{Fe}_{1/2}\text{Co}_{1/2}]\text{O}_2$  existed only at the beginning of charge process as O3–P3 phase transition,<sup>71</sup> and

thus, it is expected that excellent rate capability is achieved. The Co-free system, e.g.,  $\text{Na}[\text{Fe}_{0.4}\text{Ni}_{0.3}\text{Mn}_{0.3}]\text{O}_2$ , also shows the O3–P3 phase transition and good electrode performance with small polarization as shown in Figure 13. The rate capability of  $\text{Na}[\text{Fe}_{0.4}\text{Ni}_{0.3}\text{Mn}_{0.3}]\text{O}_2$ <sup>117</sup> is, however, inferior to that of the Co-substituted system.<sup>71,119</sup> The results probably originate from the superior in-plane electrical conductivity of Co as experimentally observed for  $\text{Li}_x\text{CoO}_2$ <sup>122</sup> and  $\text{Na}_x\text{CoO}_2$ .<sup>85</sup>

**3.1.4.2. O3-Type and P2-Type  $\text{Na}_x[\text{Ni}_{1/2}\text{Me}_{1/2}]\text{O}_2$  (Me = Mn and Ti).**  $\text{LiNi}_{1/2}\text{Mn}_{1/2}\text{O}_2$  containing  $\text{Ni}^{2+}$  and  $\text{Mn}^{4+}$  is one of the most widely studied electrode materials for LIBs.<sup>123</sup>  $\text{LiNi}_{1/2}\text{Mn}_{1/2}\text{O}_2$  delivers large reversible capacity (approximately  $200 \text{ mAh g}^{-1}$ ) based on the  $\text{Ni}^{2+}/\text{Ni}^{4+}$  redox (and  $\text{Mn}^{4+}$  is inactive). However, ionic radii of  $\text{Li}^+$  and  $\text{Ni}^{2+}$  are similar in size; formation of antisite defects (cation intermixing between  $\text{Li}^+$  and  $\text{Ni}^{2+}$ ) is unavoidable. The nickel ions in the lithium layer lead to slow kinetics for solid-state diffusion of lithium ions. To solve this problem,  $\text{LiNi}_{1/2}\text{Mn}_{1/2}\text{O}_2$  ideally without the antisite defects was prepared by  $\text{Na}^+/\text{Li}^+$  ion exchange from O3-type  $\text{Na}[\text{Ni}_{1/2}\text{Mn}_{1/2}]\text{O}_2$ .<sup>41,124</sup> O3-type  $\text{Na}[\text{Ni}_{1/2}\text{Mn}_{1/2}]\text{O}_2$  can be also utilized as a positive electrode material for NIBs.<sup>97,125</sup> Typical charge/discharge curves of O3- $\text{Na}_{1-x}[\text{Ni}_{1/2}\text{Mn}_{1/2}]\text{O}_2$  are shown in Figure 13.  $\text{Na}_{1-x}[\text{Ni}_{1/2}\text{Mn}_{1/2}]\text{O}_2$  delivers large reversible capacity ( $\sim 185 \text{ mAh g}^{-1}$ ) based on  $\text{Ni}^{2+}/\text{Ni}^{4+}$  redox with the O3–P3 phase transition. Almost all of sodium ions are extracted by charge to 4.5 V vs Na without irreversible structural change. Good capacity retention is achieved when the voltage range is limited below 3.8 V.<sup>125</sup> P3-type  $\text{Na}_{2/3}[\text{Ni}_{1/2}\text{Mn}_{1/2}]\text{O}_2$  can be also prepared as a low-temperature phase.<sup>126</sup> The electrode performance of the Co-substituted system, O3-type  $\text{Na}[\text{Co}_{1/3}\text{Ni}_{1/3}\text{Mn}_{1/3}]\text{O}_2$ , was also reported as an electrode material.<sup>127</sup>

$\text{LiNi}_{1/2}\text{Ti}_{1/2}\text{O}_2$ , which contains  $\text{Ni}^{2+}$  and  $\text{Ti}^{4+}$ , instead of  $\text{Mn}^{4+}$ , crystallizes into the cation-disordered rock-salt phase because the ionic radius of  $\text{Ti}^{4+}$  is quite close to those of  $\text{Li}^+$  and  $\text{Ni}^{2+}$ . The electrode performance of  $\text{LiNi}_{1/2}\text{Ti}_{1/2}\text{O}_2$  is not attractive as a positive electrode material.<sup>128</sup> In contrast,  $\text{Na}[\text{Ni}_{1/2}\text{Ti}_{1/2}]\text{O}_2$  crystallizes into the O3-type layered phase. This fact is also another example of the increase in the flexibility of materials design as electrode materials for the Na system. The electrode performance of O3- $\text{Na}[\text{Ni}_{1/2}\text{Ti}_{1/2}]\text{O}_2$  is found in the literature.<sup>129,130</sup> Approximately 50% of sodium ions is reversibly extracted/reinserted into  $\text{Na}_{1-x}[\text{Ni}_{1/2}\text{Ti}_{1/2}]\text{O}_2$  with a relatively high operating voltage using the redox reaction of nickel.

P2-type  $\text{Na}_{2/3}[\text{Ni}_{1/3}\text{Mn}_{2/3}]\text{O}_2$  was also first prepared as a precursor to synthesize the new layered material for the Li system, i.e., T2-type  $\text{Li}_{2/3}[\text{Ni}_{1/3}\text{Mn}_{2/3}]\text{O}_2$ .<sup>41</sup> The electrode performance of  $\text{Na}_{2/3}[\text{Ni}_{1/3}\text{Mn}_{2/3}]\text{O}_2$  in Na cells was also reported.<sup>42,43</sup> All sodium ions are reversibly extracted based on the  $\text{Ni}^{2+}/\text{Ni}^{4+}$  redox, which realizes high operating voltage as a sodium insertion host. A long voltage plateau at 4.2 V vs Na metal appears in the range of  $1/3 \leq x \leq 2/3$  in  $\text{Na}_{2/3-x}[\text{Ni}_{1/3}\text{Mn}_{2/3}]\text{O}_2$ , as shown in Figure 13. The two-phase coexistence of P2- $\text{Na}_{1/3}[\text{Ni}_{1/3}\text{Mn}_{2/3}]\text{O}_2$  and O2- $[\text{Ni}_{1/3}\text{Mn}_{2/3}]\text{O}_2$  (the sample seems to have stacking faults, but a clear decrease in the interlayer distance from  $11.4 \text{ \AA}$  for the P2 phase and  $8.9 \text{ \AA}$  for the O2 phase was observed) has been evidenced by in-situ XRD in the plateau region.<sup>43</sup> A large volume change (more than 20%) is unavoidable in this region associated with the O2-phase transition, and therefore, cyclability is insufficient as electrode materials as shown in

Figure 13. Its cyclability as electrode materials is drastically improved in the electrochemical cycle in the region of  $0 \leq x \leq 1/3$  in  $\text{Na}_{2/3-x}[\text{Ni}_{1/3}\text{Mn}_{2/3}]_x\text{O}_2$  without the phase transition into the O<sub>2</sub> phase.<sup>70</sup> P2-Na<sub>2/3</sub>[Ni<sub>1/3</sub>Mn<sub>2/3</sub>]O<sub>2</sub> is stable in moist air, and water molecules cannot be inserted into the structure.<sup>80</sup>

Sufficient cyclability can be demonstrated by titanium substitution for manganese ions, i.e., P2-type  $\text{Na}_{2/3}[\text{Ni}_{1/3}\text{Mn}_{2/3-x}\text{Ti}_x]\text{O}_2$ .<sup>131</sup> Although titanium substitution reduces the reversible limit, the P2–O<sub>2</sub> phase transition is effectively suppressed, leading to good cyclability.  $\text{Na}_{2/3}[\text{Ni}_{1/3}\text{Mn}_{1/2}\text{Ti}_{1/6}]\text{O}_2$  delivers 127 mAh g<sup>-1</sup> of reversible capacity with ca. 3.7 V of average discharge voltage vs Na metal (Figure 13). A relatively high operating voltage as sodium insertion host is highly beneficial to increase the energy density for the NIBs. The estimated energy density as positive electrode materials reaches 470 Wh kg<sup>-1</sup> based on metallic sodium as a negative electrode.<sup>131</sup>

Additionally, many different P2-type layered materials were newly synthesized, and the electrode performance in Na cells was provided: Co–Mn,<sup>132,133</sup> Co–Ni–Mn,<sup>134,135</sup> and Fe–Ni–Mn.<sup>136</sup> Not only these transition-metal ions but also lithium ions can be also substituted for the nickel and manganese ions. P2-type  $\text{Na}_{1.0}\text{Li}_{0.2}\text{Ni}_{0.25}\text{Mn}_{0.75}\text{O}_\delta$  (this composition can be reformulated as P2-type  $\text{Na}_{5/6}[\text{Li}_{1/6}\text{Ni}_{5/24}\text{Mn}_{5/8}]\text{O}_2$ ) has been proposed as a potential positive electrode material for NIBs.<sup>137</sup> The sample delivers about 100 mAh g<sup>-1</sup> of reversible capacity based on Ni<sup>2+</sup>/Ni<sup>4+</sup> redox in the voltage range of 2.0–4.2 V. Moreover, the sample shows excellent rate capability without cobalt ions.<sup>137</sup> Available reversible capacity is further increased to 200 mAh g<sup>-1</sup> after charge to 4.8 V.<sup>4</sup> Such anomalous large capacity has been also evidenced for the Li-substituted manganese system, P2-type  $\text{Na}_{5/6}[\text{Li}_{1/4}\text{Mn}_{3/4}]\text{O}_2$ , even without nickel ions, whereas similar electrochemical reaction to Li<sub>2</sub>MnO<sub>3</sub> in the Li cell is observed.<sup>67</sup>

### 3.2. Other Oxides as Na Insertion Host

**3.2.1. Iron-Based Oxides.**  $\text{NaFeO}_2$  with trivalent iron ions crystallizes into two different polymorphs. The electrode performance of the low-temperature phase,  $\alpha$ -type (O<sub>3</sub>-type)  $\text{NaFeO}_2$ , has been described in a former section (Figure 6). Synthesis at higher temperature (>760 °C) easily results in the phase transition into  $\beta$ -type  $\text{NaFeO}_2$  as the high-temperature polymorph. The crystal structure of  $\beta$ - $\text{NaFeO}_2$  is related to the mineral wurtzite. Packing of oxide ions is a hexagonal close-packed array, and both sodium and iron ions are located at tetrahedral sites (Figure 14a).<sup>138</sup> The electrode performance of  $\beta$ - $\text{NaFeO}_2$  was examined in Na cells. Charge/discharge curves of a Na/ $\beta$ - $\text{NaFeO}_2$  cell are shown in Figure 15a.  $\beta$ - $\text{NaFeO}_2$  seems to be electrochemically inactive as an electrode material in the voltage range of 2.0–4.0 V vs Na metal. From these results it is speculated that Fe<sup>3+</sup> at tetrahedral sites could be difficult to oxidize to the Fe<sup>4+</sup> state, which could be energetically stable only at octahedral sites.

Inverse spinel-type  $\text{Fe}_3\text{O}_4$  (and  $\gamma$ -type  $\text{Fe}_2\text{O}_3$ ) and corundum-type ( $\alpha$ -type)  $\text{Fe}_2\text{O}_3$  were also examined as host materials for sodium insertion. A reduction in particle size to the nanoscale often activates the electrode reversibility of transition-metal oxides, which had been thought to be inactive in Li cells.<sup>139,140</sup> Similar to the Li system, nanosized  $\text{Fe}_3\text{O}_4$  and  $\text{Fe}_2\text{O}_3$  are reported to be electrochemically active in Na cells<sup>141,142</sup> even though micrometer-sized  $\text{Fe}_3\text{O}_4$  (and other oxides) are electrochemically inactive. The reversible capacity is less than 10 mAh g<sup>-1</sup> for the submicrometer-sized  $\text{Fe}_3\text{O}_4$ ,

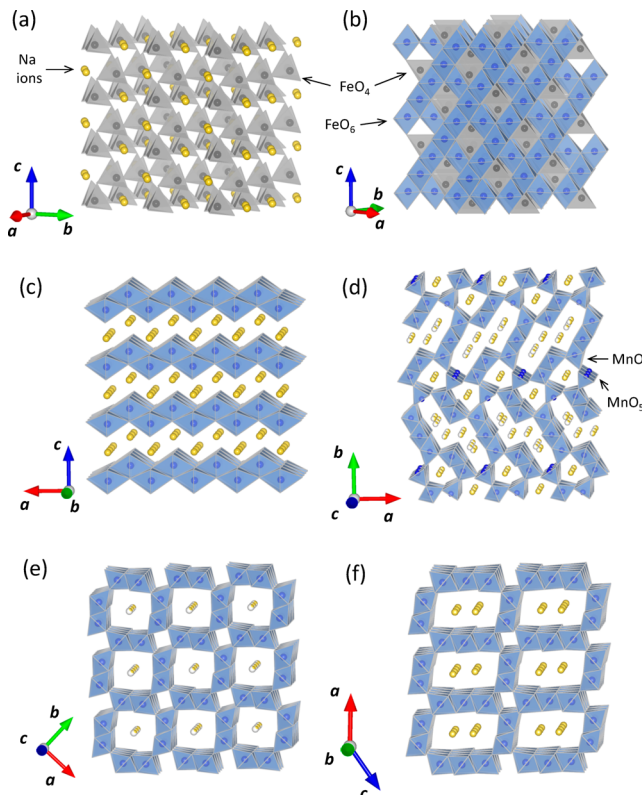


**Figure 14.** Comparison of crystal structures for miscellaneous iron/manganese-based oxides: (a)  $\beta$ - $\text{NaFeO}_2$ , (b)  $\text{Fe}_3\text{O}_4/\gamma$ - $\text{Fe}_2\text{O}_3$ , (c)  $\beta$ - $\text{NaMnO}_2$ , (d)  $\text{Na}_{0.44}\text{MnO}_2$ , (e)  $\alpha$ - $\text{MnO}_2$ , and (f)  $\text{Na}_{0.4}\text{MnO}_2$ .

whereas the rechargeable capacity reaches 190 mAh g<sup>-1</sup>, which corresponds to the 1.6 mol of Li in  $\text{Fe}_3\text{O}_4$ , for the nanosized  $\text{Fe}_3\text{O}_4$  particles prepared by a precipitation method.<sup>141,142</sup> Similar to the Li system, the nanocrystalline  $\text{Fe}_3\text{O}_4$  powder is electrochemically active in the  $\text{NaClO}_4$  electrolyte.<sup>141,142</sup> The 400 nm  $\text{Fe}_3\text{O}_4$  sample is electrochemically inactive in the Na system, similar to the Li system. For the nanocrystalline  $\text{Fe}_3\text{O}_4$  powder, the reversible capacity increases to 170 mAh g<sup>-1</sup>. Although the reversible capacity of 10 nm sample is slightly smaller compared to the  $\text{LiClO}_4$  electrolyte, acceptable capacity retention for the 30 cycle test was observed in the  $\text{NaClO}_4$  electrolyte. The electrochemical reactivity of the  $\text{Fe}_3\text{O}_4$  powder is activated by controlling the size of particles for both Li and Na systems. Recently, it has been demonstrated that a binder-free nanocomposite with carbon nanotube and nano iron oxides shows excellent electrode performance as an electrode material in Na cells.<sup>143</sup> Further reduction to 0 V vs Na metal results in the partial conversion reaction: reversible formation of nanosized  $\text{Na}_2\text{O}$  and Fe metal.<sup>144,145</sup>

**3.2.2. Manganese-Based Oxides.** Early studies on Na–Mn–O ternary compounds as a sodium insertion host are found in the literature published in the 1980s.<sup>39</sup> The structural chemistry of Na–Mn–O ternary compounds is complicated, and many different phases, including polymorphs, are obtained as the atomic ratio of Na to Mn changes.<sup>146</sup> Two different Na–Mn layered phases, O'3-type  $\text{NaMnO}_2$  and P2-type  $\text{Na}_x\text{MnO}_2$  ( $x = \text{ca. } 0.7$ ), have been described in the former section. Two polymorphs are known for  $\text{NaMnO}_2$ : one is  $\alpha$ -type (O'3-type)  $\text{NaMnO}_2$  as the low-temperature phase and another is  $\beta$ -type  $\text{NaMnO}_2$  as the high-temperature phase.<sup>146</sup>  $\beta$ - $\text{NaMnO}_2$  is prepared at >900 °C, and the crystal structure is different from

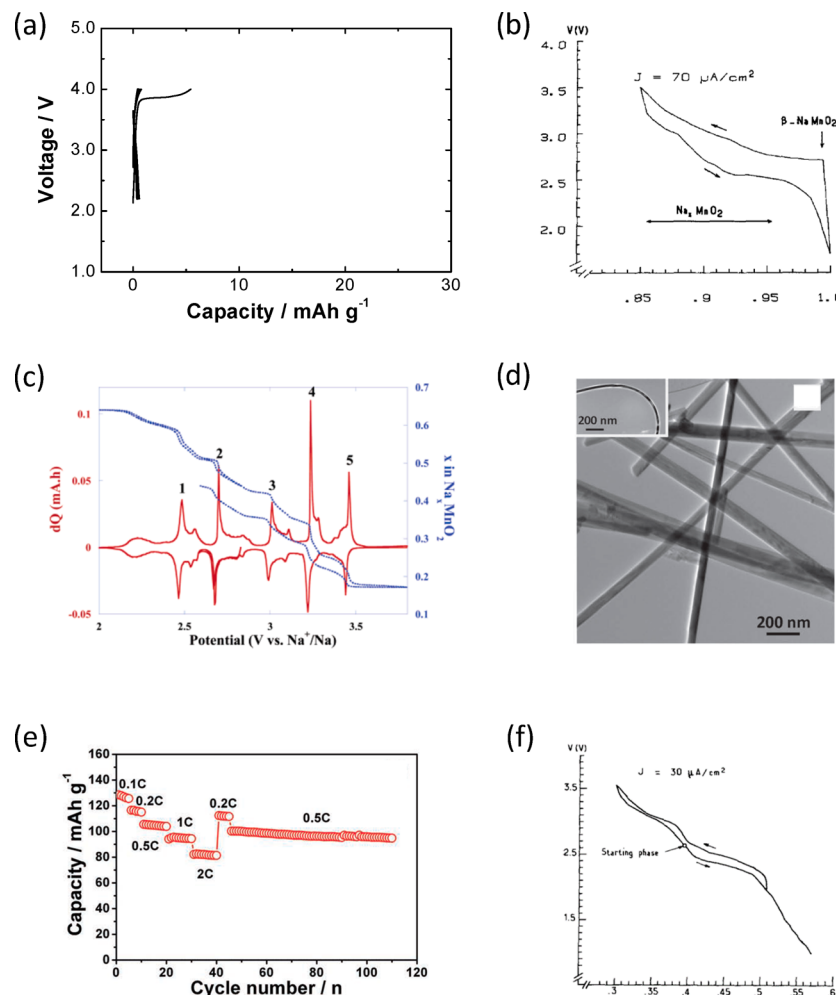


**Figure 15.** Electrode performance of miscellaneous iron/manganese-based oxides: (a)  $\beta$ -NaFeO<sub>2</sub>, (b)  $\beta$ -NaMnO<sub>2</sub>, and (c) Na<sub>0.44</sub>MnO<sub>2</sub>. (d, e) Nanowire of Na<sub>0.44</sub>MnO<sub>2</sub> is highly active as electrode material in the Na cell. (f) Charge/discharge curves of Na<sub>0.44</sub>MnO<sub>2</sub> in the Na cell. (a) Reprinted with permission from ref 62. Copyright 2014 IOP Publishing, National Institute for Materials Science (NIMS). CC BY-NC-SA. (b, f) Reprinted with permission from ref 39. Copyright 1983 Elsevier. (c) Reprinted with permission from ref 149. Copyright 2007 American Chemical Society. (d, e) Reprinted with permission from ref 151. Copyright 2011 WILEY-VCH Verlag GmbH&Co. KGaA, Weinheim.

$\beta$ -NaFeO<sub>2</sub> with the wurtzite-related structure. Packing of oxide ions for  $\beta$ -NaMnO<sub>2</sub> is the same as that of  $\alpha$ -NaFeO<sub>2</sub> with the CCP lattice, and the distribution of Na and Fe at octahedral sites in the CCP lattice is different. The crystal structure of  $\beta$ -NaMnO<sub>2</sub> is the same with orthorhombic LiMnO<sub>2</sub>, a so-called zigzag-type layered phase (Figure 14c). The electrode performance of  $\beta$ -NaMnO<sub>2</sub> in a Na cell was also reported.<sup>39</sup> The potential difference between charge/discharge processes in the Na cell seems to be relatively small, similar to  $\alpha$ -NaMnO<sub>2</sub> (Figure 15b).

When the fraction of sodium to manganese ions is reduced, two different phases, Na<sub>0.44</sub>MnO<sub>2</sub> and Na<sub>0.4</sub>MnO<sub>2</sub>, are obtained. Na insertion properties of Na<sub>0.44</sub>MnO<sub>2</sub> (Na<sub>4</sub>Mn<sub>9</sub>O<sub>18</sub>) were first examined in 1990s at 85 °C with solid-state polymer electrolyte<sup>147,148</sup> and revisited in 2007 to be examined at room temperature with aprotic solvent.<sup>149</sup> A crystal structure of Na<sub>0.44</sub>MnO<sub>2</sub> is also shown in Figure 14d. The framework structure of Na<sub>0.44</sub>MnO<sub>2</sub> (space group Pbam) consists of four MnO<sub>6</sub> octahedral sites and one MnO<sub>5</sub> square-pyramidal site. Trivalent manganese ions are energetically stabilized at the square-pyramidal sites. These octahedral and square-pyramidal sites are connected to each other by either edge or corner share (vertex share), forming the complicated framework structure

with two different tunnels along the *c*-axis direction. Sodium ions are accommodated at three different sites in the framework structure, and sodium ions in both large and small tunnels are highly mobile.<sup>150</sup> However, trivalent manganese ions at the square-pyramidal sites cannot be oxidized to the tetravalent state,<sup>150</sup> and thus, 20% sodium ions cannot be extracted from the framework structure. During the discharge (reduction) process, Na<sub>x</sub>MnO<sub>2</sub> is reversibly uptaking sodium ions to form Na<sub>0.67</sub>MnO<sub>2</sub>, and approximately 120 mAh g<sup>-1</sup> of reversible capacity is obtained as electrode materials. Complicated phase transitions occur in the insertion/extraction processes of sodium ions as expected from the galvanostatic charge/discharge curves in Figure 15c.<sup>149</sup> Detailed configurations of sodium-ion ordering in Na<sub>x</sub>MnO<sub>2</sub> upon electrochemical cycles have been studied by first-principles calculations.<sup>150</sup> Recently, a well-crystallized and uniform nanowire (diameter ≈ 50 nm and the growth orientation along [001]) of Na<sub>0.44</sub>MnO<sub>2</sub> was prepared (Figure 15d) by a polymer-pyrolysis method.<sup>151</sup> The Na<sub>0.44</sub>MnO<sub>2</sub> nanowire shows relatively good rate capability and excellent capacity retention as shown in Figure 15e. Approximately 100 mAh g<sup>-1</sup> of reversible capacity is obtained even after 100 cycles in Na cells.

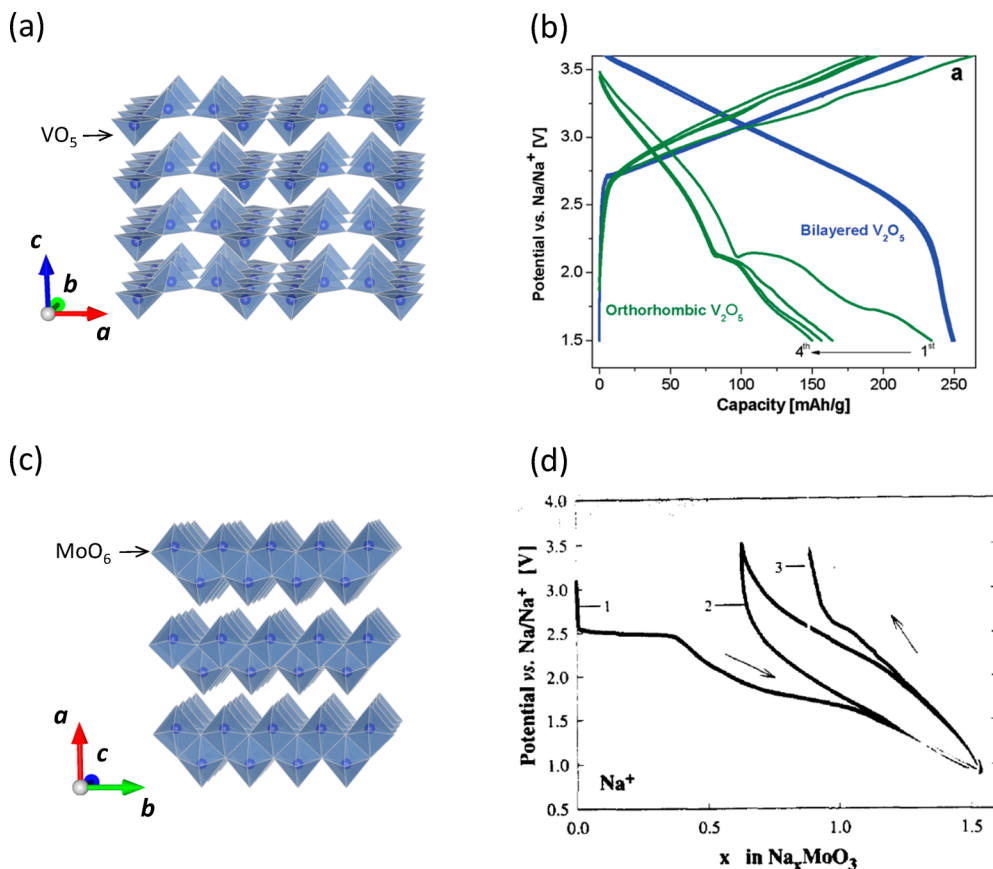


**Figure 16.** Crystal structures and electrode performance of  $\text{V}_2\text{O}_5$  (a, b) and  $\text{MoO}_3$  (c, d). (a, b) Reprinted with permission from ref 159. Copyright 2011 American Chemical Society. (c, d) Reprinted with permission from ref 164. Copyright 1995 Elsevier.

Other manganese (di)oxides studied for lithium insertion materials, such as  $\alpha\text{-MnO}_2$  and  $\beta\text{-MnO}_2$ , were also tested as sodium insertion host materials.<sup>152</sup> The framework structure of both  $\alpha\text{-MnO}_2$  and  $\beta\text{-MnO}_2$  consists of  $\text{MnO}_6$  octahedra that are connected by both edge and corner sharing. The structure of  $\beta\text{-MnO}_2$  is classified as rutile type with relatively small  $1 \times 1$  tunnels along the  $c$ -axis direction, which is built up with chains of edge-shared  $\text{MnO}_6$  octahedra. Alkali ions, even small lithium ions, cannot be inserted into the small tunnels of bulk  $\beta\text{-MnO}_2$ .<sup>153</sup> However, nanosized  $\beta\text{-MnO}_2$  with ordered mesopores is electrochemically active in Li cells.<sup>153</sup> A large reversible capacity of  $>250 \text{ mAh g}^{-1}$  is obtained using nanosized  $\beta\text{-MnO}_2$ . Although the crystalline phase is lost (changes into an amorphous phase) after electrochemical cycles, the electrode performance of  $\beta\text{-MnO}_2$  is effectively activated using such nanoengineered samples. Therefore, it is also expected that this methodology could be used for Na insertion materials, similar to iron oxides as described in the former section. Indeed, recently it has been reported that  $\beta\text{-MnO}_2$  nanorods with a diameter of 100 nm, which preferably grows along [001], deliver large reversible capacity ( $>200 \text{ mAh g}^{-1}$ ) in a Na cell.<sup>152</sup> Since the size of sodium ions is much larger than that of lithium ions, phase transitions from the rutile structure are expected to take place in Na cells. Although a large reversible capacity is obtained with the  $\beta\text{-MnO}_2$  nanorod, note that the difference in voltage between the charge/discharge in Na cells is much larger compared with Na insertion reactions in highly crystallized particles based on the topotactic reaction.

$\alpha\text{-Type MnO}_2$ , which is called hollandite as a group of minerals, has been also studied in a Na cell. The structure of  $\alpha\text{-}$

$\text{MnO}_2$  shown in Figure 14e is built up with edge- and corner-shared  $\text{MnO}_6$  octahedra, similar to  $\beta\text{-MnO}_2$ . Large  $2 \times 2$  tunnels are formed with double chains of edge-shared  $\text{MnO}_6$  octahedra. The open tunnels in  $\alpha\text{-MnO}_2$  are generally stabilized by incorporation of large cations, such as  $\text{K}^+$ , and sodium migration in the open diffusion path is expected to be efficient. Although  $\alpha\text{-MnO}_2$  nanorods show a large reversible capacity of  $>200 \text{ mAh g}^{-1}$  in a Na cell, polarization between charge/discharge curves seem to be large similar to  $\beta\text{-MnO}_2$  nanorods.<sup>152</sup> Results of the DFT calculation suggest that migration barrier of Na ions in  $\alpha\text{-MnO}_2$  is comparable to or slightly smaller than that of Li ions.<sup>154</sup>  $\lambda\text{-Type MnO}_2$ , prepared from spinel-type  $\text{LiMn}_2\text{O}_4$ , is also used as an electrode material for Na cells.<sup>155,156</sup> The phase transition behavior is unique in Na cells;  $\lambda\text{-type MnO}_2$  partly translates into the O'3-type layered phase on electrochemical cycles.

Manganese oxides with an even more open path for Na migration,  $2 \times 3$  tunnels consisting of double and triple  $\text{MnO}_6$  chains, are also found in a mineral called romanechite as shown in Figure 14f.<sup>157</sup> Large  $\text{Ba}^{2+}$  ions and water molecules are incorporated as a template to stabilize such large tunnels in romanechite. A  $\text{Na}^+$ -substituted sample for  $\text{Ba}^{2+}$  and  $\text{H}_2\text{O}$  in romanechite,  $\text{Na}_{0.4}\text{MnO}_2$ , is also prepared by a simple solid-state method.<sup>39,146</sup> The sample shows quite small polarization in a Na cell even though the sodium insertion mechanism into  $\text{Na}_{0.4}\text{MnO}_2$  with  $2 \times 3$  tunnels is not fully understood. At least 0.3 mol of sodium ions are reversibly inserted/extracted into/from the framework structure of romanechite with the large tunnels.<sup>39</sup>

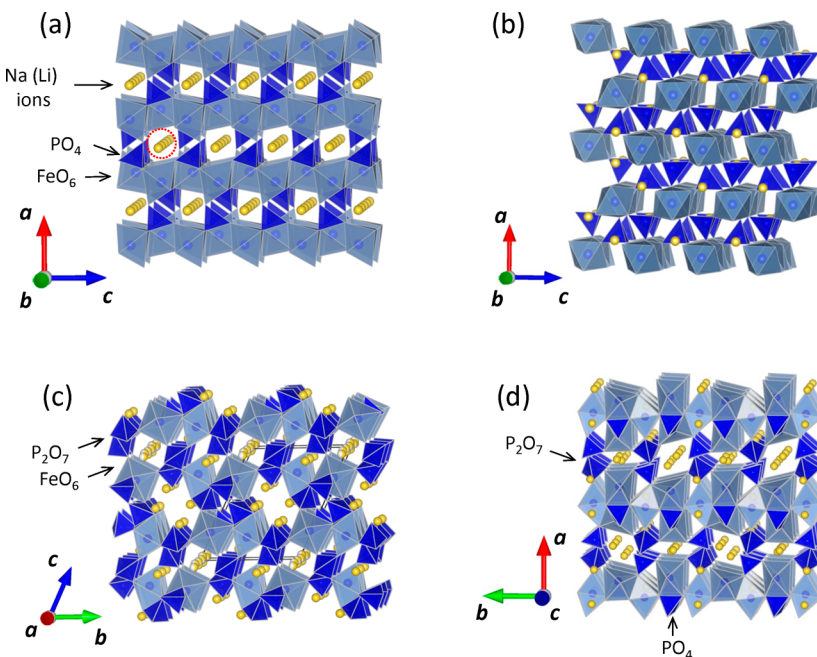


**Figure 17.** Crystal structure of phosphate-based compounds with Fe(II): (a) Na(Li)FePO<sub>4</sub> (triphylite-type), (b) NaFePO<sub>4</sub> (maricite-type), (c) Na<sub>2</sub>Fe(P<sub>2</sub>O<sub>7</sub>), and (d) Na<sub>4</sub>Fe<sub>3</sub>(PO<sub>4</sub>)<sub>2</sub>(P<sub>2</sub>O<sub>7</sub>).

**3.2.3. Vanadium-Based Oxides.** Vanadium pentoxide was studied as a sodium insertion host in 1980s,<sup>158</sup> similar to the Li system. The layered structure of  $\alpha$ -V<sub>2</sub>O<sub>5</sub> is built up with edge- and corner-shared VO<sub>5</sub> square pyramids as shown in Figure 16a. Both Li<sup>+</sup> and Na<sup>+</sup> are inserted into  $\alpha$ -V<sub>2</sub>O<sub>5</sub> with the layered structure, and a large discharge capacity is obtained regardless of the difference in the size of alkali ions. Na<sub>x</sub>V<sub>2</sub>O<sub>5</sub> bronzes are also electrochemically active in Na cells.<sup>158</sup> Recently,  $\alpha$ -V<sub>2</sub>O<sub>5</sub> has been revisited as a positive electrode material.<sup>159</sup> The electrode performance of  $\alpha$ -V<sub>2</sub>O<sub>5</sub> is exhibited in Figure 16b. A large initial reversible capacity of over 200 mAh g<sup>-1</sup> is obtained with well-crystallized  $\alpha$ -V<sub>2</sub>O<sub>5</sub> particles. The electrode performance of V<sub>2</sub>O<sub>5</sub> is significantly increased using nanostructured V<sub>2</sub>O<sub>5</sub>, which was synthesized by electrochemical deposition. Thus, prepared V<sub>2</sub>O<sub>5</sub> has a wide interlayer distance of approximately 13.5 Å and a morphology of nanoribbons with highly porous structure. Nanostructured V<sub>2</sub>O<sub>5</sub> electrodes deliver theoretical reversible capacity based on formation of Na<sub>2</sub>V<sub>2</sub>O<sub>5</sub> (approximately 250 mAh g<sup>-1</sup>) with good cyclability. Energy and power density reaches over 700 Wh kg<sup>-1</sup> and 1200 W kg<sup>-1</sup>, respectively, with metallic sodium as the negative electrode.<sup>159</sup> Vanadium phosphates and fluorophosphates are further reviewed in a later section.

**3.2.4. Oxides of 4d Transition Metals.** Compared with 3d transition-metal oxides, limited research has been conducted for 4d transition-metal oxides so far. Some early studies on molybdenum-based materials, mainly for sulfides, as the sodium insertion host were published before 1990.<sup>160–162</sup> Molybdenum sulfides MoS<sub>3</sub><sup>160</sup> and Chevrel phases Mo<sub>6</sub>S<sub>8-x</sub>I<sub>x</sub><sup>162</sup> were reported to be electrochemically active as the sodium insertion host. Recently, layered MoS<sub>2</sub>, in which Mo is located at prismatic sites formed by sulfide ions, has been also studied as a Na insertion host.<sup>163</sup> MoS<sub>2</sub> shows a low operating voltage (approximately 1.0 V) in Na cells and can be classified as negative electrode materials. In addition to sulfides, molybdenum trioxide<sup>164</sup> and sodium-containing layered molybdenum oxide<sup>161</sup> are also electrochemically active. The crystal structure

of  $\alpha$ -MoO<sub>3</sub> with hexavalent molybdenum ions is shown in Figure 16c. The framework structure of  $\alpha$ -MoO<sub>3</sub> is built up with 1D zigzag chains formed by edge-shared MoO<sub>6</sub> octahedra. The 1D zigzag chains share each corner, forming the 2D MoO<sub>3</sub> layers. Relatively large sodium ions can be electrochemically inserted between MoO<sub>3</sub> layers bridged by van der Waals forces. The voltage profile changes almost linearly from 3.0 to 1.0 V vs Na metal (Figure 16d). Approximately 1 mol of Na<sup>+</sup> is reversibly inserted/extracted into/from MoO<sub>3</sub> even though the cyclability was reported to be inferior to the lithium system in the original publication in 1995.<sup>164</sup> A clearly different behavior has been reported in layered Na<sub>x</sub>Mo<sub>2</sub>O<sub>4</sub> ( $x \approx 1.0$  for the as-prepared sample).<sup>161</sup> Several sets of voltage plateaus, presumably associated with sodium ordering and biphasic behavior, were found in Na<sub>x</sub>Mo<sub>2</sub>O<sub>4</sub> ( $0.55 < x < 1.9$ ) as electrode materials.

The electrode performance of Na<sub>2</sub>RuO<sub>3</sub> with the O<sub>3</sub>-type layered structure has been recently reported.<sup>165</sup> Na<sub>2</sub>RuO<sub>3</sub> delivers approximately 150 mAh g<sup>-1</sup> of reversible capacity with good capacity retention based on the redox reaction of ruthenium ions. The average operating voltage is slightly lower than 3 V with the slope profile. Two-phase coexistence has been found only in the narrow range ( $0.5 < x < 0.6$  in Na<sub>2-x</sub>RuO<sub>3</sub>).<sup>165</sup>

### 3.3. Polyanionic Compounds

**3.3.1. Phosphates with Fe(II) and Mn(II).** Since the layered lithium iron(III) oxide, LiFeO<sub>2</sub>, shows unimpressive battery performance based on the Fe<sup>2+</sup>/Fe<sup>3+</sup> redox couple after oxygen loss in the Li cells as discussed above, polyanionic compounds of iron were extensively studied based on the use of the Fe<sup>2+</sup>/Fe<sup>3+</sup> redox couple.<sup>29</sup> Lithium iron(II) phosphate, LiFePO<sub>4</sub>, is the most widely studied polyanionic compound as a positive electrode material for LIBs because of the interest for practical applications.<sup>166</sup> A crystal structure of LiFePO<sub>4</sub> is classified as the triphylite-type structure (space group *Pnma*) with a distorted hcp oxygen lattice. The structure is closely related to the olivine-type structure, and two cations (lithium

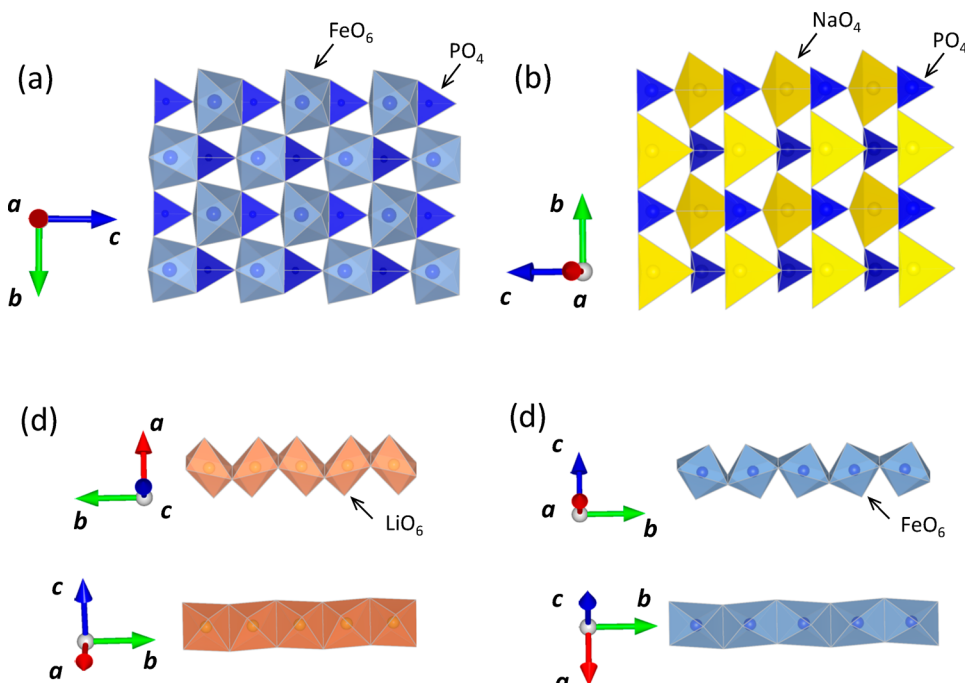


**Figure 18.** Similarity and difference of crystal structures of  $\text{Na}(\text{Li})\text{FePO}_4$  (triphylite-type) and  $\text{NaFePO}_4$  (maricite-type); arrangement of (a)  $\text{FeO}_6$ - $\text{PO}_4$  in triphylite and (b)  $\text{NaO}_4$ - $\text{PO}_4$  in maricite and 1D chains of (c)  $\text{LiO}_6$  octahedra in triphylite and (d)  $\text{FeO}_6$  octahedra in maricite.

and iron ions in the case of  $\text{LiFePO}_4$ ) are located in two distinct octahedral sites in the common framework structure composed of  $\text{XO}_4$  ( $\text{X} = \text{Si, P, Mo etc.}$ ) tetrahedra. Phosphate ions,  $(\text{PO}_4)^{3-}$  tetrahedra, share one edge and four corners with  $\text{FeO}_6$  octahedra, forming the framework structure of triphylite-type  $\text{FePO}_4$  as shown in Figure 17a. Formation of edge-shared sites between  $\text{FeO}_6$  octahedral and  $\text{PO}_4$  tetrahedral units relatively stabilizes the energy of the  $\text{Fe}^{2+}/\text{Fe}^{3+}$  redox couple through the inductive effect, resulting in the high-voltage (3.45 V vs Li metal) positive electrode materials as iron-based compounds based on the  $\text{Fe}^{2+}/\text{Fe}^{3+}$  redox.<sup>58,166</sup> Although the  $\text{FeO}_6$  octahedra share corners in the triphylite-type structure (Figure 18a), electrical conductivity is still too low to use it as an electrode material. The electrode performance of  $\text{LiFePO}_4$  is significantly improved by carbon coating<sup>167</sup> and shortening of a Li diffusion path with nanosized particles. Such engineered nanosized particles deliver large reversible capacity in Li cells, which now almost reaches its theoretical limit (170 mAh g<sup>-1</sup>). Conduction mechanisms of Li ions in triphylite-type  $\text{LiFePO}_4$  have been extensively studied.<sup>168,169</sup>  $\text{LiO}_6$  octahedra are connected to each other by edge-sharing along  $[010]$ , forming 1D chains as shown in Figure 18c. Li ions can migrate with a low diffusion barrier (~150 meV<sup>33</sup>) along the 1D chains throughout particles if formation of antisite defects between Li and Fe sites is negligible.<sup>169</sup>

A sodium counterpart,  $\text{NaFePO}_4$ , is also studied as an electrode material for NIBs.<sup>170</sup>  $\text{NaFePO}_4$  crystallizes into maricite-type structure as the thermodynamically stable phase. Its crystal structure is also closely related to the olivine-type structure with a distorted hcp oxygen lattice. A large gap in the size of ionic radii between Na and Fe results in significant distortion in the hcp oxygen lattice (Figure 18b) in comparison to triphylite-type  $\text{LiFePO}_4$ . Iron ions are located at octahedral sites, and  $\text{FeO}_6$  octahedra share edges, forming 1D chains as shown in Figure 18d. The structure of 1D chains of  $\text{FeO}_6$  in the maricite phase is essentially the same with the 1D  $\text{LiO}_6$  chains

in the triphylite phase. Sodium ions are located at large tetrahedral sites (note that this site is also regarded as an irregular site coordinated by 10 oxygen within 3 Å<sup>171</sup>), which share corners with  $\text{PO}_4$  tetrahedra (Figure 18b). Since sodium sites are isolated in the structure as shown in Figure 18b, a large barrier for sodium migration is expected in the maricite-type  $\text{NaFePO}_4$ . Indeed, the reversibility of Na extraction/insertion for maricite-type  $\text{NaFePO}_4$  seems to be unacceptable as an electrode material.<sup>170,172</sup>

In contrast, triphylite-type  $\text{NaFePO}_4$ , which is a metastable polymorph of  $\text{NaFePO}_4$ , is electrochemically active.<sup>170,173</sup> Triphylite-type  $\text{NaFePO}_4$  can be prepared by an ion-exchange method from  $\text{LiFePO}_4$ . Li ions are chemically (and electrochemically) extracted from triphylite- $\text{LiFePO}_4$  without destruction of its core structure, forming heterosite-type  $\text{FePO}_4$ . Chemical (and electrochemical) Na insertion into heterosite-type  $\text{FePO}_4$ , which possesses the same framework structure with triphylite- $\text{LiFePO}_4$ , results in formation of triphylite-type  $\text{NaFePO}_4$ . Triphylite-type  $\text{NaFePO}_4$  is stable below 480 °C under steady nitrogen flow and transforms into maricite- $\text{NaFePO}_4$  by further heating above 480 °C.<sup>173,174</sup> Charge/discharge (oxidation/reduction) curves of triphylite- $\text{NaFePO}_4$  in a Na cell<sup>173</sup> are shown in Figure 19a. Nearly 1 mol of Na ions is reversibly inserted/extracted into/from triphylite- $\text{NaFePO}_4$ . Since the ionic radius of the sodium ion is much larger than that of the lithium ion, the unit cell volume of triphylite- $\text{NaFePO}_4$  is approximately 10% larger than that of triphylite- $\text{LiFePO}_4$ . Two voltage plateaus are observed on discharge (Figure 19a). The open-circuit voltage on the plateaus is observed to be between 2.87 and 2.97 V,<sup>173</sup> which is slightly lower than that of ~3.1 V vs Na expected from  $\text{LiFePO}_4$  (3.45 V vs Li). The voltage difference between Li and Na cells is, however, less significant than those typically observed for the layered oxides (Figure 3). The appearance of two voltage plateaus originates from formation of an intermediate phase (a sodium-ion ordered phase) as

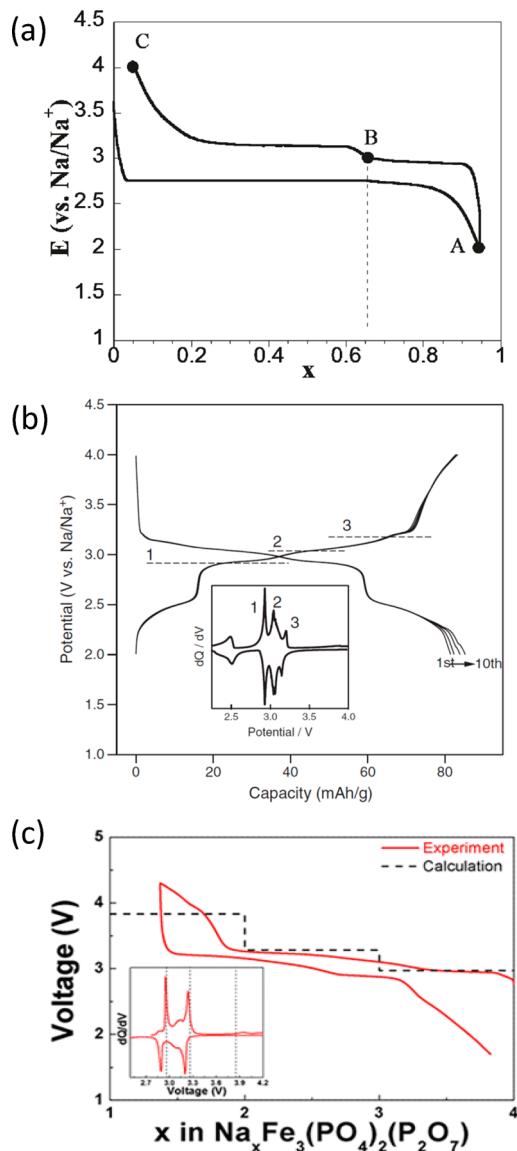


**Figure 19.** Electrode performance of phosphate-based compounds with Fe(II) in Na cells: (a)  $\text{NaFePO}_4$  (triphylite-type), (b)  $\text{Na}_2\text{Fe}(\text{P}_2\text{O}_7)$ , and (c)  $\text{Na}_4\text{Fe}_3(\text{PO}_4)_2(\text{P}_2\text{O}_7)$ . (a) Reprinted with permission from ref 173. Copyright 2010 American Chemical Society. (b) Reprinted with permission from ref 184. Copyright 2012 Elsevier. (c) Reprinted with permission from ref 190. Copyright 2012 American Chemical Society.

$\text{Na}_{0.4}\text{FePO}_4$  (point B in Figure 19a). Such an intermediate phase is not generally found for  $\text{Li}_x\text{FePO}_4$  under equilibrium conditions. The larger interaction of Na ions, in comparison to Li ions, could result in the occurrence of an intermediate phase,<sup>173,175</sup> similar to layered oxides. According to the DFT calculation, a barrier of sodium migration in narrow 1D chains is much larger (270 meV) compared with Li ions (150 meV).<sup>33</sup> Diffusion barriers highly correlate with diffusion paths in the host structures. Indeed, the experimentally measured sodium insertion kinetics in triphylite- $\text{Na}_x\text{FePO}_4$  seems to be much slower compared with Li ions.<sup>176</sup>

A thermodynamically stable phase of  $\text{NaMnPO}_4$  is also maricite type.<sup>177</sup> Similar to triphylite- $\text{NaFePO}_4$ , it is also expected that lithiophilite-type  $\text{NaMnPO}_4$ , which is isostructural with triphylite-type  $\text{Li}(\text{Na})\text{FePO}_4$ , could be obtained by ion-exchange reaction and/or related soft chemical methods. It

has been demonstrated that lithiophilite-type  $\text{NaMnPO}_4$  is prepared by topochemical reaction below 100 °C from  $\text{NH}_4\text{MnPO}_4 \cdot \text{H}_2\text{O}$  as the precursor.<sup>177</sup> The electrode performance of triphylite- $\text{NaMn}_{1/2}\text{Fe}_{1/2}\text{PO}_4$  prepared by the topochemical reaction was also reported.<sup>177</sup> Electrode reversibility of lithiophilite- $\text{NaMnPO}_4$  could be limited without preparation of nanoengineered particles, similar to  $\text{LiMnPO}_4$  because of formation of antisite defects<sup>178,179</sup> and/or the slow nucleation rate for the delithiated (desodiated) phase.<sup>180</sup>

**3.3.2. Pyrophosphates with Fe(II) and Mn(II).** After the reports on lithium iron(II) pyrophosphate,  $\text{Li}_2\text{FeP}_2\text{O}_7$ , as a positive electrode material for LIBs,<sup>181,182</sup> many studies have been published in relation to the pyrophosphate system. Use of pyrophosphate, instead of phosphate, as the framework structure has been further extended to the Na system, i.e.,  $\text{Na}_2\text{FeP}_2\text{O}_7$ .<sup>183–185</sup>  $\text{Na}_2\text{FeP}_2\text{O}_7$  is isostructural with one of the polymorphs of  $\text{Na}_2\text{CoP}_2\text{O}_7$  with space group P1.<sup>186</sup> The crystal structure of  $\text{Na}_2\text{FeP}_2\text{O}_7$  contains corner-shared  $\text{FeO}_6$  octahedra ( $\text{Fe}_2\text{O}_{11}$  units), which are connected by  $\text{P}_2\text{O}_7$  units, forming the 3D framework structure with an open sodium diffusion path (Figure 17c). Na ions are located at large distorted square-pyramidal sites. One Na ion is reversibly extracted from  $\text{Na}_2\text{FeP}_2\text{O}_7$  based on the  $\text{Fe}^{2+}/\text{Fe}^{3+}$  redox couple, and reversible capacity reaches 90 mAh g<sup>-1</sup> (theoretical capacity 97 mAh g<sup>-1</sup>) as shown in Figure 19b. Although the available energy density is lower than that of triphylite- $\text{NaFePO}_4$ , direct synthesis of  $\text{Na}_2\text{FeP}_2\text{O}_7$  is possible by conventional solid-state methods. Additionally, the rate capability seems to be much better for  $\text{Na}_2\text{FeP}_2\text{O}_7$  even though  $\text{FeO}_6$  octahedra and  $\text{FeO}_5$  square pyramids are completely isolated by the pyrophosphate ions in the framework structure. This result is probably because of the presence of an open diffusion path formed by pyrophosphate ions. Na diffusion barriers in  $\text{Na}_x\text{FeP}_2\text{O}_7$  have been also calculated by the first-principles calculation.<sup>185</sup> Sodium ions can diffuse through 1D paths along [011] with a relatively low migration barrier (~480 meV), and all Na sites are interconnected by 1D/2D paths with a diffusion barrier below 540 meV.

Recently, it has been reported that one of the  $\text{Na}_2\text{MnP}_2\text{O}_7$  polymorphs,  $\beta\text{-Na}_2\text{MnP}_2\text{O}_7$ , which is isostructural to  $\text{Na}_2\text{FeP}_2\text{O}_7$ , also shows good electrode performance in Na cells.<sup>187</sup> Although polarization seems to be large,  $\text{Na}_2\text{MnP}_2\text{O}_7$  is potentially used as a 3.6 V-class electrode material. Off-stoichiometric synthesis for sodium metal pyrophosphates induces formation of Na-rich phases.<sup>188</sup> Thus, the prepared sample shows better electrode performance compared with the stoichiometric samples without nanosizing and carbon coating. Pyrophosphate-based electrode materials containing other transition-metal elements have been reviewed in the literature.<sup>189</sup>

An interesting character to design the electrode materials for NIBs is the high structural complexity of sodium-based compounds, e.g., the P2-type layered structure as mentioned in the former section. It is impossible to prepare the P2-type layered structure for the Li system (O2/T2-type structures related to the P2-type structure are prepared by the soft-chemistry technique<sup>41,44,45,50</sup>). Similarly, a unique framework structure, with mixed polyanion groups of phosphate ( $\text{PO}_4$ )<sup>3-</sup> and pyrophosphate ( $\text{P}_2\text{O}_7$ )<sup>4-</sup> ions, is also stabilized in the Na system (and it is not known in the Li system). Recently,  $\text{Na}_4\text{Fe}_3(\text{PO}_4)_2(\text{P}_2\text{O}_7)$  was synthesized as the first mixed polyanion compound with Fe(II).<sup>190</sup> The structure is isostructural to  $\text{Na}_4\text{Me}_3(\text{PO}_4)_2(\text{P}_2\text{O}_7)$  (Me = Co, Mn, and

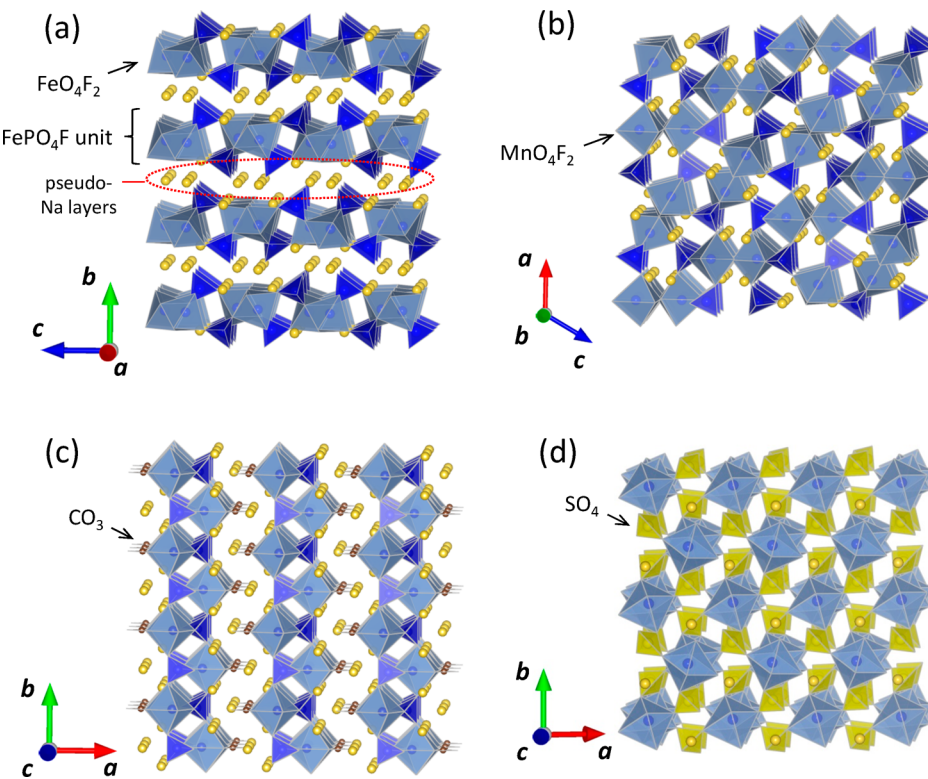


**Figure 20.** Schematic illustrations of the crystal structures of (a)  $\text{Na}_2\text{FePO}_4\text{F}$ , (b)  $\text{Na}_2[\text{Fe}_{1/2}\text{Mn}_{1/2}]\text{PO}_4\text{F}$ , (c)  $\text{Na}_3\text{MnPO}_4\text{CO}_3$ , and (d)  $\text{NaFeSO}_4\text{F}$ .

Ni) with space group  $Pn2_1a$ .<sup>191</sup>  $\text{FeO}_6$  octahedra are connected to each other by edge and corner shares, and  $\text{PO}_4$  tetrahedra also share one edge and two corners with the  $\text{FeO}_6$  octahedra, forming a layer-like unit along the  $b-c$  direction. These layer units consisting of  $\text{FeO}_6$  and  $\text{PO}_4$  are further connected by  $\text{P}_2\text{O}_7$  pyrophosphate ions, forming the crystal structure of  $\text{Na}_4\text{Fe}_3(\text{PO}_4)_2(\text{P}_2\text{O}_7)$  as shown in Figure 17d.  $\text{Na}_4\text{Fe}_3(\text{PO}_4)_2(\text{P}_2\text{O}_7)$  delivers approximately 100  $\text{mAh g}^{-1}$  of reversible capacity, which is higher than that of  $\text{Na}_2\text{FeP}_2\text{O}_7$  (Figure 19c). Three Na ions are reversibly extracted from  $\text{Na}_4\text{Fe}_3(\text{PO}_4)_2(\text{P}_2\text{O}_7)$  based on the  $\text{Fe}^{2+}/\text{Fe}^{3+}$  redox. The sample shows good capacity retention as an electrode material in the Na cell.<sup>190</sup>

**3.3.3. Fluorophosphates, Carbophosphates, and Fluorosulfates with Fe(II) and Mn (II).** A mixed anion system containing fluoride and phosphate ions is also utilized as an electrode material for NIBs. The layered fluorinated iron phosphate,  $\text{Na}_2\text{FePO}_4\text{F}$ , was widely examined as a positive electrode material for rechargeable batteries.<sup>192,193</sup> The crystal structure of  $\text{Na}_2\text{FePO}_4\text{F}$  is isostructural to the  $\text{Na}_2\text{CoPO}_4\text{F}$ -type structure<sup>194</sup> (or  $\text{Na}_2\text{FePO}_4(\text{OH})$  type) as the two-dimensional layered fluorophosphates (Figure 20a). Na ions are accommodated between  $\text{FePO}_4\text{F}$  layers, in which  $\text{FeO}_4\text{F}_2$  octahedra share edge and corners. According to the results of first-principles calculation, sodium ions migrate between  $\text{FePO}_4\text{F}$  layers with two-dimensional paths.<sup>195</sup> The crystal structure of  $\text{Na}_2\text{MnPO}_4\text{F}$  is different from  $\text{Na}_2\text{FePO}_4\text{F}$ .<sup>196</sup> All  $\text{MnO}_4\text{F}_2$  octahedra share each corner and form 1D  $\text{Mn}_2\text{F}_2\text{O}_8$  chains. The chains are connected by  $\text{PO}_4$  tetrahedra with corner sharing, forming a less dense 3D framework structure (Figure 20b).  $\text{Na}_2[\text{Fe}_x\text{Mn}_{1-x}]\text{PO}_4\text{F}$  ( $0 < x < 1.0$ ) samples were also synthesized, and it was found that the  $\text{Na}_2\text{MnPO}_4\text{F}$ -type 3D structure is thermodynamically stable at  $x < 0.75$  in  $\text{Na}_2[\text{Fe}_x\text{Mn}_{1-x}]\text{PO}_4\text{F}$ .<sup>193</sup>

The electrochemical behavior of the carbon-coated  $\text{Na}_2\text{FePO}_4\text{F}$  and  $\text{Na}_2[\text{Fe}_{1/2}\text{Mn}_{1/2}]\text{PO}_4\text{F}$  in Na cells is compared in Figure 21.<sup>197,198</sup>  $\text{Na}_2\text{FePO}_4\text{F}$  shows a relatively high operating voltage (ca. 3.0 V vs Na) and fair reversibility. The carbon-coated  $\text{Na}_2\text{FePO}_4\text{F}$  sample can deliver approximately 110  $\text{mAh g}^{-1}$  of reversible capacity, which corresponds to approximately 90% of the theoretical capacity based on the one-electron redox of iron ( $\text{Fe}^{2+}/\text{Fe}^{3+}$ ). Two well-defined voltage plateaus, which are centered at 3.06 and 2.91 V with small polarization, are observed in Figure 21a. The Na/ $\text{Na}_2[\text{Fe}_{1/2}\text{Mn}_{1/2}]\text{PO}_4\text{F}$  cell also shows a high reversible capacity of 110  $\text{mAh g}^{-1}$  (Figure 21b). In addition, from the operating voltage, the reaction in the Na cell consists of three different regions. Differential capacity  $dQ/dV$  plots of both samples are also shown in Figure 21a and 21b (insets). On the discharge process for the Na/ $\text{Na}_2[\text{Fe}_{1/2}\text{Mn}_{1/2}]\text{PO}_4\text{F}$  cell, three peaks are clearly observed at 3.36, 3.04, and 2.86 V. A redox couple centered at 3.53 V is found in the  $dQ/dV$  plot of  $\text{Na}_2[\text{Fe}_{1/2}\text{Mn}_{1/2}]\text{PO}_4\text{F}$ , which could be assigned to the  $\text{Mn}^{2+}/\text{Mn}^{3+}$  redox reaction. The polarization of the Mn redox is clearly larger compared with that of  $\text{Fe}^{2+}/\text{Fe}^{3+}$ , similar to the iron/manganese phosphates. Although the layered framework structure seems to be preferable for the sodium migration process in the fluorophosphates system, carbon-coated and nanosized  $\text{Na}_2[\text{Fe}_{1/2}\text{Mn}_{1/2}]\text{PO}_4\text{F}$  samples show good reversibility as an electrode material in Na cells.<sup>198</sup>

Recently, the synthesis and electrode performance of sodium-based carbonophosphates,  $\text{Na}_3\text{MePO}_4\text{CO}_3$ , which are a new series of mixed anion compounds used as electrode materials similar to  $\text{Na}_4\text{Fe}_3(\text{PO}_4)_2(\text{P}_2\text{O}_7)$ , have been reported.<sup>199,200</sup>  $\text{Na}_3\text{MePO}_4\text{CO}_3$  contains two different anions of carbonate ( $\text{CO}_3$ )<sup>2-</sup> and phosphate ( $\text{PO}_4$ )<sup>3-</sup> ions, and its Mn compound,  $\text{Na}_3\text{MnPO}_4\text{CO}_3$ , is found in the natural mineral called sidorenkite.<sup>199</sup> The crystal structure of  $\text{Na}_3\text{MnPO}_4\text{CO}_3$  is

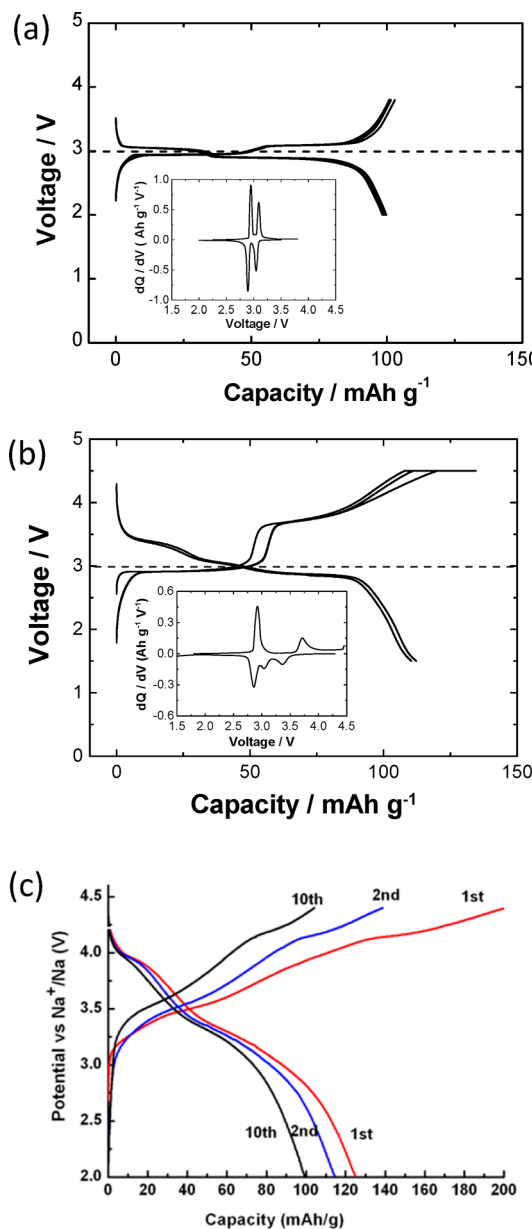


**Figure 21.** Charge/discharge curves of the (a)  $\text{Na}/\text{Na}_2\text{FePO}_4\text{F}$  cell, (b)  $\text{Na}/\text{Na}_2[\text{Fe}_{1/2}\text{Mn}_{1/2}]\text{PO}_4\text{F}$  cell, and (c)  $\text{Na}/\text{Na}_3\text{MnPO}_4\text{CO}_3$  cell. (a, b) Reprinted with permission from ref 198. Copyright 2012 The Electrochemical Society of Japan. (c) Reprinted with permission from ref 199 Copyright 2013 American Chemical Society.

shown in Figure 20c.  $\text{FeO}_6$  octahedra and  $\text{PO}_4$  tetrahedra share each corner, and  $\text{CO}_3$  triangles share one edge with  $\text{FeO}_6$  octahedra, resulting in the large distortion of  $\text{FeO}_6$  octahedra.  $\text{Na}_3\text{MnPO}_4\text{CO}_3$  can be prepared by hydrothermal reaction at 120 °C.<sup>189</sup> Two Na ions are extracted from  $\text{Na}_3\text{MnPO}_4\text{CO}_3$  based on the  $\text{Mn}^{2+}/\text{Mn}^{4+}$  two-electron redox reaction, resulting in a large initial charge capacity (Figure 21c). Although the initial charge capacity is large ( $\sim 200 \text{ mAh g}^{-1}$ ), it has been reported that the sample shows a relatively large irreversible capacity ( $\sim 75 \text{ mAh g}^{-1}$ ) at the initial cycle with acceptable capacity retention in following continuous cycles.<sup>199</sup>

Metal fluorosulfates are also a potential framework structure for the Na insertion host. Recently, sodium iron fluorosulfate,  $\text{NaFeSO}_4\text{F}$ , was successfully prepared, and its electrode performance was examined in Na cells. The crystal structure

of  $\text{NaFeSO}_4\text{F}$  is isostructural to the mineral called tavorite,  $\text{LiFe}(\text{PO}_4)\text{OH}$ .<sup>201</sup> Although the results of first-principles calculation suggest diffusion of sodium ions in the 1D path along [101],<sup>202</sup> the reversibility of  $\text{NaFeSO}_4\text{F}$  as an electrode material is limited to a narrow range.<sup>201</sup> Very recently, a new alluaudite-type Fe-based sulfate,  $\text{Na}_2\text{Fe}_2(\text{SO}_4)_3$ , was synthesized and exhibits ca. 100 mAh g⁻¹ of reversible capacity with the highest operating voltage of 3.8 V vs Na/Na<sup>+</sup> among all Fe-based insertion compounds.<sup>203</sup> They successfully increased the operating voltage by replacing phosphate  $\text{PO}_4^{4-}$  with sulfate  $\text{SO}_4^{2-}$  units having higher electronegativity and forming edge-sharing  $\text{FeO}_6$  octahedra.

Some other phosphates with Fe(III) and Mn (II), which are often found in natural minerals, were also reported as host materials for Na insertion. These materials have been further reviewed in the literature.<sup>62</sup>

**3.3.4. Polyanionic Compounds with Other Transition Metals.** **3.3.4.1. Vanadium System.** Sodium vanadium(III) phosphate,  $\text{Na}_3\text{V}_2(\text{PO}_4)_3$ , has the NASICON-type framework structure consisting of corner-shared  $\text{FeO}_6$  octahedra and  $\text{PO}_4$  tetrahedra with a 3D network (Figure 22a). The name of NASICON originates from  $\text{Na}_{1+x}\text{Zr}_2\text{P}_{3-x}\text{Si}_x\text{O}_{12}$ , which has superior sodium-ion conductivity<sup>204</sup> and is called “Na<sup>+</sup> super ionic conductor (NASICON)”. For  $\text{Na}_3\text{V}_2(\text{PO}_4)_3$ , ordering of Na ions is observed in the NASICON-type framework structure.<sup>205</sup> Full sodium-extracted phase,  $\text{V}_2(\text{PO}_4)_3$ , is obtained by chemical oxidation using  $\text{Cl}_2$  gas without destruction of the framework structure.<sup>206</sup> Additionally,  $\text{Li}_3\text{V}_2(\text{PO}_4)_3$  can be prepared by  $\text{Na}^+/\text{Li}^+$ -ion exchange from  $\text{Na}_3\text{V}_2(\text{PO}_4)_3$ , and its electrode performance in Li cells was reported.<sup>205</sup> The electrode performance of  $\text{Na}_3\text{V}_2(\text{PO}_4)_3$  was also found in the literature.<sup>207</sup> Approximately 2 mol of Na are extracted based on the  $\text{V}^{3+}/\text{V}^{4+}$  redox from  $\text{Na}_3\text{V}_2(\text{PO}_4)_3$  with 3.3 V of flat operating voltage. One mole of Na<sup>+</sup> is also inserted into  $\text{Na}_3\text{V}_2(\text{PO}_4)_3$  based on the  $\text{V}^{2+}/\text{V}^{3+}$  redox at around 1.5 V.<sup>207</sup> This reaction with relatively low potential is used as the negative electrode material, and  $\text{Na}_3\text{V}_2(\text{PO}_4)_3$  is, therefore, used as an electrode material for a symmetrical  $\text{Na}_3\text{V}_2(\text{PO}_4)_3/\text{Na}_3\text{V}_2(\text{PO}_4)_3$  cell.<sup>208</sup> Recently, carbon-coated nanosized  $\text{Na}_3\text{V}_2(\text{PO}_4)_3$  has been prepared by a one-pot method.<sup>209</sup> The carbon-coated sample delivers 120 mAh g⁻¹ of reversible capacity (Figure 23a) with excellent capacity retention.<sup>210</sup> Sodium insertion and diffusion mechanisms are extensively found in the literature.<sup>211</sup>

Vanadium fluorophosphate,  $\text{NaV}(\text{PO}_4)\text{F}$ , was proposed as a positive electrode material for NIBs in 2003.<sup>212</sup>  $\text{NaV}(\text{PO}_4)\text{F}$  can be prepared by solid-state reaction of  $\text{VPO}_4$  and  $\text{NaF}$ . Two polymorphs of  $\text{NaV}(\text{PO}_4)\text{F}$  exist as the low-temperature monoclinic phase and high-temperature tetragonal phase.<sup>213</sup> The crystal structure of tetragonal  $\text{NaV}(\text{PO}_4)\text{F}$  seems to be related to  $\text{Na}_3\text{V}_2(\text{PO}_4)_2\text{F}_3$  as described below. Tetragonal  $\text{NaV}(\text{PO}_4)\text{F}$  delivers approximately 100 mAh g⁻¹ of reversible capacity (theoretical capacity 143 mAh g⁻¹ based on  $\text{V}^{3+}/\text{V}^{4+}$ ) with relatively high voltage and is used as a 4 V-class electrode material. Capacity retention in Na cells is improved by partial substitution of aluminum<sup>214</sup> and chromium<sup>215</sup> for the vanadium in the low-temperature phase.

In 2006, the electrode performance of an additional two compounds as sodium insertion materials was reported: sodium vanadium(III) fluorophosphate,  $\text{Na}_3\text{V}_2(\text{PO}_4)_2\text{F}_3$ ,<sup>216</sup> and sodium vanadium(IV) oxyfluorophosphate,  $\text{Na}_3\text{V}_2(\text{PO}_4)_2\text{O}_2\text{F}$ .<sup>217</sup> Structures of both phases are crystallographically the same as each other and isostructural with  $\text{Na}_3\text{Fe}_2(\text{PO}_4)_2(\text{OH})_2\text{F}$ .<sup>218</sup> The

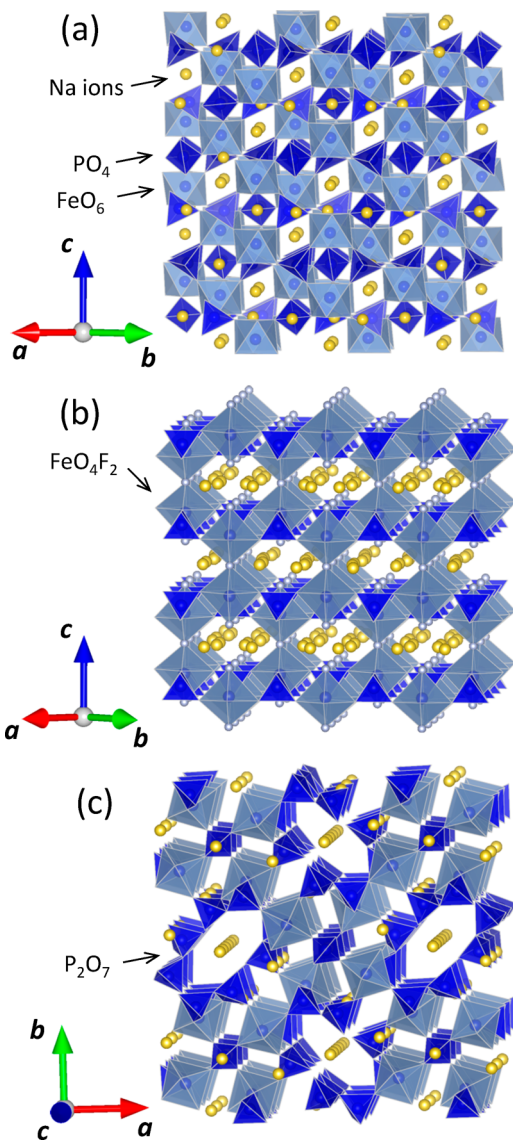


**Figure 22.** Crystal structures for vanadium-based polyanionic compounds: (a)  $\text{Na}_3\text{V}_2(\text{PO}_4)_3$  (NASICON-type), (b)  $\text{Na}_3\text{V}_2(\text{PO}_4)_2\text{F}_3$ , and (c)  $\text{Na}_7\text{V}_4(\text{P}_2\text{O}_7)_4\text{PO}_4$ .

framework structure of  $\text{Na}_3\text{V}_2(\text{PO}_4)_2\text{F}_3$  consists of  $\text{VO}_4\text{F}_2$  octahedra and  $\text{PO}_4$  tetrahedra, while that of  $\text{Na}_3\text{V}_2(\text{PO}_4)_2\text{O}_2\text{F}$  consists of  $\text{VO}_5\text{F}$  octahedra and  $\text{PO}_4$  tetrahedra. The  $\text{VO}_4\text{F}_2$  and  $\text{VO}_5\text{F}$  octahedra share four corners with  $\text{PO}_4$  tetrahedra, forming  $\text{V}_2(\text{PO}_4)_2\text{O}_2\text{F}$  and  $\text{V}_2(\text{PO}_4)_2\text{F}_3$  layers. The  $\text{VO}_4\text{F}_2$  and  $\text{VO}_5\text{F}$  octahedra in the  $\text{V}_2(\text{PO}_4)_2\text{O}_2\text{F}$  and  $\text{V}_2(\text{PO}_4)_2\text{F}_3$  layers further share corners, forming the framework structure with a two-dimensional path for sodium along the  $a-b$  plane (Figure 22b). Recently,  $\text{Na}_3\text{V}_2(\text{PO}_4)_2\text{F}_3$  has been revisited, and excellent electrode performance has been reported.<sup>219,220</sup>  $\text{Na}_3\text{V}_2(\text{PO}_4)_2\text{F}_3$  delivers 120 mAh g<sup>-1</sup> of reversible capacity (Figure 23b) with excellent cyclability and rate capability with the appearance of two voltage plateaus at 3.6 and 4.1 V.<sup>219</sup> The 2D diffusion path for sodium ions in  $\text{Na}_3\text{V}_2(\text{PO}_4)_2\text{F}_3$  was also evidenced by the results of first-principles calculation.<sup>220</sup> Since  $\text{Na}_3\text{V}_2(\text{PO}_4)_2\text{F}_3$  and  $\text{Na}_3\text{V}_2(\text{PO}_4)_2\text{O}_2\text{F}$  are isostructural, a solid solution phase can be also obtained.<sup>221</sup> As one composition of the solid solution phase between  $\text{Na}_3\text{V}_2(\text{PO}_4)_2\text{F}_3$  and  $\text{Na}_3\text{V}_2(\text{PO}_4)_2\text{O}_2\text{F}$ ,  $\text{Na}_3\text{V}_2(\text{PO}_4)_2\text{O}_{1.6}\text{F}_{1.4}$  has been prepared and excellent electrode performance has been demonstrated.<sup>222</sup>

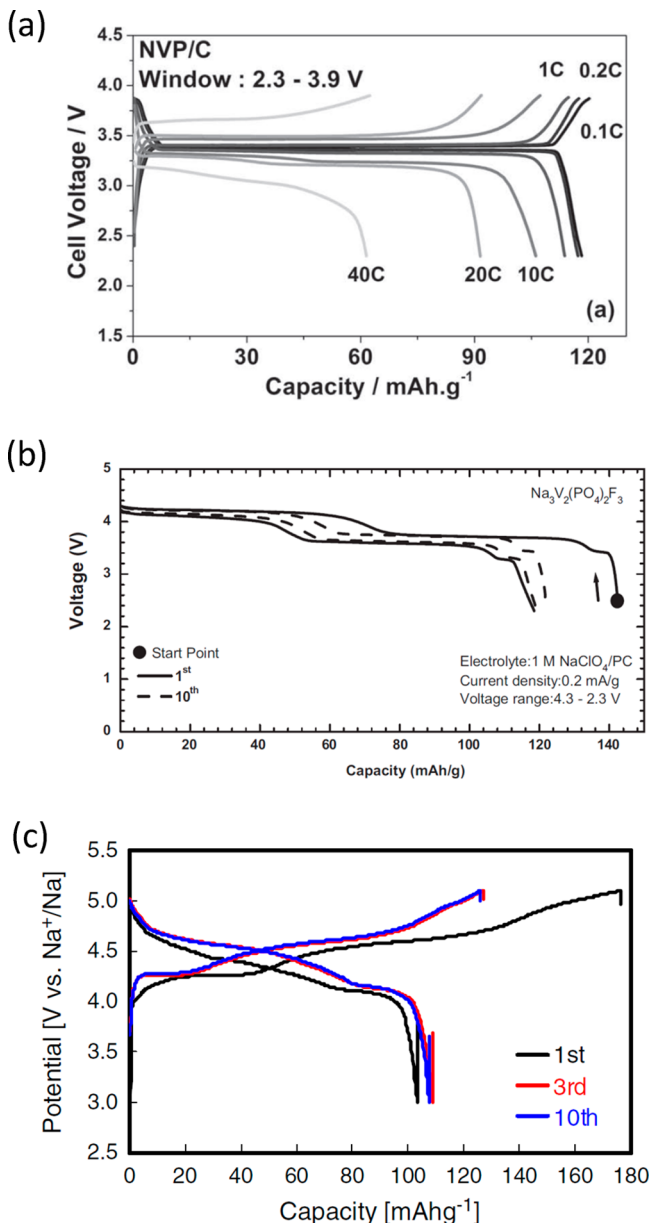


**Figure 23.** Comparison of electrode performance of different polyanionic compounds: (a)  $\text{Na}_3\text{V}_2(\text{PO}_4)_3$ , (b)  $\text{Na}_3\text{V}_2(\text{PO}_4)_2\text{F}_3$ , and (c)  $\text{Na}_4\text{Co}_{2.4}\text{Mn}_{0.3}\text{Ni}_{0.3}(\text{PO}_4)_2\text{P}_2\text{O}_7$ . (a) Reprinted with permission from ref 210. Copyright 2013 WILEY-VCH Verlag GmbH&Co. KGaA, Weinheim. (b) Reprinted with permission from ref 219. Copyright 2013 Elsevier. (c) Reprinted with permission from ref 225. Copyright 2013 Elsevier.

$\text{Na}_3\text{V}_2(\text{PO}_4)_2\text{O}_{1.6}\text{F}_{1.4}$  can deliver approximately 130 mAh g<sup>-1</sup> of reversible capacity with excellent capacity retention even at 60 °C. The excellent capacity retention is proposed to originate from the small volume expansion (less than 3%) on electrochemical cycling.<sup>222</sup>

Similar to  $\text{Na}_4\text{Fe}_3(\text{PO}_4)_2(\text{P}_2\text{O}_7)$ , the mixed polyanion system of phosphate ( $\text{PO}_4$ )<sup>3-</sup> and pyrophosphate ( $\text{P}_2\text{O}_7$ )<sup>4-</sup> ions is also found in the vanadium system. Recently, the electrode performance of  $\text{Na}_7\text{V}_4(\text{P}_2\text{O}_7)_4\text{PO}_4$  in Na cells has been reported.<sup>223</sup> All vanadium ions at octahedral sites in  $\text{Na}_7\text{V}_4(\text{P}_2\text{O}_7)_4\text{PO}_4$  are isolated by corner-shared  $\text{P}_2\text{O}_7$  and  $\text{PO}_4$  units.  $\text{Na}_7\text{V}_4(\text{P}_2\text{O}_7)_4\text{PO}_4$  can be reversibly oxidized to  $\text{Na}_3\text{V}_4(\text{P}_2\text{O}_7)_4\text{PO}_4$  via  $\text{Na}_5\text{V}_4(\text{P}_2\text{O}_7)_4\text{PO}_4$  as the intermediate

phase.  $\text{Na}_7\text{V}_4(\text{P}_2\text{O}_7)_4\text{PO}_4$  shows nearly 3.9 V flat operating voltage even though the reversible capacity is limited to 80  $\text{mAh g}^{-1}$ .

**3.3.4.2. Cobalt-Based System.**  $\text{Na}_4\text{Co}_3(\text{PO}_4)_2\text{P}_2\text{O}_7$ , which is isostructural with  $\text{Na}_4\text{Fe}_3(\text{PO}_4)_2(\text{P}_2\text{O}_7)$  shown in Figure 17c, has been also proposed as a potential candidate as a high-voltage positive electrode for NIBs.<sup>224</sup> Approximately 95  $\text{mAh g}^{-1}$  of reversible capacity is observed for a Na/ $\text{Na}_4\text{Co}_3(\text{PO}_4)_2\text{P}_2\text{O}_7$  cell. This capacity corresponds to 2.2 mol of sodium-ion extraction from  $\text{Na}_4\text{Co}_3(\text{PO}_4)_2(\text{P}_2\text{O}_7)$ , and a high operating voltage of >4 V has been also reported based on  $\text{Co}^{2+}/\text{Co}^{3+}$  redox. Similar to the O3- and P2-type layered  $\text{Na}_x\text{CoO}_2$  system, several sets of voltage plateaus appear in the Na/ $\text{Na}_4\text{Co}_3(\text{PO}_4)_2\text{P}_2\text{O}_7$  cell, indicating the complicated phase transitions associated with the sodium-ion ordering.

Partial substitution of Mn and Ni for Co is possible in  $\text{Na}_4\text{Co}_3(\text{PO}_4)_2\text{P}_2\text{O}_7$ , and the electrode performance of the manganese- and nickel-substituted sample,  $\text{Na}_4\text{Co}_{2.4}\text{Mn}_{0.3}\text{Ni}_{0.3}(\text{PO}_4)_2\text{P}_2\text{O}_7$ , has been reported.<sup>225</sup>  $\text{Na}_4\text{Co}_{2.4}\text{Mn}_{0.3}\text{Ni}_{0.3}(\text{PO}_4)_2\text{P}_2\text{O}_7$  shows more than 100  $\text{mAh g}^{-1}$  of reversible capacity, and surprisingly, some extent of discharge capacity in the voltage region of 5.0–4.5 V (5.34–4.84 V vs Li metal) has been reported (Figure 23c). The origin of the anomalously high voltage has been suggested to be the contribution of the nickel-ion redox in the polyanionic framework structure.<sup>225</sup>

**3.3.4.3. Polyanionic Compounds with 4d Transition Metals.** Only a few studies are available for oxoanion compounds with 4d transition metals as sodium insertion materials. NASICON-type  $\text{Fe}_2(\text{MoO}_4)_3$  is electrochemically active in both Li and Na cells based on the  $\text{Fe}^{2+}/\text{Fe}^{3+}$  redox.<sup>226</sup> Additionally, the electrode performance of molybdenum oxypyrophosphate,  $\text{Mo}_2\text{O}_4\text{P}_2\text{O}_7$ , in Li and Na cells was reported.<sup>227</sup> Approximately 3 mol of sodium ions are reversibly inserted/extracted into/from  $\text{Mo}_2\text{O}_4\text{P}_2\text{O}_7$  in a voltage range of 3–2 V. Electrode performance (rate capability and cyclability) seems to be better in the Li cells.

### 3.4. Miscellaneous Na Insertion Materials as Positive Electrode Materials

Iron trifluoride,  $\text{FeF}_3$ , has been studied as a potential candidate to achieve high energy density as an iron-based electrode material in Li cells. The electrode performance of  $\text{FeF}_3$  in Li cells was first examined by Arai and co-workers.<sup>228</sup> Fe–F bonds in  $\text{FeF}_3$  are strongly polarized because of the high electronegativity of fluorine in comparison to that of oxygen. Electrons are, therefore, localized in  $\text{FeF}_3$ , resulting in insufficient electrical conductivity as an electrode material.  $\text{FeF}_6$  octahedra share all corners, forming the framework structure with open channels (Figure 24a). The structure of  $\text{FeF}_3$  is isostructural to distorted  $\text{ReO}_3$  (it is also classified as an A-site deficient perovskite structure). Although  $\text{FeF}_3$  has an open structure with three-dimensional pathways for lithium insertion, the electrode performance of micrometer-sized  $\text{FeF}_3$  is limited by its insulating character. The electrode performance of  $\text{FeF}_3$  in Li cells is significantly improved using nanocomposite materials consisting of  $\text{FeF}_3$  and conductive carbon.<sup>229</sup> This concept has been extended to the Na system, and it was demonstrated that  $\text{FeF}_3/\text{C}$  nanocomposite delivers a large reversible capacity (~150  $\text{mAh g}^{-1}$ ) in Na cells (Figure 25a).<sup>230</sup> Since  $\text{LiFeF}_3$  is formed as a metastable phase by electrochemical (or chemical) reduction of  $\text{FeF}_3$  in Li cells, it is impossible to prepare directly  $\text{LiFeF}_3$  by a simple solid-state method. Such lithiated phase is

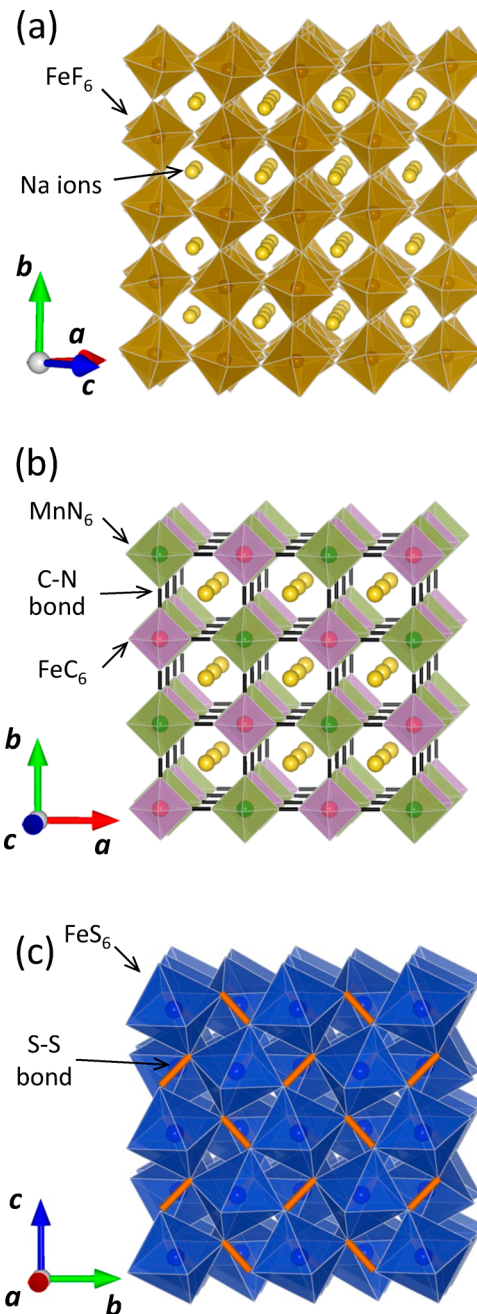
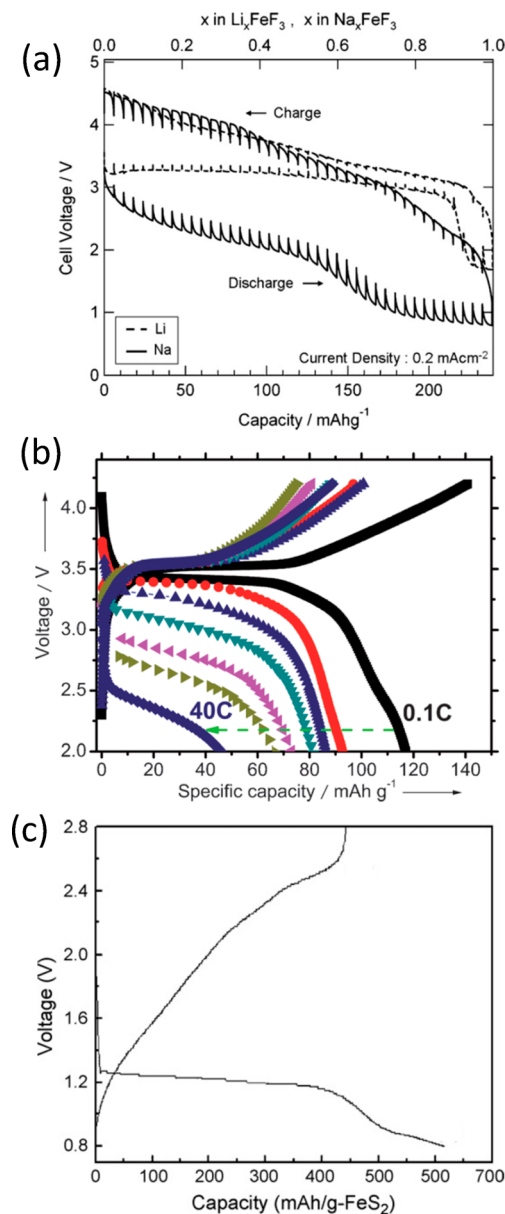


Figure 24. Comparison of crystal structures for (a)  $\text{NaFeF}_3$ , (b)  $\text{Na}_x\text{MnFe}(\text{CN})_6$ , and (c)  $\text{FeS}_2$  (pyrite).

preferable as a positive electrode material to assemble a full cell combined with carbonaceous materials as a negative electrode. In contrast to  $\text{LiFeF}_3$ ,  $\text{NaFeF}_3$  is easily prepared as a thermodynamically stable phase because the large Na ions are energetically stabilized at A sites of the perovskite structure (and the sites are too large for Li ions) as shown in Figure 24a. Nanosized  $\text{NaFeF}_3$  is electrochemically active in Na cells and used as a positive electrode even though a relatively large polarization for charge and discharge cycles was observed.<sup>231,232</sup>

Na ions are apparently coordinated by four fluoride ions at bottleneck sites when the Na ions migrate across the perovskite-type framework structure. Therefore, use of cyanide ions has been proposed to reduce the activation energy at the bottleneck sites for the Na migration process.<sup>233</sup> Moreover, the cyanide ions as strong-field ligands drastically influence the



**Figure 25.** Electrode performance of (a)  $\text{FeF}_3$ , (b)  $\text{Na}_x\text{MnFe}(\text{CN})_6$ , and (c)  $\text{FeS}_2$  (pyrite) in Na cells. (a) Reprinted with permission from ref 231. Copyright 2009 Elsevier. (b) Reprinted with permission from ref 233. Copyright 2013 WILEY-VCH Verlag GmbH&Co. KGaA, Weinheim. (c) Reprinted with permission from ref 239. Copyright 2007 Elsevier.

crystal field splitting for the 3d orbital of iron ions. Recently, Prussian blue analogues, which have a similar framework structure to that of perovskite as shown in Figure 24b, have been studied as the Na insertion host structures. The iron and manganese system with potassium ions,  $KFe_2(CN)_6$  and  $KMnFe(CN)_6$ ,<sup>234</sup> and the iron(III) system without alkaline metal ions,  $Fe_2(CN)_6$ ,<sup>235</sup> shows 80–120 mAh g<sup>-1</sup> of reversible capacity as positive electrode materials in Na cells. Polarization of Prussian blue analogues in the Na cells is much smaller than that of the perovskite system with fluoride ions. Goodenough's research group has reported the Na-enriched iron manganese system,  $Na_{1.72}MnFe(CN)_6$  (an ideal crystal structure without sodium vacancies is illustrated in Figure 24b), as a potential positive electrode material for NIBs.<sup>233</sup> Magnetic measure-

ments of  $\text{Na}_{1.72}\text{MnFe}(\text{CN})_6$  suggest the presence of low-spin Fe(II) coordinated by carbon, and the low-spin Fe(II)/Fe(III) is redox active in Na cells.<sup>233</sup> Reversible capacity reaches 130 mAh g<sup>-1</sup> with an average operating voltage of 3.2 V. The sample also shows excellent rate capability in the Na cell as shown in Figure 25b. The electrode performance of a similar sodium manganese ferrocyanide has been also recently reported.<sup>236</sup> The activation energy of the charge transfer reaction for Na insertion into Prussian blue analogues highly depends on the electrolyte solution used, and an extremely small activation energy (5 kJ mol<sup>-1</sup>) in water-based electrolyte solution has been reported.<sup>237</sup> Additionally, sodium ferrocyanide,  $\text{Na}_4\text{Fe}(\text{CN})_6$ , was reported to be electrochemically active in Na cells. The sample delivers ~90 mAh g<sup>-1</sup> of reversible capacity with a flat voltage plateau at 3.4 V.<sup>238</sup> This reversible capacity nearly corresponds to the capacity defined by one-electron redox reaction of iron for  $\text{Na}_4\text{Fe}(\text{CN})_6$ .

Pyrite,  $\text{FeS}_2$ , which is the most common sulfide minerals, is also utilized as an electrode material for Na cells even though its reaction mechanism is not classified as an insertion reaction.<sup>239</sup>  $\text{FeS}_2$  consists of  $\text{Fe}^{2+}$  and  $\text{S}_2^{2-}$  (persulfide ions), and clear evidence for the presence of a S–S bond is found in the structure as shown in Figure 24c. On the reduction process in Na cells,  $\text{Fe}^{2+}$  is reduced to metallic Fe and  $\text{S}_2^{2-}$  is potentially reduced to form  $\text{Na}_2\text{S}$ . If this reaction (so-called conversion reaction<sup>139</sup>) is a reversible process, the theoretical capacity exceeds  $950 \text{ mAh g}^{-1}$ . Although a large initial discharge capacity was obtained (Figure 25c), reversibility is insufficient as an electrode material. Use of the conversion reaction could be one strategy to design the battery system with a high energy density provided that round trip efficiencies and capacity retention upon cycling can be improved.

In this section, many different positive electrode materials have been reviewed. The energy density of selected materials, oxides and polyanionic compounds, are plotted in Figure 26. Here, the energy density was estimated by calculation with the assumption of 300 mAh g<sup>-1</sup> for hard carbon as a negative electrode material as full cells, as further discussed in the next section. Combined with hard carbon, the estimated energy

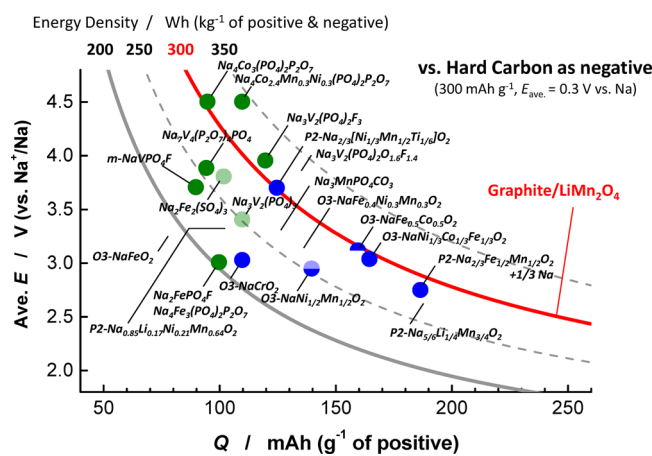


**Figure 26.** Average voltage ( $V_{\text{ave}}$ ) and energy density ( $\text{Wh kg}^{-1}$ ) versus gravimetric capacity ( $\text{mAh g}^{-1}$ ) for selected positive electrode materials for NIBs. Energy density was calculated with the hard carbon (reversible capacity of  $300 \text{ mAh g}^{-1}$  with  $V_{\text{ave}} = 0.3 \text{ V}$  vs Na metal, see Figure 27) as negative electrode materials. Data derived from refs 51, 61, 67, 71, 96, 117, 119, 125, 131, 137, 190, 197, 199, 203, 209, 212, 220, and 222–225.

density of NIBs with some of the electrode materials almost reaches and/or exceeds  $300 \text{ mWh g}^{-1}$  based on the mass of active materials (Note that carbon materials are in general needed to increase the electrode performance). The gravimetric energy density of NIBs is now competitive to the graphite/LiMn<sub>2</sub>O<sub>4</sub> system. Research progress on positive electrode materials will further enhance the energy density of NIBs in the future. The possibility of NIBs as full cells will be further discussed in a later section.

#### 4. NEGATIVE ELECTRODE MATERIALS

Research on negative electrode materials for NIBs has been developed on the four different categories, which are basically identical to those for LIB: (1) carbonaceous materials, (2) oxides and polyanionic compounds (such as phosphates) as topotactic insertion materials for sodium, (3) p-block elements (metals, alloys, phosphorus/phosphide) showing reversible sodiation/desodiation, and (4) oxides and sulfides with conversion reaction. In this section, recent research progress on negative electrodes for NIBs is summarized. The electrode performance of different electrode materials in Na cells is given focusing on the reaction mechanisms for sodiation/desodiation processes. Since the electrode potential is generally low around 0–1 V vs Na<sup>+</sup>/Na (i.e., from –3 to –2 V vs NHE), decomposition of electrolyte solution at the negative electrode is a severe issue to realize long cycle life for battery applications. Selection of binders, additives, and electrolyte, therefore, has a significant impact on the electrochemical behavior of negative electrodes, associated with formation of surface passivation layers, namely, solid electrolyte interphase (SEI).<sup>240</sup> Potential breakthroughs in negative electrode materials and practical issues are also provided to discuss the possibility of NIBs without metallic sodium in the future.

##### 4.1. Carbon-Based Electrode Materials

**4.1.1. Na Insertion into Hard Carbon.** For LIBs, graphite is widely used as a negative electrode material in comparison with other carbon materials because of its high gravimetric and volumetric capacity. Graphite electrodes deliver a reversible capacity of more than  $360 \text{ mAh g}^{-1}$ , comparable to the theoretical capacity of  $372 \text{ mAh g}^{-1}$ .<sup>241</sup> By electrochemical reduction, Li<sup>+</sup> ions are inserted between graphene layers and Li–graphite intercalation compounds (GIC) are formed with stage transformations.<sup>20</sup> At the first stage, all graphite layers are completely filled by Li, forming LiC<sub>6</sub> at the end of the electrochemical reduction process.<sup>242</sup> However, graphite is electrochemically less active in Na cells. Although a small amount of Na atoms seems to be inserted into the graphite by heating with Na metal under helium or vacuum atmosphere and by electrochemical reduction, resulting in formation of NaC<sub>64</sub>,<sup>21,243</sup> the Na insertion amount is much smaller than that for Li and K insertion into graphite. In 2014, the reversible Na intercalation into graphite in diglyme-based electrolyte was demonstrated.<sup>244</sup> Although Na<sup>+</sup> ions probably cointercalate with diglyme into graphite and the Na//graphite cell exhibits  $100 \text{ mAh g}^{-1}$  of reversible capacity with excellent capacity retention, the reversible capacity is still less than that of a Li//graphite cell.

The relatively larger reversible capacity of carbonaceous electrode materials in Na cells was first reported by Doeuff et al.<sup>22</sup> in 1993 using a soft carbon prepared by pyrolysis of petroleum cokes; however, cells were cycled at 86 °C. Soft carbon in general consists of a disordered structure and is

graphitizable at high temperature above 2800 °C. The soft carbon carbonized at 600–700 °C delivers a larger reversible capacity than that of graphite in Li cells. Although soft carbon electrodes exhibit high capacity and good rate performance in Li cells, a large irreversible capacity was observed at an initial cycle due to electrolyte decomposition on the surface of soft carbon. As another disordered carbon material, hard carbon (so-called nongraphitizable carbon) is also intensively studied as a negative electrode materials of LIBs, especially for the high-power application. Hard carbon has a disordered structure similar to soft carbon. Although many structural models have been proposed so far,<sup>245–255</sup> the detailed structure of soft and hard carbon is, however, still a debatable subject. The structure of hard carbon depends on the synthesis conditions such as carbon sources and carbonization temperatures, resulting in the difficulty to construct a universal structural model of hard carbon. In all of the proposed models hard carbon is composed of two domains, that is, carbon layers (graphene-like) and micropores (nanosized pores) formed between disorderly stacked carbon layers.

Hard carbon had been utilized as a negative electrode in the first commercial Li-ion battery, and the hard-carbon electrodes deliver comparable reversible capacity without a staging transition due to the structural disorder. The reversible capacity exceeds the theoretical capacity of graphite,<sup>256</sup> even though the volumetric capacity is lower than that of graphite. The electrochemical reversibility of Na insertion/extraction into/from hard carbon at room temperature was first reported by Stevens and Dahn in 2000.<sup>257</sup> They prepared a hard-carbon sample by carbonization of glucose at 1000 °C. The hard-carbon electrodes delivered ca.  $300 \text{ mAh g}^{-1}$  of reversible capacity in Na cells. In contrast to graphite, a much higher amount of Na ions can reversibly insert into hard carbon by electrochemical reduction in Na cells.

Charge and discharge curves of a Na cell with hard carbon which was synthesized by carbonization of sucrose at 1300 °C are shown in Figure 27. An irreversible reduction plateau at around 0.8 V is observed at only an initial reduction (sodiation) process, indicating decomposition of electrolyte solvent, salts,

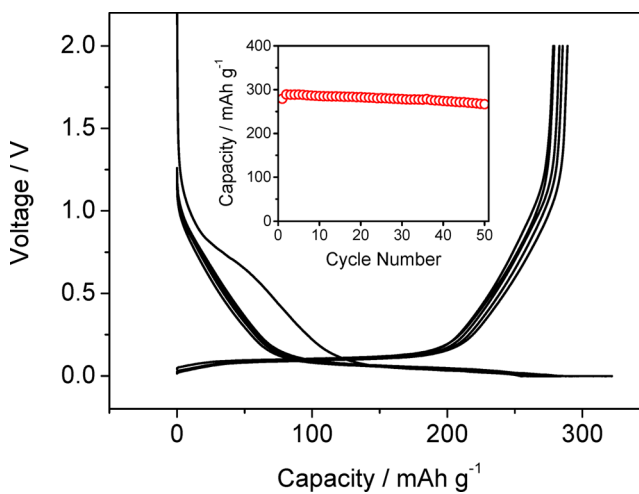


**Figure 27.** Charge/discharge curves of hard-carbon electrodes, derived from sucrose carbonized at 1300 °C, at a rate of  $25 \text{ mA g}^{-1}$  in  $1 \text{ mol dm}^{-3} \text{ NaClO}_4$  dissolved in PC:FEC (98:2 in vol %), and its capacity retention is also shown in the inset. Reprinted with permission from ref 364. Copyright 2014 PCCP Owner Societies.

and additives associated with formation of a passivation layer on the surface of hard carbon. The potentiogram slopes down from 1.2 to 0.1 V during the initial reduction, followed by a long plateau region at about 0.1 V vs Na, approaching 300 mAh g<sup>-1</sup> of reversible capacity. During the following oxidation, a reversible capacity of approximately 200 mAh g<sup>-1</sup> is observed near 0.1 V vs Na/Na<sup>+</sup> and then the potential gradually increases to 1.2 V, suggesting reversible Na insertion/extraction for hard carbon. Hard-carbon electrodes exhibit good capacity retention during the subsequent cycles with fluoroethylene carbonate (FEC) as an electrolyte additive (Figure 27, inset). Detailed studies on electrolyte and additives are described in a later section in this review.

Extensive research efforts have been devoted to studying the reaction mechanisms for Li and Na (de)insertion into the disordered carbons to explain the origin of the anomalous high capacity, and mainly two reaction models have been proposed. Sato and Yata et al. proposed the model based on the LiC<sub>2</sub> stage as a GIC where Li<sup>+</sup> ions are accommodated at ionic sites and Li<sub>2</sub> “covalent” sites between the carbon layers.<sup>256,258</sup> The second model, that is, Li insertion into micropores, is more broadly accepted as the lithium insertion mechanism to explain the anomalously high reversible capacity for disordered carbon materials. During the reduction process, lithium and sodium ions are intercalated into the interstitial space sandwiched with hexagonally bonding carbon layers (interlayer distance is generally extended in comparison to that of graphite) at first and then further inserted into the micropores.<sup>259,260</sup> Li and Na insertion into micropores is supported by small angle neutron and X-ray scattering analysis in the Li and Na systems, respectively.<sup>5,255,260,261</sup> The potentiogram can be divided into two regions: the slope region above 0.2 V and the plateau region close to the equilibrium potential of Na/Na<sup>+</sup> as described above (see Figure 27) and Li or Na insertion between carbon layers and into micropores of hard carbon occurs in the slope and plateau regions, respectively. Although their insertion process for Li and Na would proceed in a similar way, each capacity in the two regions is different for the Li and Na systems when the same hard carbon is used as an electrode in Li and Na cells.<sup>5</sup> This fact suggests that suitable micropore size and interlayer distances of hexagonally bonding carbon layers are not the same for the case of Li and Na insertion.<sup>5</sup> Furthermore, the presence of quasi-metallic Li clusters at the fully Li inserted state observed by <sup>7</sup>Li NMR was reported.<sup>251,262–264</sup> In contrast, formation of quasi-metallic Na clusters was not evidenced by <sup>23</sup>Na NMR so far.<sup>265</sup> The finding might originate from the difference in the insertion and stabilization mechanisms for Li and Na in micropores. Therefore, the electrode performance of hard carbon could be further improved through optimization of structures. Indeed, recently, more than 300 mAh g<sup>-1</sup> of reversible capacity for hard carbon derived from a sucrose precursor in Na cells has been reported,<sup>266–268</sup> even though the volumetric capacity is still low in comparison to that of graphite electrode in the Li system.

**4.1.2. Electrolyte and Additive for Na Cells.** By designing better electrolyte it is possible to enhance the energy/power density and cycle life of hard-carbon electrodes in Na cells. In the case of LIBs, various electrolytes, such as organic electrolyte solution, solid polymer electrolyte, gel polymer electrolyte, inorganic solid electrolyte, molten salt including ionic liquid, aqueous solution, etc., have been studied to date, and their development is still in progress. It is thought that one of the most successful electrolyte media is organic

electrolyte solution based on carbonate ester polar solvents where lithium salts are dissolved with small portions of functional additive(s) for practical LIBs, due to its wide potential window, high ionic conductivity, good temperature performance, low toxicity, etc. Therefore, it is reasonably expected that carbonate ester-based solution containing sodium salts is one of the most appropriate electrolyte media for battery applications. In this section, the major focus is the impact of carbonate ester electrolyte solutions as well as sodium salts and additives on the electrode performance of hard carbon in Na cells.

An early study on electrolyte solutions for hard-carbon electrodes for Na cells was reported by Alcántara et al.<sup>269</sup> The electrode performance of hard-carbon electrodes was tested and compared in different solvents: ethylene carbonate (EC)/dimethyl carbonate (DMC) as a mixed cyclic and linear carbonate system, which is a conventional system in the Li system, tetrahydrofuran (THF) as a cyclic ether, EC/THF (1:1 by v:v), and 1,2-dimethoxyethane (DME). However, the capacity decline within a few initial cycles was unavoidable regardless of the difference in the electrolyte solutions.<sup>269</sup>

Some of the authors of this review recently reported systematic studies on electrolyte solvents with NaClO<sub>4</sub> as the electrolyte salt.<sup>5</sup> The electrochemical cycling test of commercially available hard carbon was carried out in propylene carbonate (PC) and binary solvent electrolyte based on ethylene carbonate (EC) and linear carbonate esters containing NaClO<sub>4</sub> in beaker-type cells as shown in Figure 28a. When PC and EC/diethyl carbonate (DEC) mixed solution is used, the hard-carbon electrodes exhibit a high reversible capacity of more than 200 mAh g<sup>-1</sup> with excellent capacity retention over 100 cycles. On the other hand, in the case of EC/DMC and EC/ethyl methyl carbonate (EMC), the cycle performance in beaker-type cells is insufficient. Moreover, the cycle performance of the hard-carbon electrodes in coin-type cells is compared using the PC-based electrolyte solution containing different electrolyte salts in Figure 28b. Despite the fact that the beaker-type cell with NaClO<sub>4</sub> in PC shows good capacity retention, the decrease in capacity is observed using a coin-type cell in which a thin glass fiber separator is soaked with a minimal amount of electrolyte solution sandwiched between the Na metal foil and the hard-carbon electrodes. On the other hand, the coin-type cells with NaPF<sub>6</sub> and NaTFSA dissolved in PC solutions exhibit better cycle performance. Palacin et al. also tested various electrolyte solutions with different Na salts (NaClO<sub>4</sub>, NaPF<sub>6</sub>, and NaTFSA), solvents (PC, EC, DMC, DME, DEC, THF, and triglyme), and solvent mixtures (EC/DMC, EC/DME, EC/PC, and EC/triglyme) using three-electrode Swagelok cells.<sup>270</sup> The results are in good agreement with the previous study;<sup>5</sup> the best cycle performance was found to be in the case of NaClO<sub>4</sub> dissolved in cyclic carbonates, EC and PC. Note that powder of NaClO<sub>4</sub> is shock sensitive. If solutions are allowed to dry out there is a risk of violent decomposition. This is not an issue with NaPF<sub>6</sub> as the electrolyte salt.

Another key material to improve the performance of hard-carbon electrodes is electrolyte additives. The film-forming additives into electrolyte solutions are widely known to improve the electrode properties for the LIBs.<sup>271–274</sup> Vinylene carbonate is the most widely used film-forming additive in the practical LIBs with the graphite negative electrode.<sup>275,276</sup> FEC is also known as an effective electrolyte additive for improving SEI films and passivation, especially used for lithium metal and

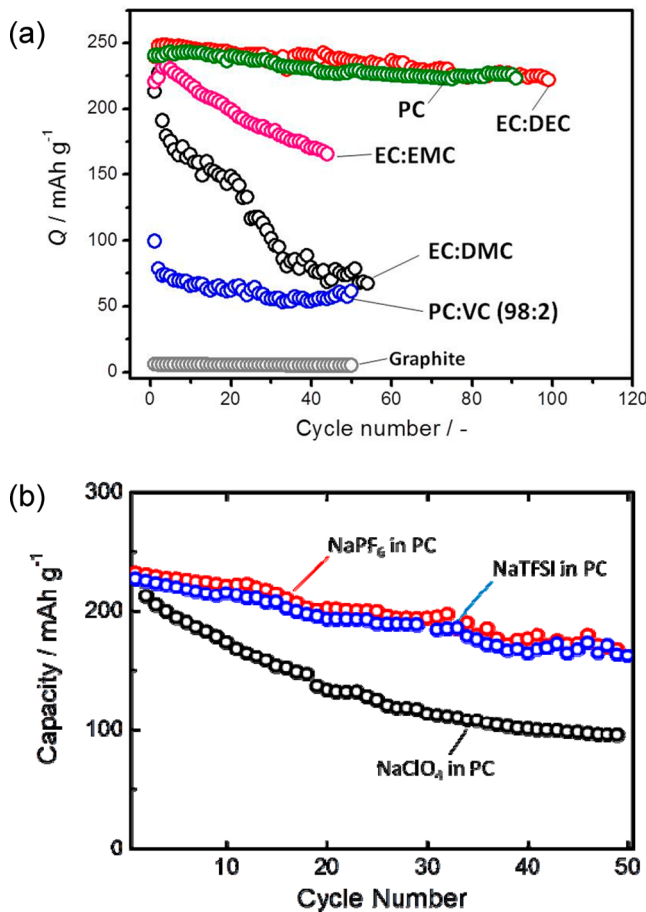


**Figure 28.** (a) Capacity retention for hard-carbon electrodes in the beaker-type cells with  $1 \text{ mol dm}^{-3}$   $\text{NaClO}_4$  dissolved in different solvent mixtures. (b) Capacity retention for hard-carbon electrodes in the coin-type cells with PC-based electrolyte solvent containing different Na salts;  $1 \text{ mol dm}^{-3}$   $\text{NaPF}_6$ , LiTFSI, and  $\text{NaClO}_4$  at a rate of  $25 \text{ mA g}^{-1}$ . Reprinted with permission from ref 5. Copyright 2011 WILEY-VCH Verlag GmbH&Co. KGaA, Weinheim.

silicon-based electrode materials.<sup>272,273,277</sup> The influence of the addition of FEC into electrolyte solution on the electrode performance of hard-carbon electrodes in Na cells has been also reported (Figure 29).<sup>278</sup> When a small amount of FEC is added into  $1 \text{ mol dm}^{-3}$   $\text{NaClO}_4/\text{PC}$  solution, an additional voltage plateau at ca. 0.7 V appears during the first reduction due to decomposition of FEC. By FEC addition, capacity degradation as observed for the electrolyte without FEC is sufficiently suppressed.<sup>278</sup> Indeed, FEC addition is noticeably effective to achieve good reversibility of the Na insertion, presumably associated with formation of a stable passivation layer at the surface of hard carbon (and sodium metal<sup>278</sup>). Ponroux et al.<sup>268</sup> recently compared the electrochemical performance of hard-carbon electrodes in  $1 \text{ mol dm}^{-3}$   $\text{NaClO}_4$  EC:PC electrolyte solution with and without FEC additive. A decrease in the reversible capacity and Coulombic efficiency by FEC addition has been demonstrated. The reduction process would not be able to access the low potential plateau (at ca. 0.1 V vs  $\text{Na}^+/\text{Na}$ ) region probably due to the high resistive nature of the surface layer formed by FEC addition with EC:PC mixtures. Water contamination might affect the different influence of FEC in the literature. Both the purity of the electrolyte solution and the atmosphere of the Ar-filled glovebox in which Na cells are assembled influence the amount of contaminated water in

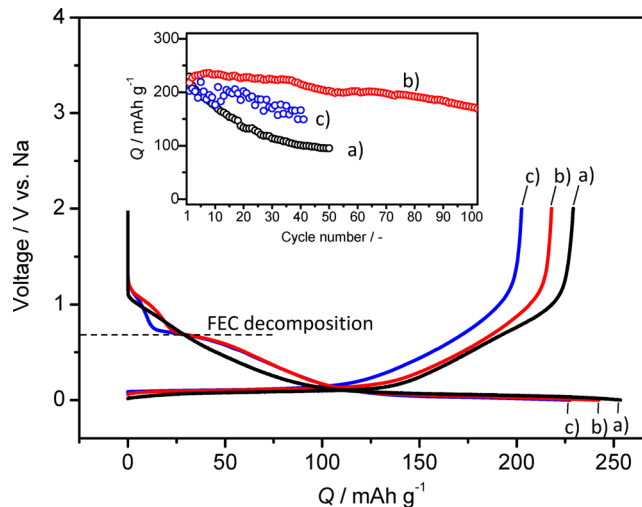


**Figure 29.** Initial galvanostatic reduction/oxidation curves for hard-carbon electrodes in  $1 \text{ mol dm}^{-3}$   $\text{NaClO}_4/\text{PC}$  solution (a) without and with (b) 2 and (c) 10 vol % FEC. (Inset) Oxidative capacity retention for the hard-carbon electrodes. Commercial hard-carbon powder was used as electrode materials. Reprinted with permission from ref 278. Copyright 2011 American Chemical Society.

electrochemical cells, leading to the difference in the passivation process. The amount of electrolyte (relative amount of additive to hard carbon and/or sodium) would also influence the passivation process. An increase in the polarization by 5% FEC addition into  $1 \text{ mol dm}^{-3}$   $\text{NaPF}_6$  PC solution is observed when Na carboxymethyl cellulose (CMC) binder is used as further described in the next section. Further optimization of the additive amount with a suitable combination of solvents and salts is necessary for each electrode material to enhance the electrode performance for battery applications.

Since the issue associated with the flammability of carbonate- and ether-based solvent cannot be ignored, ionic liquids have attracted much interest as electrolyte due to their flame retardancy (nonvolatility), thermal stability, and wide electrochemical windows.<sup>279–281</sup> Fukunaga et al. examined the hard carbon in several ionic liquids without conventional solvent at relatively high temperature ( $90^\circ\text{C}$ ) with different compositions of NaFSA and  $\text{C}_1\text{C}_3\text{pyrFSA}$  (FSA, bis(fluorosulfonyl)amide;  $\text{C}_1\text{C}_3\text{pyr}$ , *N*-methyl-*N*-propylpyrrolidinium).<sup>282</sup> The hard-carbon electrode exhibited a good reversible capacity of  $260 \text{ mAh g}^{-1}$  at a constant rate of  $50 \text{ mA g}^{-1}$  with high Coulombic efficiency (>99.9%) for 40 cycles at  $90^\circ\text{C}$ . The cell also shows good rate capability at a rate of  $\sim 1000 \text{ mA g}^{-1}$ . Further studies on the possibility of surface film formation by decomposition of ionic liquids (with organic cations) are necessary to understand the detailed sodium insertion mechanism of hard carbon in the pure ionic liquid.<sup>283</sup>

**4.1.3. Binders.** Since Li-ion batteries became commercially available in 1991, poly(vinylidene fluoride) (PVdF) has been widely used as a binder to form an electrode layer from powdery electrode materials on metallic foil because of its good chemical and electrochemical stability for long-time use. However, this polymer is relatively costly and requires the use of volatile organic solvents to make a slurry paste that is often toxic such as *N*-methyl pyrrolidone (NMP) in the processing. Moreover, defluorination from PVdF is observed when the polymer is attacked by alkali hydroxides.<sup>284</sup> In contrast, water-soluble binders such as sodium carboxymethyl

cellulose (CMC), which is derived from cellulose as natural polymers, provide an environmentally friendly and cost effectiveness for battery manufacturing.<sup>285–287</sup> Additionally, adhesive strength as binders and dispersion of active materials in the slurry are efficiently improved using water-soluble binders having a carboxylic group, for instance, CMC, polyacrylates, etc.<sup>277,288–291</sup> Selection of suitable binders is also an important factor to maximize the electrode performance of active materials in Na cells, similar to Li cells.

Figure 30 compares the influence of PVdF and CMC binders on the electrode performance for hard-carbon electrodes in 1

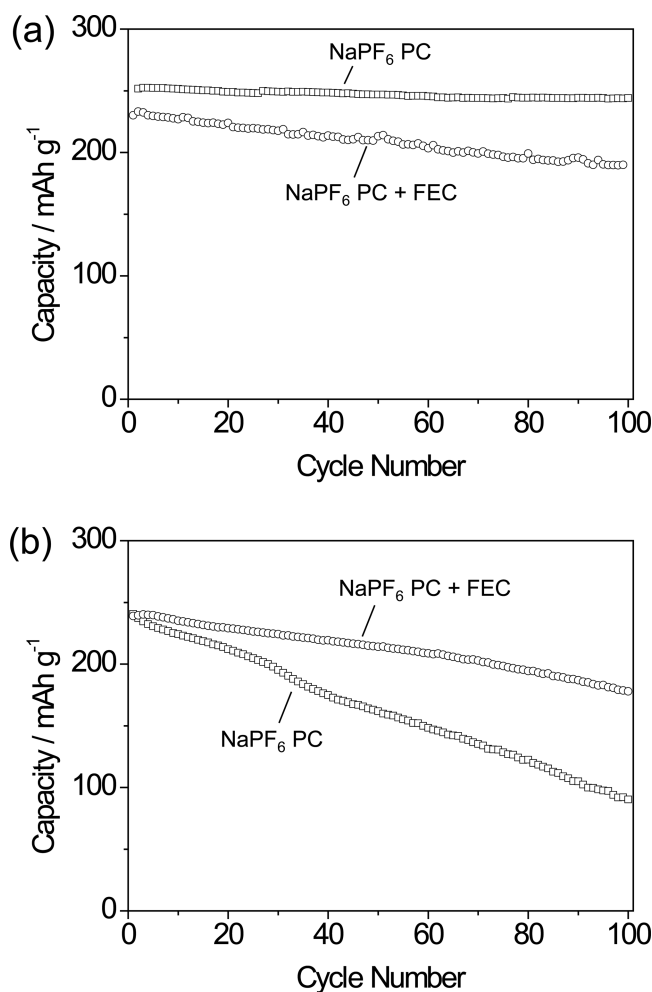


Figure 30. Cycle performance of hard-carbon electrodes with (a) CMC and (b) PVdF binders in 1 mol  $\text{dm}^{-3}$   $\text{NaPF}_6$  PC solution without FEC and with 5% FEC. Reprinted with permission from ref 292. Copyright 2014 Elsevier.

$\text{mol dm}^{-3}$   $\text{NaPF}_6/\text{PC}$  with the effect of the FEC additive.<sup>292</sup> In the case of PVdF without the FEC additive, the reversible capacity significantly declines on electrochemical cycles. In contrast, the hard-carbon electrodes with the CMC binder show excellent capacity retention, >96.5% even after 100 cycles in the coin-type cell. Furthermore, the initial and averaged Coulombic efficiency is improved by use of the CMC binder. Nevertheless, in the combination of the CMC binder and FEC additive, the capacity retention and Coulombic efficiency are deteriorated. An XPS study reveals that the CMC binder effectively covers the surface of hard-carbon particles, and the layer is expected to partly work as a passivation film. Therefore,

the decomposed compounds of the FEC additive would form excessive surface films on the binder layers and increase the resistance of the electrodes, leading to the lower reversible capacity. From these results it is proposed that the CMC binder effectively improves the electrode performance of the hard-carbon electrodes, probably related to formation of uniform passivation layers on the surface of hard-carbon particles.<sup>292</sup>

**4.1.4. Solid Electrolyte Interphase.** In the former sections it has been shown that solvents, electrolyte salts, additives, and binders highly influence the electrode performance of hard carbon (potentially other negative electrode materials) in Na cells, and the difference originates from decomposition of electrolytes and formation of surface films (ideally passivation). Generally, almost all polar aprotic solvents, including EC and PC, are not thermodynamically stable at  $\sim 0$  V vs  $\text{Na}/\text{Na}^+$ . Therefore, passivation must play a key role to realize the stable cycle performance of electrode materials with high reversibility. Currently, there is much knowledge on passivation for negative electrodes in LIBs, so-called solid electrolyte interphase (SEI). As broadly accepted, the thin stable surface layer is formed on the surface of carbonaceous materials, which suppresses additional electrolyte decomposition. The concept of SEI was first introduced by Peled.<sup>240</sup> According to Peled's study,<sup>240</sup> alkali and alkali-earth metals are always covered by a surface layer and SEI should meet the following terms: (i) this surface layer protects a direct and free contact between the electrode and the solution, and (ii) electrons are not allowed to pass through the interphase (the SEI is a pure cationic conductor).

Although the surface passivation process has been extensively studied in the Li system, only a limited number of results were published in the Na system before 2010. Moshkovich et al.<sup>293</sup> studied and compared the surface films formed on the noble metals in aprotic solvent (PC) containing Li and Na ions ( $\text{LiClO}_4$  and  $\text{NaClO}_4$ ). The major finding is incomplete passivation of a noble metal surface and dissolution of surface films for the Na system. The results suggest that the solubility of the electrochemical decomposition products of the carbonate ester-based electrolyte solutions in the Na system is higher than that of the Li system. This fact probably originates from the difference in the Lewis acidity of  $\text{Li}^+$  and  $\text{Na}^+$  ions. As discussed in the former section, since the Lewis acidity of lithium ions is stronger than sodium ions, the Coulombic interaction of lithium ions with negatively charged species or lone pair electrons is notable compared with that of sodium ions, resulting in the difference in the solubility for the electrolyte decomposition products. One simple fact is that  $\text{Li}_2\text{CO}_3$  is hardly soluble in water, whereas  $\text{Na}_2\text{CO}_3$  is highly water soluble. According to previous studies about SEI formed at the surface of carbon materials in Li cells,<sup>294</sup> several lithium compounds, such as  $\text{Li}_2\text{CO}_3$ , lithium alkylcarbonate(s), lithium alkoxide(s),  $\text{LiF}$ , and so on, are found in the SEI layer as insoluble components on carbon and Li metal deposited by electroreductive reaction at approximately 0.8 V vs Li. Considering the difference in the Lewis acidity and solubility between lithium and sodium, it is reasonable to point that formation of the SEI passivation layer is more difficult in Na cells because of the higher solubility of the decomposition products in  $\text{Na}^+$ -based electrolyte solution.

This fact also indicates that the Na metal and sodium-inserted carbon suffer from corrosion (i.e., chemical oxidation) due to insufficient passivation. Indeed, the electrochemical reversibility of Na metal deposition/dissolution is generally

lower than that of lithium metal. Additionally, the surface layers formed on the hard-carbon particles are also expected to be different in the Li and Na systems. Therefore, surface layers for hard carbon in Na and Li cells have been comparably studied by scanning electron microscopy (SEM), transmission electron microscopy (TEM), X-ray photoelectron spectroscopy (XPS), and time-of-flight secondary ion mass spectroscopy (TOF-SIMS) with electrochemical measurements including self-discharge tests.<sup>5</sup> To clarify the surface layers on hard-carbon electrodes, hard-carbon electrodes with the PVdF binder were cycled in 1 mol dm<sup>-3</sup> NaClO<sub>4</sub> and LiClO<sub>4</sub> PC electrolyte solution. From the TEM observation, the surface film formed on the tested hard carbon in the Na cell has a thickness of approximately 30 nm in dry condition, and the morphology of the surface films was found to be clearly different in the Li and Na systems.<sup>5</sup> In the case of Na, the rough and nonuniform deposit layer was observed on the surface. On the other hand, the uniform layer covered the surface in the Li cell. The difference of the surface film components between Li and Na systems is further evidenced by TOF-SIMS as shown in Figure 31A. In the Na cell, a small number of fragment peaks was observed, their intensity is markedly higher in comparison with that of the Li cell, and the fragments were mainly assigned to the inorganic fragment components. On the contrary, a large number of fragments at every  $m/z = 1$  were observed in the Li cell, and most of them were assigned to organic fragments. These results prove that the surface film in the Li cell was mainly composed of the organic compounds, while that in Na was composed of the inorganic compounds. The above results confirm that a passivation layer different from the Li-based negative electrode exists for the Na-based electrode because the organic compounds formed in Na cells could be more soluble compared to those formed in Li cells as already described, and the hardly soluble inorganic compounds are mainly deposited on the surface of hard carbon. XPS measurements also reveal the similar difference of the surface layers formed by the electrochemical cycling in Li and Na cells. In Figure 31B, a strong peak at 284.5 eV in the spectra was assigned to the  $sp^2$  carbon in  $-C-C-$  of hard carbon. The other peaks are expected to originate from the PVdF binder ( $-CF_2-$  at 290.8 eV) and various functional groups on the hard-carbon electrodes.<sup>242,295</sup> After the electrochemical tests the peak at 284.5 eV almost disappeared, indicating that hard carbon in both cells is covered with the decomposition products of the electrolyte. The apparent difference for electrodes cycled in Na and Li cells was observed in 285.5 eV; the peak intensity in  $-CH_2-$  is stronger for the Li cell than that in the Na cell. Since  $-CH_2-$  would be assigned to the alkyl and alkylene groups and polymer species, the larger amount of hydrocarbon compounds was found in the surface film formed in the Li cell as also evidenced above by TOF-SIMS. To examine the passivation property of the fully Na-inserted hard carbon and stability of the surface layers formed on the hard carbon, self-discharge tests of the hard-carbon electrodes after full Na and Li insertion at the 10th cycle were further conducted as seen in Figure 31C. There is unimportant self-discharge since the discharge capacity is approximately 80% after a month, and a similar trend in both Na and Li cells was found.

These results indicate that the surface film works as a passivation film (and the findings satisfy the requirements for "SEI" described above), which similarly protects the Na- and Li-inserted hard carbon from chemical reactions with the electrolyte at the interface, whereas the morphology and

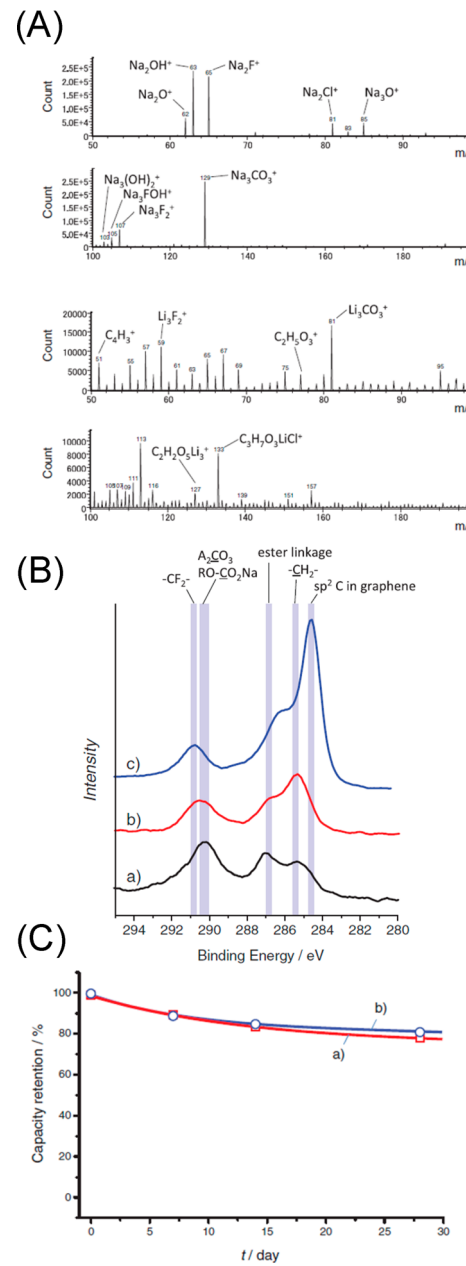


**Figure 31.** (A) TOF-SIMS positive-ion spectra for the hard-carbon electrodes after the first galvanostatic cycle in Na and Li cells. (B) XPS carbon 1s spectra for the hard-carbon electrodes tested in (a) Na and (b) Li cells after the first cycle and (c) pristine electrode. (C) Self-discharge tests of the hard-carbon electrodes after full insertion of (a) Na and (b) Li at the 10th cycle. Reprinted with permission from ref 5. Copyright 2011 WILEY-VCH Verlag GmbH&Co. KGaA, Weinheim.

chemical composition of the surface film are different between Li and Na cells. Electrolyte salts, additives, and binders also influence the components of surface layers of hard carbon, as expected from the data shown in Figures 28–30. Although NIBs are analogous to LIBs on the basis of the energy storage mechanism, understanding the characteristic behavior at bulk, surface, and interface of sodium insertion electrodes in the Na system is necessary to further improve the NIB performance.

#### 4.2. Ti-Based Compounds as Negative Electrode Materials

Titanium-based compounds, especially for titanium oxides (TiO<sub>2</sub> polymorphs) and Li titanate (spinel-type  $Li[Li_{1/3}Ti_{5/3}]$ )

$\text{O}_4$ ), have been extensively studied as potential negative electrode materials for rechargeable LIBs. Numerous titanium-based materials are known to be electrochemically active as host materials for Li insertion. In contrast, only two materials, NASICON-type  $\text{NaTi}_2(\text{PO}_4)_3$ <sup>296,297</sup> and  $\text{TiS}_2$ ,<sup>11,298</sup> were reported for the Na counterpart before 2010. Researchers in the field of battery materials have explored the titanium-based materials as potential negative electrodes for NIBs, and many publications have appeared in the past few years.<sup>299–312</sup> In this section, recent research achievements for titanium oxides and phosphates as Na insertion hosts are reviewed.

**4.2.1. Titanium Oxides and Titanates.** **4.2.1.1.  $\text{TiO}_2$  Polymorphs.** The most common form of titanium compounds is titanium dioxide,  $\text{TiO}_2$ .  $\text{TiO}_2$  consists of  $\text{TiO}_6$  octahedra with tetravalent titanium ions. Polymorphisms of  $\text{TiO}_2$  appear to be related to the difference in the linkage of  $\text{TiO}_6$  octahedra. Tetravalent titanium ions have no d electron, and all  $\text{TiO}_2$  polymorphs are therefore electrical insulators. Titanium dioxides, exceptionally stable, nontoxic, inexpensive, and abundant materials, have attracted significant attention as typical intercalation negative electrode materials for LIBs. Several  $\text{TiO}_2$  polymorphs have been synthesized and tested as insertion hosts for Li ions so far.<sup>313–317</sup> Among the polymorphs of  $\text{TiO}_2$ , anatase-type  $\text{TiO}_2$ , which is found as a natural mineral, is known as one of the oldest host structures studied for Li insertion.<sup>318</sup>  $\text{TiO}_6$  octahedra in anatase-type  $\text{TiO}_2$  share four edges with other octahedra, forming the three-dimensional framework structure with the distorted cubic close-packed (ccp) oxygen lattice (Figure 32a). Microsized anatase-type  $\text{TiO}_2$  can store reversibly 0.5 mol of lithium ions per formula. Although the first-principle calculations of Li and Na diffusion in the anatase-type lattice suggest that diffusion barriers for

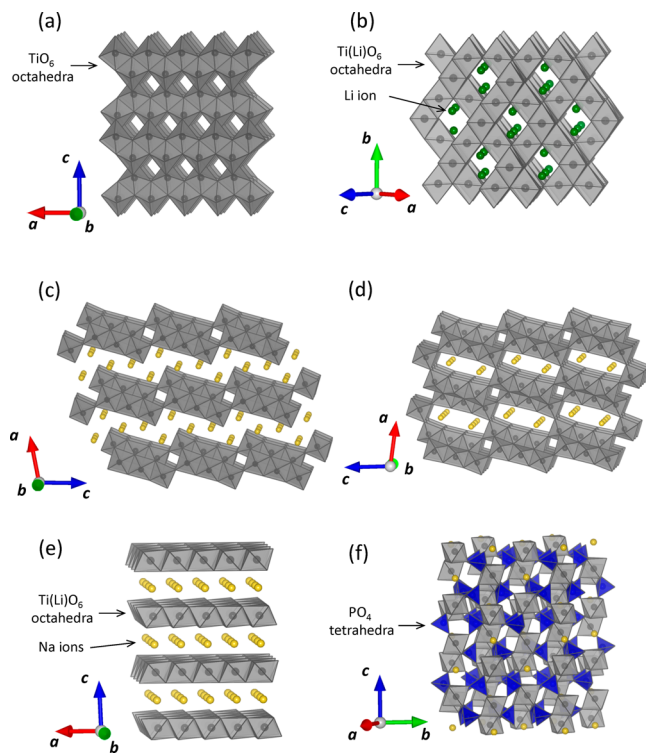


**Figure 32.** Schematic illustrations of (a) anatase-type  $\text{TiO}_2$ , (b)  $\text{Li}[\text{Li}_{1/3}\text{Ti}_{5/3}] \text{O}_4$ , (c)  $\text{Na}_2\text{Ti}_3\text{O}_7$ , (d)  $\text{Na}_2\text{Ti}_6\text{O}_{13}$ , (e) P2- $\text{Na}_{0.66}[\text{Li}_{0.22}\text{Ti}_{0.78}] \text{O}_2$ , and (f)  $\text{NaTi}_2(\text{PO}_4)_3$ .

both ions are similarly small,<sup>319</sup> micrometer-sized anatase is electrochemically inactive in Na cells. Recently, nanosized anatase (<30 nm) has been reported to be electrochemically active in Na cells.<sup>320,321</sup> Shortening of the migration length for Na insertion is an effective method to improve the electrode performance of  $\text{TiO}_2$ . A large reversible capacity of more than 150 mAh g<sup>-1</sup> is obtained (corresponding to approximately 0.5 mol of sodium insertion) in the voltage range of 0–2.0 V vs Na/Na<sup>+</sup> even though a large surface area of nanosized anatase inevitably results in low Coulombic efficiency (42%) in the initial cycle as shown in Figure 33a. The voltage profile of

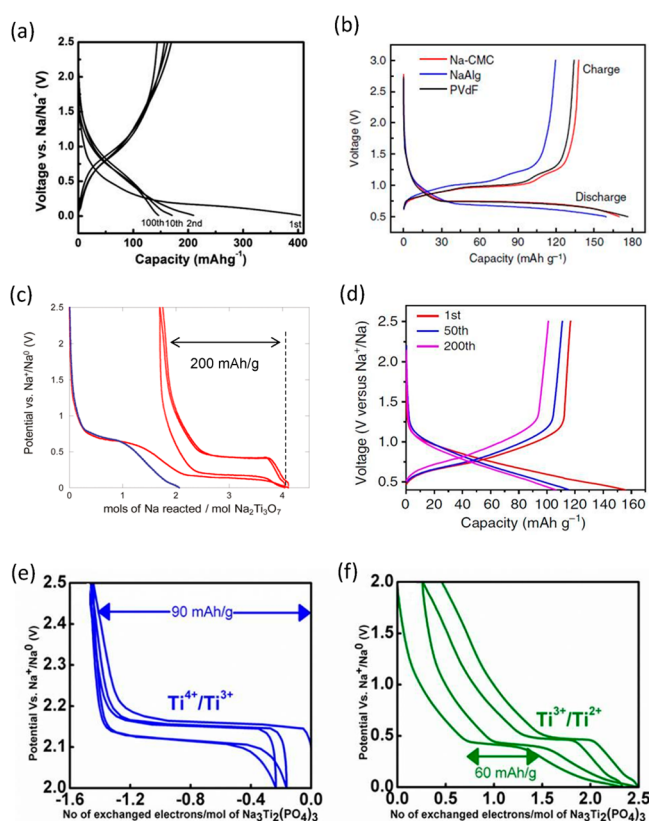


**Figure 33.** Charge/discharge profiles of titanium oxides, titanates, and phosphates in Na cells. (a) Nanosized anatase-type  $\text{TiO}_2$  electrodes. (b) Comparison of the initial charge/discharge curves of  $\text{Li}[\text{Li}_{1/3}\text{Ti}_{5/3}] \text{O}_4$  electrodes with PVdF, NaAlg, and CMC binders. (c) Electrode performance of the  $\text{Na}_2\text{Ti}_3\text{O}_7$  electrode. (d) Charge/discharge curves of a P2- $\text{Na}_{0.66}[\text{Li}_{0.22}\text{Ti}_{0.78}] \text{O}_2$  electrode and  $\text{Na}_3\text{Ti}_2(\text{PO}_4)_3$  electrodes cycled in the voltage range of (e) 2.5–2.0 and (f) 2.0 and 0.0 V. (a) Reprinted with permission from ref 320. Copyright 2013 The Royal Society of Chemistry. (b) Reprinted with permission from Macmillan Publishers Ltd.: (*Nature Communications*) (ref 302), copyright 2013. (c) Reprinted with permission from ref 308. Copyright 2011 American Chemical Society. (d) Reprinted by permission from Macmillan Publishers Ltd.: (*Nature Communications*) (ref 331), copyright 2013. (e, f) Reprinted with permission from ref 332. Copyright 2013 American Chemical Society.

nanosized anatase in Na cells is a sloping curve, and voltage plateaus are not observed. Note that similar voltage profiles are also reported for amorphous  $\text{TiO}_2$ <sup>322</sup> and nanosized bronze-type  $\text{TiO}_2$ ,<sup>323</sup> which is often described as  $\text{TiO}_2(\text{B})$ . Such behavior reminds us of the particle size dependency of rutile-type  $\text{TiO}_2$ ,<sup>324</sup> which consists of only corner-shared  $\text{TiO}_6$  octahedra and is known as the most energetically stable polymorph of  $\text{TiO}_2$ , as the Li insertion host. Micrometer-sized

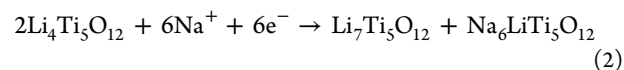
rutile-type  $\text{TiO}_2$  is less active in Li cells, while nanosized sample is highly active. Moreover, a similar sloping voltage profile to that of nanosized  $\text{TiO}_2$  in Na cells is reported.<sup>324</sup> Very recently, Passerini's research group<sup>321</sup> investigated the electrochemical performance dependence of  $\text{TiO}_2$  electrode on various electrolyte compositions (different salts and solvents). The best electrochemistry performance (specific capacity, cycling stability, and Coulombic efficiency) was obtained using  $\text{NaClO}_4$  salt in EC:PC binary solvents. Further systematic study is needed to understand the size dependency and voltage profile for the  $\text{TiO}_2$  polymorphs as Na/Li insertion host materials.

**4.2.1.2. Lithium Titanate,  $\text{Li}[\text{Li}_{1/3}\text{Ti}_{5/3}]O_4$ .** The most widely studied Li titanate is spinel-type  $\text{Li}[\text{Li}_{1/3}\text{Ti}_{5/3}]O_4$  (space group  $F\bar{d}3m$ ). This framework structure is classified as a cation-ordered rock-salt phase in which one-quarter of Li ions and all titanium ions are located at octahedral sites. The octahedral sites share edges, forming three-dimensional tunnels in the structure. Remaining Li ions are originally located at tetrahedral sites in the spinel framework structure as shown in Figure 32b. When  $\text{Li}^+$  ions are electrochemically inserted into  $\text{Li}[\text{Li}_{1/3}\text{Ti}_{5/3}]O_4$ , lithium ions at tetrahedral sites migrate into the adjacent octahedral sites, finally forming  $\text{Li}_2[\text{Li}_{1/3}\text{Ti}_{5/3}]O_4$ , accompanied by reduction from Ti(IV) to Ti(III). The most interesting character is no volume change of the unit cell after Li insertion, which is well known as a "zero-strain" negative electrode material.<sup>325,326</sup> Zero strain as an electrode material is highly beneficial, especially for long-term cycling. Additionally, the operating potential of  $\text{Li}[\text{Li}_{1/3}\text{Ti}_{5/3}]O_4$  is relatively high as a negative electrode: 1.55 V vs Li/ $\text{Li}^+$ . Therefore,  $\text{Li}[\text{Li}_{1/3}\text{Ti}_{5/3}]O_4$  is free from the electrolyte decomposition and the risk of unsafe Li plating and dendritic growth even though the energy density is inevitably lower than carbonaceous materials.

Recently, Zhao et al. reported for the first time electrochemical Na insertion into  $\text{Li}[\text{Li}_{1/3}\text{Ti}_{5/3}]O_4$ .<sup>301</sup> The reversible capacity in a Na cell is approximately 155 mAh g<sup>-1</sup> with a relatively low insertion/extraction voltage with a plateau at 0.7 V for discharge and the good cyclability as the oxide-based negative electrode material. Because of the lower potential operation of less than 1 V, electrolyte decomposition including the film-forming process is, however, inevitable in Na cells, leading to the lower Coulombic efficiency.<sup>302</sup> Similar to carbonaceous materials described in the former section, selection of binders is, therefore, important to improve the cyclability. Figure 33b compares the initial discharge and charge curves of  $\text{Li}[\text{Li}_{1/3}\text{Ti}_{5/3}]O_4$  electrodes with PVdF, Na alginate (NaAlg), and CMC binders cycled in 1 mol dm<sup>-3</sup> NaFSA EC:DEC electrolyte solution. The electrode with the NaAlg binder displays a relatively low discharge capacity (159 mAh g<sup>-1</sup>) and Coulombic efficiency of 75%, while the electrode with the CMC binder exhibits a high discharge capacity of 170 mAh g<sup>-1</sup> and Coulombic efficiency of 81%. The capacity of  $\text{Li}[\text{Li}_{1/3}\text{Ti}_{5/3}]O_4$  electrodes rapidly fades for the conventional PVdF electrode. In the case of the electrode with NaAlg binder, a relatively low reversible capacity is obtained in the initial few cycles; in subsequent cycles, the reversible capacity increases and reaches a stable value of approximately 150 mAh g<sup>-1</sup> after 20 cycles. Similarly, the electrode with the CMC binder exhibits a stable capacity of ~155 mAh g<sup>-1</sup> with excellent cyclic performance.

According to Sun et al., a reduction product of  $\text{Li}[\text{Li}_{1/3}\text{Ti}_{5/3}]O_4$  ( $\text{Li}_4\text{Ti}_5\text{O}_{12}$ ) in Na cells is a mixture between  $\text{Li}_2[\text{Li}_{1/3}\text{Ti}_{5/3}]O_4$  ( $\text{Li}_7\text{Ti}_5\text{O}_{12}$ ) and  $\text{Na}_2[\text{Li}_{1/3}\text{Ti}_{5/3}]O_4$  ( $\text{Na}_6\text{LiTi}_5\text{O}_{12}$ ) as shown

in eq 2 as a result of the segregation of Li and Na in the spinel framework structure.<sup>302,303</sup>



Diffusion of large  $\text{Na}^+$  ions in the narrow tunnels for the spinel framework structure and phase transition, however, require large barriers, and thus, the rate capability is also limited compared with the Li counterpart. The nanosize effect of Na insertion in  $\text{Li}[\text{Li}_{1/3}\text{Ti}_{5/3}]O_4$  has been systematically studied,<sup>303</sup> and the nanosize effect would be another important aspect for searching new materials for titanates.

**4.2.1.3. Sodium Titanates.** Several compounds which are formed by the Na oxides,  $\text{Na}_2\text{O}$ , with  $\text{TiO}_2$  can be represented as a composition series of  $\text{Na}_2\text{O}\cdot n\text{TiO}_2$ . Crystal structures for the series of Na titanates were studied in 1960s.<sup>327–329</sup> Recently,  $\text{Na}_2\text{O}\cdot n\text{TiO}_2$  ( $n = 3$ ),  $\text{Na}_2\text{Ti}_3\text{O}_7$ , has been studied as the host material for Na insertion.<sup>308</sup> A crystal structure of  $\text{Na}_2\text{Ti}_3\text{O}_7$  is shown in Figure 32c. The basic unit consists of a two-dimensional sheet of the composition  $(\text{Ti}_3\text{O}_7)^{2-}$  with edge-shared triple octahedral chains. Na ions are accommodated between the sheets of  $(\text{Ti}_3\text{O}_7)^{2-}$ .  $\text{Na}_2\text{Ti}_3\text{O}_7$  has the ability to reversibly accommodate two Na ions per formula unit (0.67 Na per Ti with 200 mAh g<sup>-1</sup>, corresponding to the reduction of 2/3 of the  $\text{Ti}^{4+}$  to  $\text{Ti}^{3+}$ ) at an average potential of 0.3 V vs Na (Figure 33c), which is the lowest voltage ever reported as topotactic insertion into oxide electrodes in Li/Na-ion batteries.

The  $\text{Na}_2\text{Ti}_3\text{O}_7$ /carbon black composite electrodes also have delivered large capacity at slow cycling rates with a small amount of capacity fade per cycle (177 mAh g<sup>-1</sup> at C/10).<sup>305</sup> Additionally, nanosized  $\text{Na}_2\text{Ti}_3\text{O}_7$  samples show high charge/discharge rate capability,<sup>300,305</sup> which seems to be much better than that of the spinel-type Li titanate. DFT calculation also suggests the relatively low diffusion barrier (0.18–0.22 eV for the adjacent site) for sodium ions in  $\text{Na}_2\text{Ti}_3\text{O}_7$ .<sup>330</sup> An important challenge for low-potential oxides is the reduction of irreversible capacity at the initial cycle and to extend cycle life. A large irreversible capacity is typically observed in the initial cycle, presumably related to electrolyte decomposition and the film-forming process at the titanium oxide surface (and carbon black) similar to carbon materials discussed above.<sup>305,308</sup> Capacity degradation probably originates from insufficient surface passivation of the particle of  $\text{Na}_2\text{Ti}_3\text{O}_7$ .

The electrode performance of  $\text{Na}_2\text{O}\cdot n\text{TiO}_2$  ( $n = 6$ ),  $\text{Na}_2\text{Ti}_6\text{O}_{13}$ , has been also reported.<sup>306</sup> Structural similarity between  $\text{Na}_2\text{Ti}_3\text{O}_7$  and  $\text{Na}_2\text{Ti}_6\text{O}_{13}$  was discussed in the literature.<sup>328</sup> Both samples are composed of the same unit of  $(\text{Ti}_3\text{O}_7)^{2-}$ . The chain of  $(\text{Ti}_3\text{O}_7)^{2-}$  is isolated in  $\text{Na}_2\text{Ti}_3\text{O}_7$ , forming the two-dimensional layered structure. In contrast, the unit of  $(\text{Ti}_3\text{O}_7)^{2-}$  shares each corner of  $\text{TiO}_6$  octahedra, forming the tunnel-type structure (Figure 32d). The electrochemical properties and reaction mechanisms have been examined; it can accommodate 0.85 mol of Na per formula unit and delivers a discharge capacity of more than 65 mAh g<sup>-1</sup> with a flat plateau at approximately 0.8 V.  $\text{Na}_2\text{Ti}_6\text{O}_{13}$  composite electrodes with carbon additives show stable cycling and good rate performance, which can be used for 5000 cycles at 20 C rate with acceptable capacity retention even though the energy density is much lower compared with layered  $\text{Na}_2\text{Ti}_3\text{O}_7$ .

Another layered sodium titanate has been prepared from  $\text{NaTi}_3\text{O}_6(\text{OH})\cdot 2\text{H}_2\text{O}$ .<sup>304</sup> The dehydrated form of  $\text{NaTi}_3\text{O}_6(\text{OH})\cdot 2\text{H}_2\text{O}$  can store approximately 1.3 Na<sup>+</sup> ions per

formula unit of the active material. A voltage plateau is observed at a low average potential of about 0.3 V vs Na. This sodium titanate is also used as the lithium insertion host and delivers a large reversible capacity ( $\sim 200 \text{ mAh g}^{-1}$ ) with a linear voltage profile from 0 to 1.5 V vs Li.<sup>304</sup>

Recently, a Li/Na-mixed titanate,  $\text{Na}_{0.66}[\text{Li}_{0.22}\text{Ti}_{0.78}]O_2$ , is also studied as the insertion host for Na ions.<sup>331</sup> A crystal structure of  $\text{Na}_{0.66}[\text{Li}_{0.22}\text{Ti}_{0.78}]O_2$  is classified as the P2-type layered structure. Titanium and lithium ions, which have similar ionic radii, are located at the edge-shared octahedral sites, forming  $[\text{Li}_{0.22}\text{Ti}_{0.78}]O_2^{0.66-}$  layers.  $\text{Na}^+$  ions are located at six oxygen-coordinated prismatic sites between the  $[\text{Li}_{0.22}\text{Ti}_{0.78}]O_2^{0.66-}$  layers as shown in Figure 32e. The theoretical capacity is calculated to be 104 mAh g<sup>-1</sup> based on the vacant sites in Na layers, and the observed reversible capacity nearly reaches the theoretical value using well-crystallized micrometer-sized particles. The average voltage of 0.75 V in Na cells is rather high compared to layered  $\text{Na}_2\text{Ti}_3\text{O}_7$ . It is noted that the volume change during Na insertion and extraction is quite small, less than 1.0%. Such a nearly zero-strain character with a single-phase reaction could be the remarkable advantage of  $\text{Na}_{0.66}[\text{Li}_{0.22}\text{Ti}_{0.78}]O_2$  as the electrode materials with good cyclability (Figure 33d). Indeed, long cycle life, more than 1200 cycles, with a fair capacity retention of 75% has been reported. The activation energy of Na diffusion in  $\text{Na}_{0.66}[\text{Li}_{0.22}\text{Ti}_{0.78}]O_2$  has been calculated to be relatively small, less than 0.4 eV. This result is also supported by the good rate capability in Na cells. Open diffusion paths for  $\text{Na}_2\text{Ti}_3\text{O}_7$  and  $\text{Na}_{0.66}[\text{Li}_{0.22}\text{Ti}_{0.78}]O_2$  are beneficial as Na insertion hosts. Micrometer-sized  $\text{Na}_{0.66}[\text{Li}_{0.22}\text{Ti}_{0.78}]O_2$  with zero-strain character on the charge/discharge process is a good candidate for cost-effective stationary use with a long cycle life.

The Na layered oxide,  $\text{NaTiO}_2$ , with Ti(III) has been described in the former section (Figure 12).

**4.2.2. Titanium Phosphates.** Similar to the vanadium(III) phosphate in the former section, NASICON-type  $\text{NaTi}_2(\text{PO}_4)_3$  can be used as an electrode material for NIBs. Delmas et al. first reported reversible electrochemical Na insertion into NASICON-type  $\text{NaTi}_2(\text{PO}_4)_3$ .<sup>296,297</sup>  $\text{TiO}_6$  octahedra are isolated from each other by corner-shared  $\text{PO}_4$ , forming the open structure with some sets of vacant sites for alkali ions. Four moles of sodium ions are accommodated in the framework structure of  $\text{Me}_2(\text{PO}_4)_3$  (Figure 32f). For the case of  $\text{NaTi}_2(\text{PO}_4)_3$ , 2 mol of sodium ions are electrochemically and reversibly inserted based on a  $\text{Ti}^{3+}/\text{Ti}^{4+}$  redox couple, forming  $\text{Na}_3\text{Ti}_2(\text{PO}_4)_3$ .

The theoretical capacity is calculated to be 133 mAh g<sup>-1</sup> if two  $\text{Na}^+$  are reversibly inserted/extracted. A large reversible capacity, corresponding to nearly theoretical capacity, is experimentally obtained in Na cells,<sup>332</sup> with a flat operating voltage of 2.1 V (Figure 33e). The operating voltage (vs Na) is higher compared to the oxide materials because of the inductive effect in phosphate when the same redox couple is used, in this case,  $\text{Ti}^{3+}/\text{Ti}^{4+}$ .<sup>103,104</sup> A detailed crystal structure of the sodiated phase,  $\text{Na}_3\text{Ti}_2(\text{PO}_4)_3$ , has been also reported.<sup>333</sup>  $\text{Na}_3\text{Ti}_2(\text{PO}_4)_3$  has the perfect ordering of sodium ions in the three-dimensional NASICON-type framework structure at room temperature.

Recently, Senguttuvan et al.<sup>312</sup> reported that an additional plateau appears at 0.4 V by further electrochemical reduction of  $\text{Na}_3\text{Ti}_2(\text{PO}_4)_3$  (Figure 33f), most likely corresponding to partial reduction of  $\text{Ti}^{3+}$  to  $\text{Ti}^{2+}$ . One additional  $\text{Na}^+$  is inserted into  $\text{Na}_3\text{Ti}_2(\text{PO}_4)_3$ , forming  $\text{Na}_4\text{Ti}_2(\text{PO}_4)_3$ . An interesting trial is a

symmetrical  $\text{Na}_3\text{Ti}_2(\text{PO}_4)_3$  cell using  $\text{Ti}^{3+}/\text{Ti}^{4+}$  and  $\text{Ti}^{2+}/\text{Ti}^{3+}$  redox couples as positive and negative electrodes, respectively. It has been demonstrated that the averaged operating potential is 1.7 V using the symmetrical phosphate cell.<sup>312</sup> The flat voltage of 2.1 V could restrict its use for battery application for NIBs with aprotic electrolyte. The disadvantage has turned into a benefit:  $\text{Ti}^{4+}$  can be reversibly reduced to  $\text{Ti}^{3+}$  in neutral aqueous solution without decomposition of water.<sup>309,310,334</sup> A comparative study of the electrode performance of  $\text{Na}-\text{Ti}_2(\text{PO}_4)_3$  in nonaqueous and aqueous electrolyte suggests excellent electrode performance with aqueous electrolyte at neutral pH.<sup>310</sup> Quite small polarization between reduction and oxidation with excellent rate capacity has been reported in aqueous electrolyte, which presumably originates from the small activation energy for the desolvation (dehydration) process and high ionic conductivity in aqueous electrolyte. Moreover, the cost of batteries could be reduced with aqueous electrolyte even though the sacrifice for energy density is unavoidable.

#### 4.3. Na Alloys and Other Sodiable Compounds as Negative Electrodes

In the former section, Na insertion materials, which show relatively small volume expansion by sodiation, were reviewed. In this section, electrode materials that accompany the Na insertion reaction with destruction and reconstruction of framework structures, such as Na–Me alloying electrodes, are reviewed.

##### 4.3.1. Background of Na Alloys and Compounds.

Group 14 and 15 elements (Figure 34a), including metals (Sn, Pb, Bi), metalloids (Si, Ge, As, Sb), and polyatomic nonmetal (P), are known to form binary compounds with Na. These electrode materials, alloying with Na or forming Na binary compounds, have been recently studied as potential negative

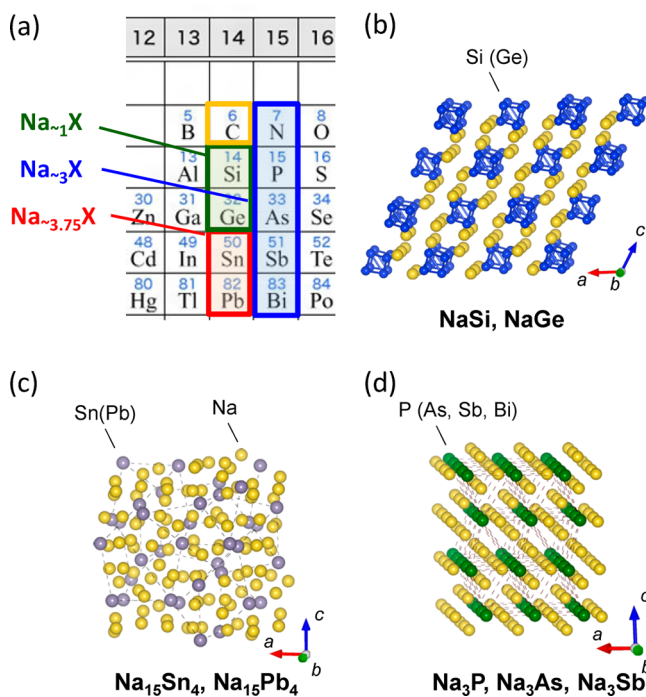


**Figure 34.** (a) Elements of groups 14 and 15 in the Periodic Table to form binary compounds with Na, and schematic illustrations of the most Na-rich phases for Si and Ge (a), Sn and Pb (b), and P, As, and Sb (c). Data derived from ref 348.

**Table 3.** Space Group, Density, and Theoretical Volume Expansion of Binary Na–Me Compounds<sup>a</sup>

element (E)	space group	density (g/cm <sup>3</sup> )	V/E (Å <sup>3</sup> / E)	reduction products (RP)	space group	density (g/cm <sup>3</sup> )	V/RP (Å <sup>3</sup> / RP)	ΔV (%)	ΔV/Na (Å <sup>3</sup> / Na)
Si	<i>Fd-3m</i>	2.33	20.0	Na	<i>Im3m</i>	0.97	39.3	39.3	
Sn	<i>I4<sub>1</sub>/amd</i>	7.29	27.1	Na <sub>15</sub> Sn <sub>4</sub> (Na <sub>3.75</sub> Sn)	<i>C2/c</i>	1.75	48.5	143	28.5
Sb	<i>R-3m</i>	6.70	30.2	Na <sub>3</sub> Sb	<i>I-43d</i>	2.40	141.8	423	30.6
P		2.16	23.8	Na <sub>3</sub> P	<i>P6<sub>3</sub>/mmc</i>	2.67	118.6	293	29.5
					<i>P6<sub>3</sub>/mmc</i>	1.78	93.3	292	23.2

<sup>a</sup>Me = Si (NaSi), Sn (Na<sub>15</sub>Sn<sub>4</sub>), Sb (Na<sub>3</sub>Sb), and P (Na<sub>3</sub>P). Data of Na metal are also shown for comparison. Phosphorus shows anomalously small volume expansion by sodiation (23.2 Å<sup>3</sup>/Na) as the binary Na–Me system. Reprinted with permission from ref 349. Copyright 2014 WILEY-VCH Verlag GmbH&Co. KGaA, Weinheim.

electrodes for rechargeable NIBs<sup>335–340</sup> and have the particularity to interact with a larger number of Na (compared to insertion materials), leading to a much higher capacity than hard carbon and titanium oxides.

In the past decade, Li alloys and binary compounds as electrode materials have been extensively studied, especially for the Li–Sn and Li–Si systems because of the much higher reversible capacity than that of the Li–graphite system, which now almost reaches its theoretical limit in practical LIBs.<sup>341–344</sup> In addition to the group 14 and 15 elements, aluminum as a group 13 element forms a binary alloy with Li. Copper is, therefore, used as a current collector for negative electrode materials for rechargeable Li batteries, while an aluminum current collector is used for a positive electrode. In contrast, Na does not form an alloy with aluminum that can be used as the current collector for rechargeable Na batteries. Use of cost-effective aluminum is an additional practical advantage of the NIB system, which could reduce the total cost of batteries, compared to LIBs.

Electrochemical lithiation of silicon to form lithium silicide, Li<sub>15</sub>Si<sub>4</sub> (Li<sub>3.75</sub>Si), is known as the most Li-rich phase, which has been evidenced experimentally in numerous studies, whereas NaSi (Figure 34b) is known as the most Na-rich phase of Na–Si binary compounds.<sup>345</sup> The capacity estimated based on formation of NaSi is inevitably lower than that of the Li system with Li<sub>3.75</sub>Si. Furthermore, to the best of our knowledge, electrochemical formation of NaSi in a Na cell has not been reported experimentally so far.<sup>346,347</sup>

Additionally, Chevrier and Ceder pointed out the significantly lower volumetric energy density for the Na-based alloys in comparison to the Li-based alloys.<sup>348</sup> The volumetric capacity of Na alloys with Pb and Sn is limited to ~1130 mAh cm<sup>-3</sup>. The volume occupied by Na atoms in a series of Na–Me alloy system during sodiation is essentially independent of Me (Si, Ge, Sn, and Pb as group 14 elements) and sodiation level, which is constant at 30.3 Å<sup>3</sup> per a Na atom, corresponding to 18.2 mL/mol as the molar volume of Na in the Na–Me alloys (see also Table 3).<sup>348</sup> The volume change is more than twice as large as that of Li (14.8 Å<sup>3</sup>/Li and 8.9 mL/mol).<sup>341</sup> This fact inevitably results in difficulty in utilizing the alloy-based negative electrode materials for energy storage devices, in comparison to insertion-based negative electrode materials. Such huge volume expansion could restrict the long-term continuous cycling as an electrode material. The large volume expansion, depending on the amount of Na ions incorporated into the structures, is unavoidable in this system, while in many cases the volume expansion for Na insertion materials does not exceed 120%. Therefore, during successive cycles of charge/discharge the material suffers from high mechanical stress and repeated passivation. The cracking in the

composite electrodes leads to a loss of electrical contact and results in capacity loss.

Several strategies have been developed to overcome these problems in relation to the large volume change as shown in the next section, including binders, electrolyte additives, preparation of nanoarchitected samples, etc. Note that the pioneering early research was published in 1987 by Jow et al.<sup>23</sup> A Na–Pb binary alloy, showing large volume expansion (>400%) on electrochemical cycling, shows surprisingly stable cycles in Na cells. A lead composite electrode with a conductive polymer, poly(*p*-phenylene), and a nonfluorinated polymer as the binder shows excellent cyclability in Na cells.<sup>23</sup> Although lead as a heavy element could limit its use in the practical application, achievement of excellent cyclability using the Na alloy is the first important discovery in this topic. Another recent important discovery would be that reversible three-electron redox of phosphorus has been demonstrated in Na cells.<sup>339,349,350</sup> Phosphorus boosts gravimetric energy density up for the Na system (theoretical capacity based on the three-electron redox reaches approximately 2600 mAh g<sup>-1</sup>) as shown in Figure 35a. Moreover, some improvement of volumetric capacity, beyond the limit of molar volume of metallic Na, is also anticipated (Figure 35b) as further discussed in a later section.<sup>349</sup>

#### 4.3.2. Tin and Antimony as Alloy Electrode Materials.

Tin and antimony form binary alloys with sodium. Electrochemical alloying/dealloying for the Na–Sn system occurs in a series of steps, Sn, Na<sub>0.6</sub>Sn, Na<sub>1.2</sub>Sn (amorphous), Na<sub>5</sub>Sn<sub>2</sub>, and Na<sub>15</sub>Sn<sub>4</sub> at 25 °C.<sup>351</sup> When the Sn forms Na<sub>15</sub>Sn<sub>4</sub> by sodiation, the theoretical capacity reaches 847 mAh g<sup>-1</sup>. Formation of Na<sub>15</sub>Sn<sub>4</sub> phase after full reduction of Sn in the Na cell has been experimentally observed.<sup>347,351–353</sup> In addition, formation of crystalline NaSn and an unidentified phase, Na<sub>x</sub>Sn ( $x \approx 2.25$ ), has been reported in Na cells at 90 °C.<sup>352</sup> This phase was later identified as Na<sub>5</sub>Sn<sub>2</sub> with a hexagonal lattice.<sup>351</sup>

Recently, it has been demonstrated that the reversibility of the alloying/dealloying for Sn electrodes is effectively improved by use of a polyacrylate (PAA) binder.<sup>347</sup> The Sn–PAA electrode delivers a high reduction and oxidation capacity of 880 and 760 mAh g<sup>-1</sup>, respectively (Figure 36). The specific capacity and Coulombic efficiency are effectively improved by adopting the PAA binder instead of PVdF as seen in Figure 36. The averaged operating potential is remarkably low for the Sn electrode, which is advantageous to increase the energy density. Nevertheless, the Sn–PAA electrode shows insufficient capacity retention, most probably due to the inevitable volume change of the electrode material and electrolyte decomposition at the active surface of Na–Sn alloys. When a small amount of FEC is added to electrolyte, the performance of the Sn electrode with PAA is further improved, similar to hard carbon and titanium

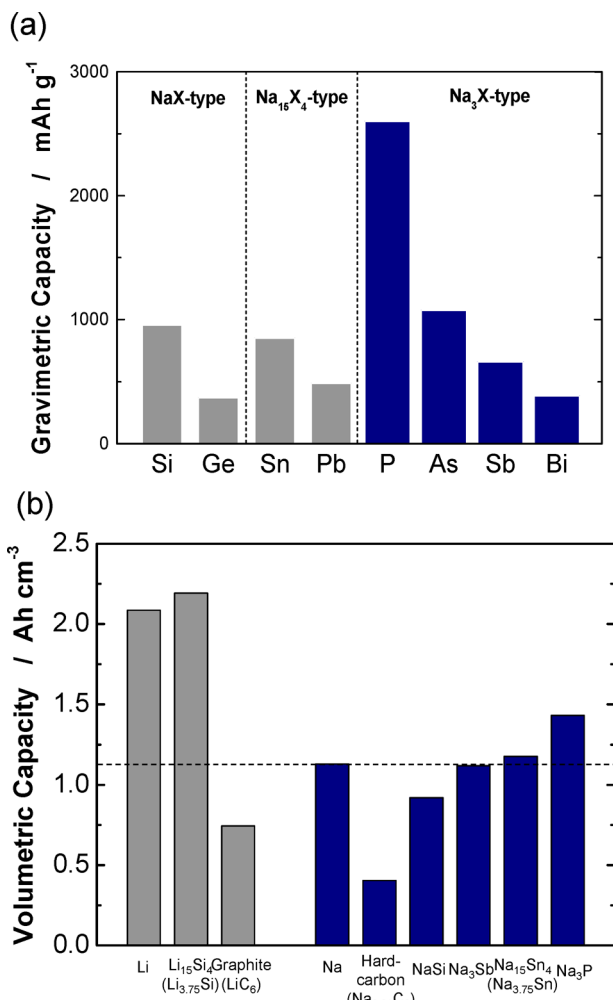


**Figure 35.** (a) Theoretical gravimetric capacity estimated from phase diagrams for the group 14 and 15 elements. (b) Theoretical volumetric capacity of Si, Sn, Sb, and P electrodes in Na cells. Hard carbon as Na insertion material is also compared. For hard carbon, 300 mAh g<sup>-1</sup> of charge capacity and formation of Na<sub>0.134</sub>C (Na<sub>0.81</sub>C<sub>6</sub>) with a density of 1.7 g cm<sup>-3</sup> are assumed for the calculation. Metallic lithium, Li–Si, and Li–graphite systems are also shown for comparison. Reprinted with permission from ref 349. Copyright 2014 WILEY-VCH Verlag GmbH&Co. KGaA, Weinheim.

oxides as discussed above. As shown in Figure 36, the Sn electrode delivers 700 mAh g<sup>-1</sup> of reversible capacity for more than 20 cycles, which is more than two times larger reversible capacity compared with a hard-carbon electrode.

Qian et al. prepared an Sb/C composite electrode by mechanical ball milling of Sb powder with conductive carbon.<sup>354</sup> They found that the Sb/C electrode delivers a reversible capacity of 610 mAh g<sup>-1</sup>, which corresponds to the capacity based on three-electron redox of Sb and alloying with Na (Figure 37a). Good rate capability is also demonstrated; 50% of capacity is retained at a high current of 2000 mA g<sup>-1</sup> with long-term cycle stability. Although the Sb/C electrode in the FEC-free electrolyte can only be cycled in the first 50 cycles, the cyclability is highly improved by adding 5% FEC into the electrolyte solution, similar to the Sn electrode. In the optimized electrolyte, the Sb/C electrode demonstrates a long-term cycling stability with 94% capacity retention over 100 cycles (Figure 37b).

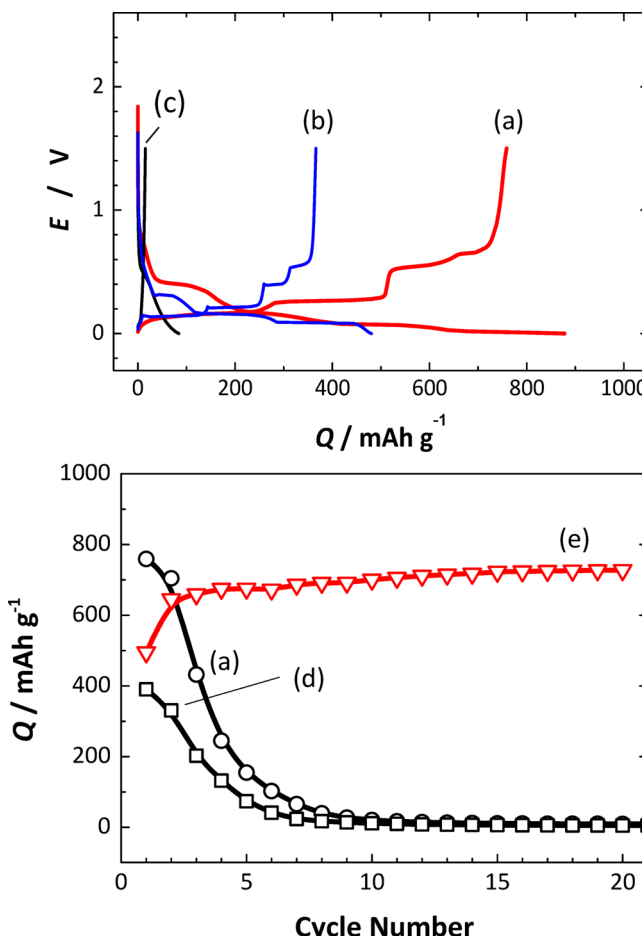


**Figure 36.** (Top) Initial galvanostatic reduction and oxidation curves and (bottom) reversible capacity variation of (a) Sn–PAA, (b) Pb–AA, (c) Si–PAA, (d) Sn–PVdF, and (e) Sn–SNO<sub>3</sub>–PANA. Reprinted with permission from ref 364. Copyright 2014 PCCP Owner Societies.

The reaction mechanism of Sb in Na cells has been studied by an in-situ XRD method.<sup>355</sup> Crystalline Sb is electrochemically reduced to form Na<sub>x</sub>Sb as an amorphous phase. Amorphous Na<sub>x</sub>Sb is further reduced to crystalline Na<sub>3</sub>Sb with a hexagonal lattice through formation of cubic Na<sub>3</sub>Sb as a metastable intermediate phase. Crystalline Na<sub>3</sub>Sb is oxidized in Na cells and changes into amorphous Sb as the oxidation product.

An alloy of Sn and Sb was also examined as a negative electrode in Na cells.<sup>356</sup> A composite electrode of SnSb/C was prepared using a high-energy mechanical milling method. The SnSb/C electrode demonstrated high initial capacity (540 mAh g<sup>-1</sup>) with good cyclability: 80% capacity retention over 50 cycles. In addition, compared with the simple metals, Sn/C and Sb/C composite electrodes, the SnSb/C electrode shows better capacity retention and good rate capability. Moreover, the charge/discharge profile is sloping, and no voltage plateaus are observed in the SnSb/C electrodes. The electrochemical behavior of the Sn–Sb alloy is clearly different from each metal.

Recently, Monconduit and co-workers reported reaction mechanisms of SnSb alloy in the Na cells.<sup>336</sup> Reduction of the SnSb alloy in Na cells results in formation of an amorphous phase (and/or nanocrystalline phase with low crystallinity), which is clearly different from the character observed for the

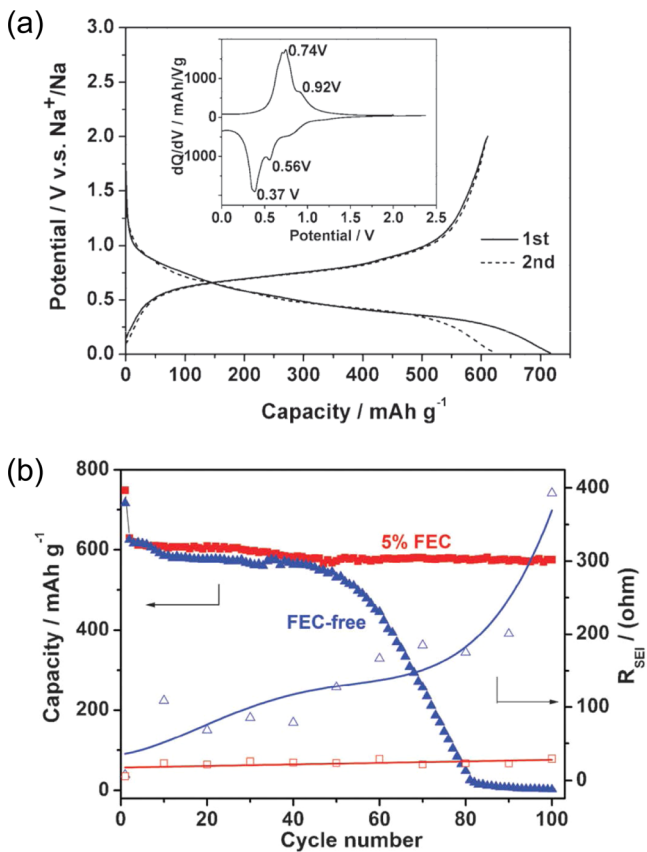


**Figure 37.** (a) Charge/discharge curves of the Sb/C composite electrode at  $100 \text{ mA g}^{-1}$ , (inset) differential capacity versus potential; (b) cycle retention and SEI film resistances of the Sb/C with (red) and without (blue) FEC addition. Reprinted with permission from ref 354. Copyright 2012 The Royal Society of Chemistry.

simple metals of Sn and Sb (formation of crystalline phases after full electrochemical reduction).

**4.3.3. Phosphorus-Based Materials.** Phosphorus, a nonmetallic element of the group 15 in the periodic table, has three main allotropes: white, red, and black phosphorus. Red phosphorus is a relatively stable allotrope of phosphorus, and both amorphous and crystalline phases are known to be present. As electrode materials for Na cells, in 2012, the three-electron reversible redox process of red phosphorus electrodes was reported in Na cells (theoretical capacity is calculated to be approximately  $2600 \text{ mAh g}^{-1}$ ) and its potential application in rechargeable Na batteries has been demonstrated.<sup>357</sup> Very recently, similar results using phosphorus–carbon composites have also been reported as electrode materials for Na cells.<sup>339,350</sup> One can note that  $\text{Na}_3\text{P}$  as the reduction product releases flammable and toxic phosphine,  $\text{PH}_3$ , upon hydrolysis. This will inevitably restrict and limit its practical use, similar to Na/S batteries. Nevertheless, phosphorus electrodes have interesting and important characteristics as electrode materials in Na cells. Briefly, it is the anomalously small volume expansion during the sodiation process that is different from other Na-based alloys.<sup>348,349</sup> Since Na atoms have covalent character in  $\text{Na}_3\text{P}$  as the reduction product, the apparent molar volume of Na is reduced to 77% and 59% based on the Na–Me alloys and metallic Na, respectively.<sup>349</sup> Therefore, the theoretical volumetric capacity of phosphorus electrodes exceeds 27% of the capacity for metallic Na (Figure 35b and Table 3).

Although the expected volume expansion by sodiation is lower than other Na alloys, a severe problem of electrolyte decomposition has been also found at the highly reactive surface of  $\text{Na}_3\text{P}$ . Cyclability is much better for a Li counterpart,  $\text{Li}_3\text{P}$ .<sup>349</sup> Similar to the Sn and Sb systems as Na alloys, the reversibility of formation of sodium phosphide in Na cells is successfully improved by utilizing nonfluorinated binders, such as sodium polyacrylate (PANA)<sup>339,349</sup> and sodium carboxymethyl cellulose (CMCNa)<sup>350</sup> with electrolyte additives such as FEC<sup>204,349</sup> as shown in Figure 38a and 38b. As recently

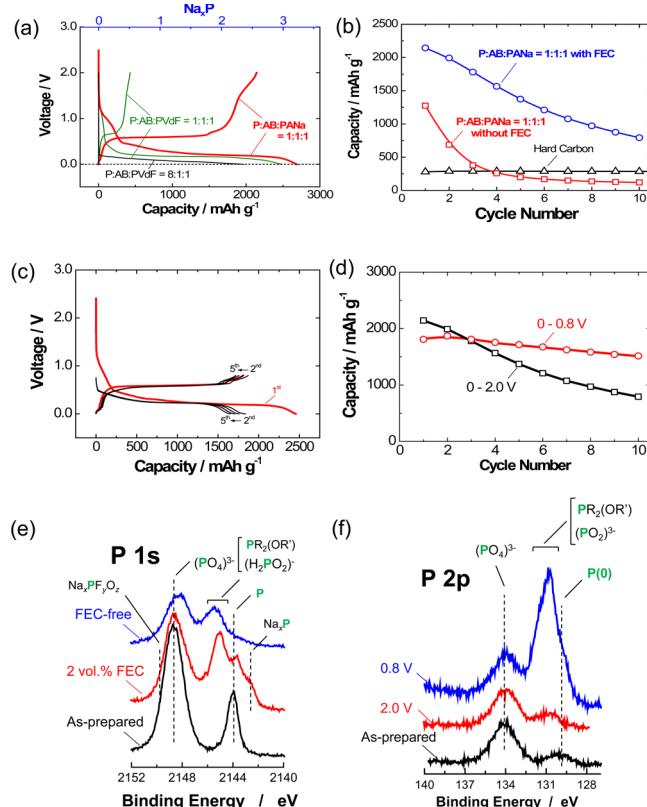


**Figure 38.** Electrochemical properties of red phosphorus//Na cells at a rate of  $50 \text{ mA g}^{-1}$ . (a) Galvanostatic charge/discharge curves with different phosphorus concentration and binders (PVDF or PANA). (b) Comparison of capacity retention with or without FEC. (c) Electrode performance of the phosphorus electrodes with an upper cutoff voltage of 0.8 V. (d) Capacity retention of the Na cells. (e) Hard X-ray photoelectron spectra of red phosphorus electrodes. Electrolyte decomposition products are enriched at the electrode surface with FEC-free electrolyte. (f) Soft X-ray absorption spectra of red phosphorus electrodes with different cutoff voltage. Compounds containing monovalent phosphorus are accumulated in the surface layer when cutoff voltage is limited to 0.8 V. Surface layer is clearly changed by oxidation to 2.0 V, probably leading to degradation of capacity retention as shown in d. Reprinted with permission from ref 349. Copyright 2014 WILEY-VCH Verlag GmbH&Co. KGaA, Weinheim.

reported, X-ray photoelectron spectroscopy reveals that phosphorus species are incorporated in the surface film, and electrolyte decomposition is effectively suppressed by the use of FEC (Figure 38e).<sup>349</sup> Cyclability is further improved by lowering the cutoff voltage to 0.8 V as shown in Figure 38c and 38d. It has been found (by X-ray photoelectron spectroscopy) that surface layers containing phosphorus species are easily oxidized on charge to 2.0 V as found by soft X-ray

photoelectron spectroscopy (Figure 38f), resulting in the loss of reversible capacity. Cyclability is also significantly improved using  $\text{NaPF}_6$  as salts of electrolyte instead of  $\text{NaClO}_4$ . Acceptable capacity retention of more than 50 cycles and good rate capability have been reported using the  $\text{NaPF}_6$ -based electrolyte solution with well-optimized phosphorus/carbon composite electrodes.<sup>339,350</sup>

Black phosphorus is the least reactive allotrope and has higher electrical conductivity compared with white and red phosphorus.<sup>358,359</sup> Black phosphorus can be prepared from red phosphorous by high-pressure synthesis under 4.5 GPa at high temperature (900 °C). It is also prepared by mechanical milling with mixer mill and planetary ball-mill apparatuses.<sup>360</sup> Similar to red phosphorus, black phosphorus is reported to show high lithiation capacity as a negative electrode for Li cells.<sup>361,362</sup> For instance, Park and Sohn<sup>362</sup> reported that black phosphorus with an orthorhombic lattice shows a large initial capacity above 2000 mAh g<sup>-1</sup>. Similar to this work, Marino and co-workers<sup>363</sup> developed a phosphorus/carbon composite electrode with ordered mesoporous carbon, which showed improved capacity retention as an electrode material in Li cells. In 2013, the electrode performance of black phosphorus in Na cells was also reported.<sup>350</sup> However, electrode performance seems to be insufficient compared with the amorphous phase. Very recently, it was demonstrated that a black phosphorus electrode with the PANa binder shows high specific capacity and excellent cycling performance in Na cells.<sup>364</sup> The black phosphorus electrode with PANa binder shows high initial charge and discharge capacities of 2050 and 1620 mAh g<sup>-1</sup>, respectively, at rate of 125 mAh g<sup>-1</sup> in 1 mol dm<sup>-3</sup>  $\text{NaPF}_6$  EC:DEC. Averaged Coulombic efficiency reaches 97% from the second cycle. The charge/discharge capacities of the black phosphorus electrode slowly decrease during a continuous cycle test. Cyclability in 1 mol dm<sup>-3</sup>  $\text{NaPF}_6$  EC:DEC solution is further improved using the FEC additive.<sup>364</sup>

Similar to allotropes of elemental phosphorus, phosphorus-containing compounds, such as nickel phosphide ( $\text{NiP}_3$ ), are also electrochemically active in Na cells. Fullenwarth et al.<sup>365</sup> reported that  $\text{NiP}_3$  electrode shows good capacity retention with a high reversible capacity of over 900 mAh g<sup>-1</sup>. It has been proposed that formation of  $\text{Na}_3\text{P}$  embedding Ni nanoparticles is the final reaction product after full electrochemical reduction. The voltage profile of  $\text{NiP}_3$  in Na cells resembles that of elemental phosphorus with an average desodiation potential between 0.3 and 0.8 V vs  $\text{Na}/\text{Na}^+$ , which is slightly higher than that of hard-carbon electrodes. This character could be beneficial to improve the safety as a negative electrode for NIB applications because of the lower chance of Na plating on charge.

In conclusion, the main problem of Na alloy and compounds as electrode materials lies in the volume expansion of electrode materials correlated with destruction of structures of starting materials in reaction with Na. There are more tough challenges in the Na system compared with the Li system because the molar volume of Na is much larger than that of Li. The current research is essentially to control at least the unfavorable effects of volume changes of the electrodes during cycling and to suppress the loss of electronic conduction in the composite electrodes. These issues greatly penalize the life and kinetics of the charge/discharge reaction for batteries on these electrode materials. Further optimization of alloy compositions and structures and careful study of the structural changes for the different alloy phases during the electrochemical reactions will

lead to further improvement of the electrochemical performance.<sup>337–339,350,353,365,366</sup> In addition, further understanding the interphase of the electrode materials,<sup>349</sup> coupled with studies on binders and electrolyte, will be an important subject as shown in this review.

In this section, many different negative electrode materials have been reviewed. The reversible capacity, average voltage, and estimated energy density as NIBs (full cells) for these electrode materials are plotted in Figure 39. Herein, high-

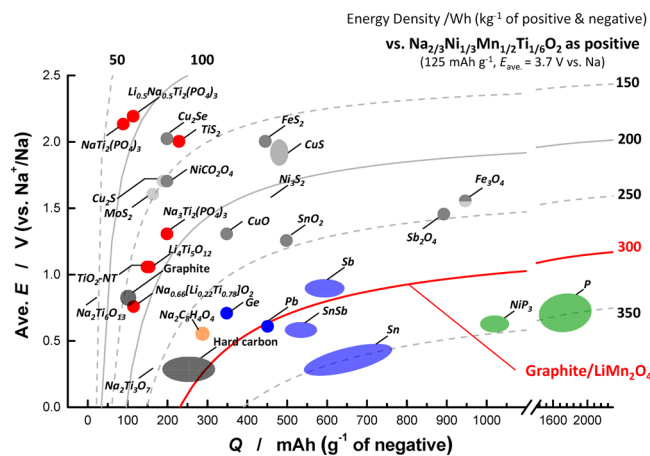


**Figure 39.** Average voltage (V) and energy density (Wh kg<sup>-1</sup>) versus gravimetric capacity (mAh g<sup>-1</sup>) for negative electrodes materials for NIBs: (black circles) carbonaceous materials, (red circles) oxides and phosphates as sodium insertion materials, (blue circles) alloy, (green) phosphide/phosphorus, and (gray circles) oxides and sulfides with conversion reaction. Energy density based on weight of active materials in positive and negative electrodes is calculated using their reversible discharge capacity. Positive electrode is assumed to be  $\text{Na}_{2/3}[\text{Ni}_{1/3}\text{Mn}_{1/2}\text{Ti}_{1/6}]_{\text{O}_2}$  for the calculation. Data derived from refs 11, 145, 163, 239, 244, 301, 305–307, 320, 331, 332, 340, 346, 349, 354, 356, 364, 365, and 367–375.

voltage  $\text{Na}_{2/3}\text{Ni}_{1/3}\text{Mn}_{1/2}\text{Ti}_{1/6}\text{O}_2$ <sup>131</sup> shown in Figure 13 is hypothetically used as a positive electrode material for NIBs as the full cells. The estimated energy density for hard carbon reaches 300 mWh g<sup>-1</sup> based on the mass of active materials. The electrode materials based on the insertion reaction (and conversion reaction) show relatively low energy density, except  $\text{Na}_2\text{Ti}_3\text{O}_7$ . The gravimetric energy density of NIBs potentially increases to 350 mWh g<sup>-1</sup> using Sn and P. Although phosphorus shows high reversible capacity, the estimated energy density as NIBs is similar to Sn. The reversible capacity for both Sn and P is much larger than that of the positive electrodes, and therefore, the energy density of NIBs highly depends on the reversible capacity and operating voltage of positive electrode materials. For instance, even for the case of Sn, NIB consists of 80% of the positive electrode material (ca. 200 mAh g<sup>-1</sup>) vs 20% of Sn as the negative electrode material (ca. 800 mAh g<sup>-1</sup>) to balance the capacity for both electrodes. In this case, the operating voltage of tin is slightly lower vs Na metal (higher as the NIBs) than that of phosphorus. High-capacity positive electrode materials, which are suitable to combine with the high-capacity phosphorus electrodes, are clearly needed to further increase the energy density of NIBs.

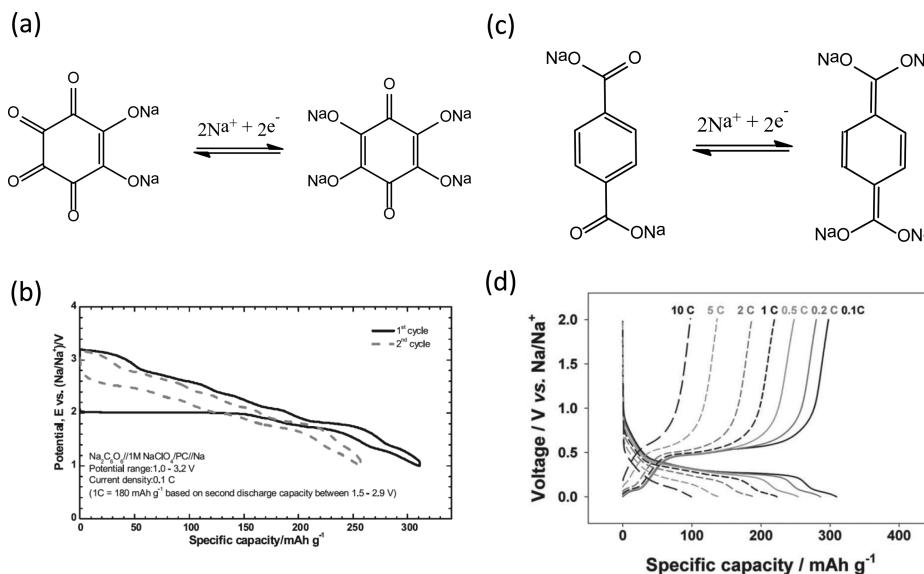


**Figure 40.** Reaction mechanism and electrode performance of organic molecules in Na cells: (a, b)  $\text{Na}_2\text{C}_6\text{O}_6$  and (c, d)  $\text{Na}_2\text{C}_8\text{H}_4\text{O}_4$ . (b) Reprinted with permission from ref 267. Copyright 2013 Elsevier. (d) Reprinted with permission from ref 367. Copyright 2012 WILEY-VCH Verlag GmbH&Co. KGaA, Weinheim.

## 5. ORGANIC COMPOUNDS AS ELECTRODE MATERIALS

On the basis of the material abundance, organic compounds without transition metals are also an attractive candidate as electrode materials. Many different organic systems with conjugated structures have been proposed in the Li system.<sup>376</sup> Historically, organic electrode materials for energy storage devices with metallic lithium started from a p-type conductive polymer with anion doping for charge compensation.<sup>377</sup> Since this type of reaction is not influenced by cation species, these electrode materials can be easily applied to the Na system. Indeed, aniline/o-nitroaniline conductive copolymer delivers a large reversible capacity of  $180 \text{ mAh g}^{-1}$  with an average potential of 3.2 V in Na cells and remains at  $170 \text{ mAh g}^{-1}$  after 50 cycles.<sup>378</sup> Polytriphenylamine also shows similar electrode performance in the Na cells.<sup>379</sup> Recently, bipolar porous organic electrode (BPOE), with a porous-honeycomb and polymeric framework consisting of benzene rings and triazine, has been also reported as a potential positive electrode material.<sup>380</sup> However, the change in the concentration of the salt in the electrolyte is unavoidable on electrochemical cycles in the anion doping system, similar to electrochemical double-layer capacitors.

Organic molecules and polymers with conjugated carbonyl groups have been also studied as potential positive electrode materials in the Li system. Dilithium rhodizonate ( $\text{Li}_2\text{C}_6\text{O}_6$ ) has been proposed as high-capacity organic electrode materials for rechargeable lithium batteries.<sup>381</sup> The conjugated carbonyl group ( $>\text{C}=\text{O}$ ) is reversibly reduced in the Li cells with aprotic solvent, and lithium ions are inserted (absorbed) for the charge compensation to form a lithium methoxide ( $>\text{C}(\text{O}-\text{Li})-\text{O}-\text{Li}$ ) group. After this work, the electrode performance of disodium rhodizonate ( $\text{Na}_2\text{C}_6\text{O}_6$ ) in Na cells has been also reported with a reduction of conjugated carbonyl groups as shown in Figure 40a and 40b.<sup>267</sup> The  $\text{Na}_2\text{C}_6\text{O}_6$  electrode exhibited good electrochemical properties (Figure 40b): a high reversible capacity of  $170 \text{ mAh g}^{-1}$  with good cycle performance when the voltage range was carefully controlled. The electrochemical properties of disodium croconate ( $\text{Na}_2\text{C}_5\text{O}_5$ ) in Na cells have

been also found in the literature.<sup>382</sup> Recently, the electrode performance of indigo carmine, which has conjugated carbonyl groups, has been also reported.<sup>383</sup> A major problem of disodium rhodizonate, presumably also for other organic molecules, is found in relatively high solubility in aprotic solvent and inferior electrical conductivity. A relatively large amount of conductive carbons is needed in the composite electrode to increase the electrode performance. As a polymer-based material with conjugated carbonyl groups, poly-anthraquinonyl sulfide) has been recently studied as an electrode material in Na cells.<sup>379</sup> Solubility would be lowered using such polymers even though the reversible capacity is also lowered compared with disodium rhodizonate.

Organic molecules with conjugated carboxyl groups have been proposed as potential negative electrode materials for the Li system. For instance, Armand et al. studied conjugated dicarboxylate-based materials, such as dilithium terephthalate, as organic negative electrodes for Li batteries.<sup>384</sup> Similar to the Li system, the electrode performance of disodium terephthalate ( $\text{Na}_2\text{C}_8\text{H}_4\text{O}_4$ ) in Na cells as organic materials has been reported.<sup>367,385,386</sup> Disodium terephthalate can reversibly insert two sodium ions in terephthalate as shown in Figure 40c and 40d. In addition, electrode performance is potentially modulated by the molecular design with different functional groups and regioisomerism in the structures.<sup>387</sup>

The discharge profile of a disodium terephthalate electrode shows a voltage plateau at 0.3–0.5 V (Figure 40d) even though irreversible electrolyte decomposition to form the surface layers results in lower Coulombic efficiency (approximately 60%) at the first cycle.<sup>367</sup> The operating potential of disodium terephthalate in Na cells is found at around 0.4 V, which is beneficial as a negative electrode similar to the phosphorus electrode. Disodium terephthalate delivers a large reversible capacity (over  $250 \text{ mAh g}^{-1}$ ) with good capacity retention in Na cells.<sup>367,385,386</sup>

The organic tetrasodium salt of 2,5-dihydroxyterephthalic acid ( $\text{Na}_4\text{C}_8\text{H}_2\text{O}_6$ ) containing both conjugated carbonyl and carboxyl groups has been proposed as a bifunctional material as a positive (based on redox of  $\text{Na}_2\text{C}_8\text{H}_2\text{O}_6/\text{Na}_4\text{C}_8\text{H}_2\text{O}_6$  at 2.3 V

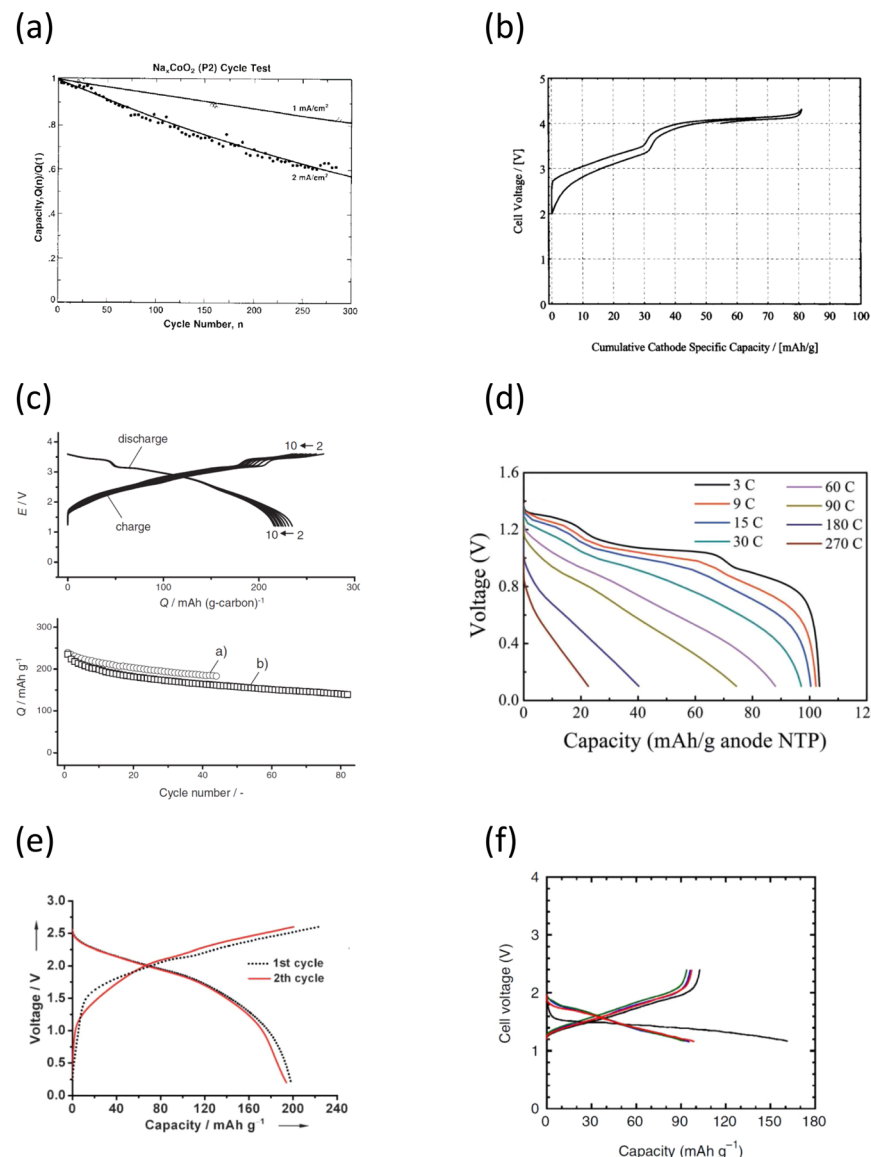


**Figure 41.** Battery performance of sodium ion full cells without metallic sodium: (a)  $\text{Na}_x\text{Pb}/\text{P2}-\text{Na}_{2/3}\text{CoO}_2$  cell, (b)  $\text{HC}/\text{NaV}(\text{PO}_4)\text{F}$  cell, (c)  $\text{HC}/\text{O}_3\text{-Na}[\text{Ni}_{1/2}\text{Mn}_{1/2}]\text{O}_2$  cell, (d)  $\text{NaTi}_2(\text{PO}_4)_3/\text{Na}_0.44\text{MnO}_2$  cell, (e)  $\text{Na}_4\text{C}_8\text{H}_2\text{O}_6/\text{Na}_4\text{C}_8\text{H}_2\text{O}_6$  cell, and (f)  $\text{Na}_x\text{Sn}/\text{Na}_3\text{PS}_4$  glass-ceramic/TiS<sub>2</sub> cell. Aprotic polar solvents with Na salts were used for a–c and e as electrolyte. (a) Reprinted with permission from ref 83. Copyright 1988 The Electrochemical Society. (b) Reprinted with permission from ref 212. Copyright 2003 The Electrochemical Society. (c) Reprinted with permission from ref 5. Copyright 2011 WILEY-VCH Verlag GmbH&Co. KGaA, Weinheim. (d) Reprinted with permission from ref 394. Copyright 2013 WILEY-VCH Verlag GmbH&Co. KGaA, Weinheim. (e) Reprinted with permission from ref 388. Copyright 2014 WILEY-VCH Verlag GmbH&Co. KGaA, Weinheim. (f) Reprinted by permission from Macmillan Publishers Ltd.: (*Nature Communications*) (ref 397), copyright 2012.

vs Na metal) and negative (redox of  $\text{Na}_4\text{C}_8\text{H}_2\text{O}_6/\text{Na}_6\text{C}_8\text{H}_2\text{O}_6$  at 0.3 V at Na metal) electrode with approximately 200 mAh g<sup>-1</sup> of reversible capacity.<sup>388</sup> This material can be used as the electrode material for transition-metal-free and symmetrical organic NIBs, even though the volumetric energy density is relatively low when compared with transition-metal oxides, polyanion compounds, and carbonaceous materials.

Recently, polymeric Schiff bases have been also reported as potential negative electrodes.<sup>389</sup> In the polymeric Schiff base,  $-\text{N}=\text{CH}-$  and  $\text{Ar}-\text{CH}=\text{N}-$  ( $\text{Ar}$  = aromatic group) are an active part for the electrochemical reduction process. Polymeric Schiff bases are reversibly reduced at 0.59 and 1.04 V versus  $\text{Na}^+/\text{Na}$  in Na cells. The reversible capacity reaches

350 mAh g<sup>-1</sup> when the composite electrode is optimized with carbon materials.<sup>389</sup>

## 6. FUTURE OUTLOOK OF NIBS

Research interest to use sodium ions as ion carriers for energy storage at ambient conditions was considered to be unattractive since materials innovations for the Li system and commercialization of LIBs were realized in 1990s. However, now research interest for sodium ions is completely changed with increasing worldwide demand for high-energy batteries. In this review, many different electrode materials for NIBs have been reviewed. Metallic sodium is generally used as a counter electrode to evaluate the electrode performance of the sodium insertion material (it is called a half-cell). The electrode

performance in half-cells is often different compared with full cells with two sodium insertion materials (Figure 2a). Moreover, it could be difficult to use metallic sodium for rechargeable battery applications because of potential safety risks. To the best of our knowledge, the first full cell without metallic sodium (i.e., sodium-ion batteries) was demonstrated in 1988.<sup>83</sup> Good cyclability for 300 cycles (Figure 41a) was reported with lead (embedded in conductive polymer matrix) as the negative electrode and P2-Na<sub>2/3</sub>CoO<sub>2</sub> as the positive electrode, even though the limited voltage range (1.5–3.3 V) was used. The full cell with P2-Na<sub>2/3</sub>CoO<sub>2</sub> and carbon material was also proposed with solid polymer electrolyte operating at 100 °C in 1993.<sup>22</sup> After Dahn's pioneering finding of hard carbon as a high-capacity material in the Na system, a full cell of hard carbon//NaV(PO<sub>4</sub>)F was also proposed.<sup>212</sup> The possibility of 4 V-class NIBs was first demonstrated using this system (Figure 41b) even though the preliminary results show insufficient cyclability (50% of retention after 30 cycles).<sup>212</sup>

After 2010, several publications in relation to full cells with Na ions as charge carriers have emerged and battery performance is significantly improved when compared with the early studies. Now, the gravimetric energy density of NIBs as full cells operable at room temperature have become competitive to that of state-of-the-art LIBs with graphite and layered oxides (Figure 26). Komaba et al. reported the full cell with hard carbon/Na[Ni<sub>1/2</sub>Mn<sub>1/2</sub>]O<sub>2</sub> and demonstrated acceptable battery performance with approximately 3 V of operating voltage as shown in Figure 41c.<sup>5</sup> The estimated gravimetric energy density reaches 60% of the high-energy graphite/LiCoO<sub>2</sub> system. Similar to this work, the full cell with hard carbon/Na[Fe<sub>1/3</sub>Ni<sub>1/3</sub>Mn<sub>1/3</sub>]O<sub>2</sub> also shows over 3 V of average operating voltage with good capacity retention. The full cell can deliver >100 mAh g<sup>-1</sup> of reversible capacity (based on the positive electrode) over continuous 150 cycles.<sup>118</sup> The possibility for further improvement of energy density in the material base has been also discussed in the former section. P2-type Na<sub>2/3</sub>[Ni<sub>1/3</sub>Mn<sub>2/3</sub>]O<sub>2</sub> and its derivatives<sup>131</sup> are potential candidates for high-voltage positive electrodes with Ni<sup>2+</sup>/Ni<sup>4+</sup> redox in the framework structure of oxide ions (Figure 13). The energy density of P2-type Na<sub>2/3</sub>[Ni<sub>1/3</sub>Mn<sub>2/3</sub>]O<sub>2</sub> exceeds 540 Wh kg<sup>-1</sup> (based on metallic sodium as negative electrode) even though its insufficient cyclability, associated with a large volume change for the P2–O<sub>2</sub> phase transition, is needed to be improved. Gravimetric/volumetric energy density is expected to be superior to those of LiFePO<sub>4</sub> and LiMn<sub>2</sub>O<sub>4</sub>. Power density would be also enhanced when compared with the Li system. Although the size of Na is relatively large compared with Li, the rate capability is not limited by size as shown in this review. Micrometer-sized and dense O3-Na[Fe<sub>1/2</sub>Co<sub>1/2</sub>]O<sub>2</sub> shows excellent rate capability (Figure 7); over 60% of reversible capacity is preserved even at the 30 C rate (7.2 A g<sup>-1</sup>).<sup>71</sup>

Research progress on full cells is also reported in the phosphate system. Na<sub>3</sub>V<sub>2</sub>(PO<sub>4</sub>)<sub>3</sub> has been used as the positive electrode and assembled the 3 V-class full cell with the hard-carbon negative electrode in the NaFSA/PC electrolyte.<sup>390</sup> Hard carbon/Na<sub>3</sub>V<sub>2</sub>(PO<sub>4</sub>)<sub>2</sub>F<sub>3</sub> as 4 V-class full cells with optimized electrolyte (EC:PC:DMC = 0.45:0.45:0.1) shows good capacity retention of more than 100 cycles.<sup>270</sup> The first 4.5 V-class full cell with hard carbon/Na<sub>4</sub>Co<sub>3</sub>(PO<sub>4</sub>)<sub>2</sub>P<sub>2</sub>O<sub>7</sub> has been also demonstrated.<sup>224</sup> Further possibility for the increase in energy density is expected from Na<sub>4</sub>Co<sub>2.4</sub>Mn<sub>0.3</sub>Ni<sub>0.3</sub>(PO<sub>4</sub>)<sub>2</sub>P<sub>2</sub>O<sub>7</sub> that surprisingly shows some

extent of discharge capacity in the voltage region of 5.0–4.5 V (5.34–4.84 V vs Li metal) as shown in Figure 23c. This anomalously high voltage probably originates from the nickel ion redox in the polyanionic framework structure.<sup>225</sup> In addition to the positive electrode materials based on the insertion reaction, interesting chemistry of oxygen molecules in aprotic solvents has been reported. Reversible electrochemical reaction between oxygen/sodium superoxide has been demonstrated with quite small polarization.<sup>391</sup> Such unique chemistry for the Na system is an important scientific finding to realize a high-energy system in the future.

A bright and optimistic future is expected for the positive electrode side. However, as the full cells, tough challenges remain for the negative electrode side to compete with the Li system. As shown in Figure 35, the volumetric energy density of hard carbon is smaller than that of graphite in the Li system even if the same gravimetric discharge capacity is obtained. One potential candidate is titanium oxides (or other oxide- or phosphates-based negative electrode materials); Na<sub>2</sub>Ti<sub>3</sub>O<sub>7</sub> delivers a relatively high gravimetric capacity (200 mAh g<sup>-1</sup>) with low voltage (0.5 V vs Na).<sup>308</sup> Since the density of titanium oxides is much higher than carbonaceous materials, the volumetric energy density is at least, theoretically, further enhanced. Although a low operating voltage as electrode materials is beneficial to increase the energy density as full cells, passivation of the materials surface is an important issue to solve. Indeed, the Coulombic efficiency in the first cycle is limited to less than 50% for Na<sub>2</sub>Ti<sub>3</sub>O<sub>7</sub>.<sup>305,308</sup> Studies on electrolyte solutions, additives, and binders to effectively passivate the surface of oxides and carbonaceous materials added as a conductive agent, which are exposed to the highly reducing condition, are needed. Full cells with titanium oxides, Li[Li<sub>1/3</sub>Ti<sub>5/3</sub>]O<sub>4</sub><sup>302</sup> and Na<sub>0.66</sub>[Li<sub>0.22</sub>Ti<sub>0.78</sub>]O<sub>2</sub>,<sup>331</sup> which show relatively good Coulombic efficiency in the initial cycle, assembled with Na<sub>3</sub>V<sub>2</sub>(PO<sub>4</sub>)<sub>3</sub> have been also reported. Three-electron redox of phosphorus in Na cells is also a recent new finding and could be used as a negative electrode for NIBs. However, passivation on the surface of the electrode material with a large volume change is the toughest challenge, similar to silicon in the Li system.

Leaving aside the energy density, another important research topic of NIBs is cost-effective batteries, especially for electrical energy storage (EES). Considering the design of better batteries for EES, the primary importance is elemental abundance (cost) with acceptable battery performance (energy density, cycle life, safety, etc.). In this regard, Fe and Mn as the Earth-abundant elements are important key elements. P2-type Na<sub>x</sub>[Fe<sub>1/2</sub>Mn<sub>1/2</sub>]O<sub>2</sub> delivers approximately 190 mAh g<sup>-1</sup> of reversible capacity and is one candidate as a positive electrode material for EES even though the compensation for deficient sodium ions is needed to use full capacity.<sup>51</sup> The full cell consisting of only abundant elements with Na<sub>0.44</sub>MnO<sub>2</sub> and carbon has been also demonstrated.<sup>151</sup> The full cell with pyrolyzed carbon/Na<sub>0.44</sub>MnO<sub>2</sub> retains over 70% of reversible capacity after 100 cycles. In addition to the electrode active materials, expensive battery components and production cost also influence the total cost. Replacement of a current collector from copper foil for the Li–graphite system to aluminum for the Na system is a great advantage to reduce the battery cost because sodium metal cannot form the binary alloy with aluminum. Similar to the Li system, since the aprotic polar solvent and salt with a porous membrane is used as electrolyte, the cost advantage is small for the sodium system. As recently

reported by Whitacre and co-workers, water-based electrolyte has been also proposed as a cost-effective system and the carbon/manganese oxide aqueous battery system has been commercialized for the EES application by Aquion Energy.<sup>392</sup> Activated carbon with electrochemical double-layer charge/discharge is used as the positive electrode, and therefore, this system is classified as a hybrid sodium-ion capacitor, not NIBs. Additionally, a hybrid potassium-ion capacitor with Prussian blue and activated carbon as positive and negative electrodes, respectively, has been also proposed.<sup>393</sup> NaTi<sub>2</sub>(PO<sub>4</sub>)<sub>3</sub>/Na<sub>0.44</sub>MnO<sub>2</sub> full cell with aqueous electrolyte has been proposed as a cost-effective and high-power system.<sup>394</sup> The full cell shows excellent rate capability as shown in Figure 41d. A symmetric Na<sub>4</sub>C<sub>8</sub>H<sub>2</sub>O<sub>6</sub> cell as all organic materials without transition metals has been also proposed. Two V-class all organic NIBs with Na<sub>4</sub>C<sub>8</sub>H<sub>2</sub>O<sub>6</sub> exhibit good capacity retention with acceptable rate capability (Figure 41e). Although many approaches are proposed as an alternative technology for conventional NIBs with aprotic polar solvents, the energy density is significantly reduced compared with the aprotic system because of the lower operating voltage of aqueous and current organic systems. Since the limitation of space to store batteries could not be a critical issue for EES compared to those of electronic devices and transportation systems, "Wh" per "cost of batteries" is, therefore, of primary importance with acceptable volumetric energy density. Therefore, the strategy of battery design for EES is needed to balance both the increase in energy density and the decrease in the total cost of batteries.

As discussed in this review, many layered oxides are hygroscopic, and such materials require dry conditions in the sample handling. This problem is similarly found in LiNiO<sub>2</sub> and layered oxides containing Ni<sup>3+</sup> in the Li system. Materials design without hygroscopic character may be required to assemble cost-effective NIBs because PVdF binders and current collectors are easily damaged by the presence of alkali ions in the slurry at ambient conditions. Cycle life is also another important factor to reduce the total cost. After 2010, the cyclability of the electrode materials in Na cells was significantly improved. However, the Coulombic efficiency per each cycle still needs to be improved, presumably because of the insufficient passivation in aprotic polar solvents when compared with the Li system.<sup>293</sup> This fact may originate from the difference in chemistry of the passivation process. Recently, a theoretical approach has been applied to investigate the interphase between electrode/electrolyte with an additive in an atomic scale in the Li system.<sup>395</sup> Such approach will be also quite beneficial to understand the passivation of the electrode materials in the Na system. Further understanding of the passivation layers (so-called SEI) is required to further extend the battery calendar life in the future.

The thermal stability of electrode materials (especially as practical applications) is also an essential issue because volatile and flammable aprotic solvents are used as electrolyte. Inorganic ionic liquid has been proposed as a potential stable electrolyte for NIBs. The NaFSA-KFSA (FSA; bis-(fluorosulfonyl)amide) system can be used as electrolyte without organic molecules at 90 °C.<sup>101,352,396</sup> Although the operating temperature is slightly high because of the limitation of the melting point of the inorganic ionic liquid, the electrolyte design without organic molecules is a simple and an efficient strategy to overcome the safety issues without the sacrifice of energy density. Moreover, the solid electrolyte is an ideal goal as the stable electrolyte, and it could remind us that research

development of the Na system for energy storage started from the solid electrolyte, i.e., molten sodium/sulfur batteries with β-alumina as the solid electrolyte. β-Alumina is a potential candidate for the solid electrolyte (ionic conductivity reaches 10<sup>-3</sup> S cm<sup>-1</sup> at room temperature), but sintering at 1800 °C is needed to reduce the resistance of the grain boundary.<sup>397</sup> The difficulty to form solid–solid contact between electrolyte and active materials also restricts the battery performance. The phosphate-based all-solid-state symmetrical cell, Na<sub>3</sub>V<sub>2</sub>(PO<sub>4</sub>)<sub>3</sub>/NASICON/Na<sub>3</sub>V<sub>2</sub>(PO<sub>4</sub>)<sub>3</sub>, has been proposed, and electrode performance at 80 °C has been reported.<sup>398</sup> However, the symmetrical cell shows inferior performance even at 80 °C when compared with the aprotic solvent system. Recently, a sulfide glass-ceramic (Na<sub>3</sub>PS<sub>4</sub>) has been proposed as the new solid-state electrolyte, and the all-solid-state NIB operable at room temperature, prepared by mechanical cold press without sintering at high temperature, has been demonstrated as shown in Figure 41f.<sup>397</sup> Use of sulfides is one approach to reduce the high resistance of the grain boundary and contact with active materials even though some extent of sacrifice for energy density is unavoidable. Since the high-energy density and safety risk as batteries are complementary to each other, inorganic ionic liquid, solid electrolyte, and other chemically stable electrolyte systems will be important materials to realize high-energy NIBs without the safety risk.

## 7. CONCLUSIONS

Research interest for NIBs has rapidly increased since 2010 as shown in Figure 2b, and many positive and negative electrode materials have been newly found in the world. Some similarity and differences in the chemistry between the Na and the Li systems are also found as summarized in this review. By studying and understanding the similarity and difference in crystallography, kinetics (solid-state ionic diffusion and desolvation process), and thermodynamics of Li-ion and Na-ion chemistry, including the passivation process in aprotic polar solvent, we can realize and design better battery performance, including new chemistry and new technology for both Li ion and Na ion. It is anticipated that demonstration for NIBs as rechargeable batteries at the industrial level will start in the near future even though we still have many tough challenges. Competing with the state-of-the-art and high-energy LIBs (graphite/LiCoO<sub>2</sub> system) does not seem to be easy, especially for the volumetric energy density. Innovations of materials are still needed. Nevertheless, sodium-ion-based technology has the great advantage for both high-power and cost-effective systems as discussed in this review. NIBs can be potentially used as battery systems for hybrid electric vehicles and electrical energy storage, which requires high-power and cost-effective batteries, respectively, if the cycle life of batteries and safety are being competitive for the lithium system. It is believed that NIBs will become the vital rechargeable battery system in our daily life, complimentarily with the high-energy lithium system.

## AUTHOR INFORMATION

### Corresponding Author

\*E-mail: komaba@rs.kagu.tus.ac.jp.

### Present Address

<sup>§</sup>Department of Green and Sustainable Chemistry, Tokyo Denki University, 5 Senju Asahi-cho, Adachi-ku, Tokyo, Japan.

**Notes**

The authors declare no competing financial interest.

**Biographies**

Naoaki Yabuuchi is an Associate Professor at the Department of Green and Sustainable Chemistry, Tokyo Denki University, Japan, and a Project Associate Professor at Kyoto University, Japan. He received his Ph.D. degree from Osaka City University, Japan, in 2006 and was a postdoctoral associate at the Massachusetts Institute of Technology (2006–2008) and an assistant professor at Osaka City University, Japan (from 2008 to 2009). In 2009, he joined Professor Komaba's research group at the Tokyo University of Science, Japan, as a postdoctoral researcher and became an assistant professor at the university in 2010. He was awarded the First International Award, "Science Award Electrochemistry" by Volkswagen and BASF in 2012, 2nd ISSI Young Scientist Award of International Society for Solid State Ionics in 2013, and ISE Prize for Applied Electrochemistry of the International Society of Electrochemistry in 2013. His research interests lie in the design, synthesis, and characterization of novel materials for Li- and Na-ion batteries.



Kei Kubota is an Assistant Professor at the Tokyo University of Science, Japan, and a Project Assistant Professor at Kyoto University, Japan. He received his Ph.D. degree in Chemistry in 2012 from the Tokyo Institute of Technology, Japan, where he also worked on positive electrode materials for Li batteries as a postdoctoral researcher from 2012 to 2013. His current research focuses on energy storage materials for Li- and Na-ion batteries.



Mouad Dahbi is a Postdoctoral Researcher at the Tokyo University of Science, Japan, and a Project Researcher at Kyoto University, Japan. He received his Ph.D. degree in Chemistry/Electrochemistry from the University Francois Rabelais of Tours, France in 2013. His Ph.D. work focused on the asymmetric Li-ion capacitor in aprotic electrolyte. His current research is studying negative electrodes for Na-ion batteries in aprotic electrolyte.



Shinichi Komaba is a Professor in the Department of Applied Chemistry at Tokyo University of Science, Japan, and a Project Professor at Kyoto University, Japan. He received his Ph.D. degree in Engineering from Waseda University, Japan, in 1998 and then was a research associate at Iwate University, Japan, from 1998 to 2005. From 2003 to 2004, he also worked at the Institut de Chimie de la Matière Condensée de Bordeaux, France, as a postdoctoral researcher. He joined the Tokyo University of Science as a faculty member in 2005. He was awarded the 2014 Resonate Award from Caltech, USA. He is the author or co-author of over 160 publications. His current research focuses on material science and electrochemistry in electrochemical devices (rechargeable Li- and Na-ion batteries, capacitor, sensor, and biofuel cell).

**ACKNOWLEDGMENTS**

We acknowledge the many students and collaborators who have contributed to this series of research over the past several years.

**REFERENCES**

- (1) Dunn, B.; Kamath, H.; Tarascon, J.-M. *Science* **2011**, *334*, 928.
- (2) Tarascon, J.-M. *Nat. Chem.* **2010**, *2*, 510.
- (3) Carmichael, R. S. *Practical Handbook of Physical Properties of Rocks and Minerals*; CRC Press: Boca Raton, FL, 1989.
- (4) Slater, M. D.; Kim, D.; Lee, E.; Johnson, C. S. *Adv. Funct. Mater.* **2013**, *23*, 947.

- (5) Komaba, S.; Murata, W.; Ishikawa, T.; Yabuuchi, N.; Ozeki, T.; Nakayama, T.; Ogata, A.; Gotoh, K.; Fujiwara, K. *Adv. Funct. Mater.* **2011**, *21*, 3859.
- (6) Kim, S. W.; Seo, D. H.; Ma, X. H.; Ceder, G.; Kang, K. *Adv. Energy Mater.* **2012**, *2*, 710.
- (7) Oshima, T.; Kajita, M.; Okuno, A. *Int. J. Appl. Ceram. Technol.* **2004**, *1*, 269.
- (8) Bones, R. J.; Teagle, D. A.; Brooker, S. D.; Cullen, F. L. *J. Electrochem. Soc.* **1989**, *136*, 1274.
- (9) Whittingham, M. S. *Prog. Solid State Chem.* **1978**, *12*, 41.
- (10) Whittingham, M. S. *Science* **1976**, *192*, 1126.
- (11) Newman, G. H.; Klemann, L. P. *J. Electrochem. Soc.* **1980**, *127*, 2097.
- (12) Mizushima, K.; Jones, P. C.; Wiseman, P. J.; Goodenough, J. B. *Mater. Res. Bull.* **1980**, *15*, 783.
- (13) Delmas, C.; Braconnier, J.-J.; Fouassier, C.; Hagenmuller, P. *Solid State Ionics* **1981**, *3–4*, 165.
- (14) Abraham, K. M. *Solid State Ionics* **1982**, *7*, 199.
- (15) Delmas, C.; Braconnier, J. J.; Maazaz, A.; Hagenmuller, P. *Rev. Chim. Miner.* **1982**, *19*, 343.
- (16) Kanno, R.; Takeda, Y.; Ichikawa, T.; Nakanishi, K.; Yamamoto, O. *J. Power Sources* **1989**, *26*, 535.
- (17) Mohri, M.; Yanagisawa, N.; Tajima, Y.; Tanaka, H.; Mitate, T.; Nakajima, S.; Yoshida, M.; Yoshimoto, Y.; Suzuki, T.; Wada, H. *J. Power Sources* **1989**, *26*, 545.
- (18) Fong, R.; von Sacken, U.; Dahn, J. R. *J. Electrochem. Soc.* **1990**, *137*, 2009.
- (19) Sawai, K.; Ohzuku, T.; Hirai, T. *Chem. Express* **1990**, *5*, 837.
- (20) Ohzuku, T.; Iwakoshi, Y.; Sawai, K. *J. Electrochem. Soc.* **1993**, *140*, 2490.
- (21) Ge, P.; Fouletier, M. *Solid State Ionics* **1988**, *28–30*, 1172.
- (22) Doeuff, M. M.; Ma, Y. P.; Visco, S. J.; Dejonghe, L. C. *J. Electrochem. Soc.* **1993**, *140*, L169.
- (23) Jow, T. R.; Shacklette, L. W.; Maxfield, M.; Vernick, D. J. *J. Electrochem. Soc.* **1987**, *134*, 1730.
- (24) Ma, Y.; Doeuff, M. M.; Visco, S. J.; De Jonghe, L. C. *J. Electrochem. Soc.* **1993**, *140*, 2726.
- (25) Okada, S.; Takahashi, Y.; Kiyabu, T.; Doi, T.; Yamaki, J.-I.; Nishida, T. *210th ECS Meeting Abstracts* **2006**, MA2006–02, 201.
- (26) Web of Science; <https://apps.webofknowledge.com/>, accessed Mar 2014.
- (27) Palomares, V.; Serras, P.; Villaluenga, I.; Hueso, K. B.; Carretero-Gonzalez, J.; Rojo, T. *Energy Environ. Sci.* **2012**, *5*, 5884.
- (28) Pan, H.; Hu, Y.-S.; Chen, L. *Energy Environ. Sci.* **2013**, *6*, 2338.
- (29) Masquelier, C.; Croguennec, L. *Chem. Rev.* **2013**, *113*, 6552.
- (30) Okoshi, M.; Yamada, Y.; Yamada, A.; Nakai, H. *J. Electrochem. Soc.* **2013**, *160*, A2160.
- (31) Yamada, Y.; Iriyama, Y.; Abe, T.; Ogumi, Z. *Langmuir* **2009**, *25*, 12766.
- (32) Yamada, Y.; Koyama, Y.; Abe, T.; Ogumi, Z. *J. Phys. Chem. C* **2009**, *113*, 8948.
- (33) Ong, S. P.; Chevrier, V. L.; Hautier, G.; Jain, A.; Moore, C.; Kim, S.; Ma, X.; Ceder, G. *Energy Environ. Sci.* **2011**, *4*, 3680.
- (34) Shannon, R. D. *Acta Crystallogr., Sect. A* **1976**, *32*, 751.
- (35) Kuratani, K.; Uemura, N.; Senoh, H.; Takeshita, H. T.; Kiyobayashi, T. *J. Power Sources* **2013**, *223*, 175.
- (36) Delmas, C.; Fouassier, C.; Hagenmuller, P. *Physica B* **1980**, *99*, 81.
- (37) Momma, K.; Izumi, F. *J. Appl. Crystallogr.* **2008**, *41*, 653.
- (38) Mather, G. C.; Dussarrat, C.; Etourneau, J.; West, A. R. *J. Mater. Chem.* **2000**, *10*, 2219.
- (39) Mendiboure, A.; Delmas, C.; Hagenmuller, P. *J. Solid State Chem.* **1985**, *57*, 323.
- (40) Stoyanova, R.; Carlier, D.; Sendova-Vassileva, M.; Yoncheva, M.; Zhecheva, E.; Nihtianova, D.; Delmas, C. *J. Solid State Chem.* **2010**, *183*, 1372.
- (41) Paulsen, J. M.; Dahn, J. R. *J. Electrochem. Soc.* **2000**, *147*, 2478.
- (42) Lu, Z.; Dahn, J. R. *J. Electrochem. Soc.* **2001**, *148*, A710.
- (43) Lu, Z.; Dahn, J. R. *J. Electrochem. Soc.* **2001**, *148*, A1225.
- (44) Delmas, C.; Braconnier, J.-J.; Hagenmuller, P. *Mater. Res. Bull.* **1982**, *17*, 117.
- (45) Paulsen, J. M.; Donaberger, R. A.; Dahn, J. R. *Chem. Mater.* **2000**, *12*, 2257.
- (46) Carlier, D.; Saadoune, I.; Croguennec, L.; Ménétrier, M.; Suard, E.; Delmas, C. *Solid State Ionics* **2001**, *144*, 263.
- (47) Lu, Z. H.; Dahn, J. R. *Chem. Mater.* **2001**, *13*, 2078.
- (48) Tournadre, F.; Croguennec, L.; Saadoune, I.; Carlier, D.; Shao-Horn, Y.; Willmann, P.; Delmas, C. *J. Solid State Chem.* **2004**, *177*, 2790.
- (49) Yabuuchi, N.; Kawamoto, Y.; Hara, R.; Ishigaki, T.; Hoshikawa, A.; Yonemura, M.; Kamiyama, T.; Komaba, S. *Inorg. Chem.* **2013**, *52*, 9131.
- (50) Eriksson, T. A.; Lee, Y. J.; Hollingsworth, J.; Reimer, J. A.; Cairns, E. J.; Zhang, X.-F.; Doeuff, M. M. *Chem. Mater.* **2003**, *15*, 4456.
- (51) Yabuuchi, N.; Kajiyama, M.; Iwatake, J.; Nishikawa, H.; Hitomi, S.; Okuyama, R.; Usui, R.; Yamada, Y.; Komaba, S. *Nat. Mater.* **2012**, *11*, 512.
- (52) Thackeray, M. M.; Johnson, P. J.; Depicciotto, L. A.; Bruce, P. G.; Goodenough, J. B. *Mater. Res. Bull.* **1984**, *19*, 179.
- (53) Ohzuku, T.; Kitagawa, M.; Hirai, T. *J. Electrochem. Soc.* **1990**, *137*, 769.
- (54) Tarascon, J. M.; Wang, E.; Shokoohi, F. K.; McKinnon, W. R.; Colson, S. J. *Electrochem. Soc.* **1991**, *138*, 2859.
- (55) Dahn, J. R.; Fuller, E. W.; Obrovac, M.; Vonsacken, U. *Solid State Ionics* **1994**, *69*, 265.
- (56) Takeda, Y.; Akagi, J.; Edagawa, A.; Inagaki, M.; Naka, S. *Mater. Res. Bull.* **1980**, *15*, 1167.
- (57) Ado, K.; Tabuchi, M.; Kobayashi, H.; Kageyama, H.; Nakamura, O.; Inaba, Y.; Kanno, R.; Takagi, M.; Takeda, Y. *J. Electrochem. Soc.* **1997**, *144*, L177.
- (58) Padhi, A. K.; Nanjundaswamy, K. S.; Masquelier, C.; Okada, S.; Goodenough, J. B. *J. Electrochem. Soc.* **1997**, *144*, 1609.
- (59) Takeda, Y.; Nakahara, K.; Nishijima, M.; Imanishi, N.; Yamamoto, O.; Takano, M.; Kanno, R. *Mater. Res. Bull.* **1994**, *29*, 659.
- (60) Zhao, J.; Zhao, L.; Dimov, N.; Okada, S.; Nishida, T. *J. Electrochem. Soc.* **2013**, *160*, A3077.
- (61) Yabuuchi, N.; Yoshida, H.; Komaba, S. *Electrochemistry* **2012**, *80*, 716.
- (62) Yabuuchi, N.; Komaba, S. *Sci. Technol. Adv. Mater.* **2014**, *15*, 043501.
- (63) McLaren, V. L.; West, A. R.; Tabuchi, M.; Nakashima, A.; Takahara, H.; Kobayashi, H.; Sakaebi, H.; Kageyama, H.; Hirano, A.; Takeda, Y. *J. Electrochem. Soc.* **2004**, *151*, A672.
- (64) Monyoncho, E.; Bissessur, R. *Mater. Res. Bull.* **2013**, *48*, 2678.
- (65) Ma, X.; Chen, H.; Ceder, G. *J. Electrochem. Soc.* **2011**, *158*, A1307.
- (66) Caballero, A.; Hernan, L.; Morales, J.; Sanchez, L.; Santos Pena, J.; Aranda, M. A. G. *J. Mater. Chem.* **2002**, *12*, 1142.
- (67) Yabuuchi, N.; Hara, R.; Kajiyama, M.; Kubota, K.; Ishigaki, T.; Hoshikawa, A.; Komaba, S. *Adv. Energy Mater.* **2014**, *4*, 1301453.
- (68) Van der Ven, A.; Ceder, G.; Asta, M.; Tepesch, P. D. *Phys. Rev. B: Condens. Matter Mater. Phys.* **2001**, *64*, 184307.
- (69) Delmas, C.; Maazaz, A.; Fouassier, C.; Réau, J.-M.; Hagenmuller, P. *Mater. Res. Bull.* **1979**, *14*, 329.
- (70) Lee, D. H.; Xu, J.; Meng, Y. S. *Phys. Chem. Chem. Phys.* **2013**, *15*, 3304.
- (71) Yoshida, H.; Yabuuchi, N.; Komaba, S. *Electrochem. Commun.* **2013**, *34*, 60.
- (72) Carlier, D.; Blangero, M.; Ménétrier, M.; Pollet, M. I.; Doumerc, J.-P.; Delmas, C. *Inorg. Chem.* **2009**, *48*, 7018.
- (73) Matsumura, T.; Sonoyama, N.; Kanno, R. *Solid State Ionics* **2003**, *161*, 31.
- (74) Yoncheva, M.; Stoyanova, R.; Zhecheva, E.; Kuzmanova, E.; Sendova-Vassileva, M.; Nihtianova, D.; Carlier, D.; Guignard, M.; Delmas, C. *J. Mater. Chem.* **2012**, *22*, 23418.
- (75) Mortemard de Boisse, B.; Carlier, D.; Guignard, M.; Delmas, C. *J. Electrochem. Soc.* **2013**, *160*, A569.

- (76) Thorne, J. S.; Dunlap, R. A.; Obrovac, M. N. *J. Electrochem. Soc.* **2013**, *160*, A361.
- (77) Hirayama, M.; Tomita, H.; Kubota, K.; Kanno, R. *J. Power Sources* **2011**, *196*, 6809.
- (78) Takeda, Y.; Naka, S.; Takano, M.; Shinjo, T.; Takada, T.; Shimada, M. *Mater. Res. Bull.* **1978**, *13*, 61.
- (79) Tabuchi, M.; Tatsumi, K.; Morimoto, S.; Nasu, S.; Saito, T.; Ikeda, Y. *J. Appl. Phys.* **2008**, *104*, No. 043909.
- (80) Lu, Z.; Dahn, J. R. *Chem. Mater.* **2001**, *13*, 1252.
- (81) Singh, G.; Acebedo, B.; Cabanas, M. C.; Shanmukaraj, D.; Armand, M.; Rojo, T. *Electrochem. Commun.* **2013**, *37*, 61.
- (82) Blangero, M.; Carlier, D.; Pollet, M.; Darriet, J.; Delmas, C.; Doumerc, J.-P. *Phys. Rev. B: Condens. Matter Mater. Phys.* **2008**, *77*, 184116.
- (83) Shacklette, L. W.; Jow, T. R.; Townsend, L. *J. Electrochem. Soc.* **1988**, *135*, 2669.
- (84) Molenda, J.; Delmas, C.; Dordor, P.; Stoklosa, A. *Solid State Ionics* **1984**, *12*, 473.
- (85) Lee, M.; Viciu, L.; Li, L.; Wang, Y.; Foo, M. L.; Watauchi, S.; Pascal, R. A., Jr.; Cava, R. J.; Ong, N. P. *Nat. Mater.* **2006**, *5*, 537.
- (86) Takada, K.; Sakurai, H.; Takayama-Muromachi, E.; Izumi, F.; Dilanian, R. A.; Sasaki, T. *Nature* **2003**, *422*, 53.
- (87) Hinuma, Y.; Meng, Y. S.; Ceder, G. *Phys. Rev. B: Condens. Matter Mater. Phys.* **2008**, *77*, 224111.
- (88) Berthelot, R.; Carlier, D.; Delmas, C. *Nat. Mater.* **2011**, *10*, 74.
- (89) Roger, M.; Morris, D. J. P.; Tennant, D. A.; Gutmann, M. J.; Goff, J. P.; Hoffmann, J. U.; Feyerherm, R.; Dudzik, E.; Prabhakaran, D.; Boothroyd, A. T.; Shannon, N.; Lake, B.; Deen, P. P. *Nature* **2007**, *445*, 631.
- (90) Platova, T. A.; Mukhamedshin, I. R.; Alloul, H.; Dooglav, A. V.; Collin, G. *Phys. Rev. B: Condens. Matter Mater. Phys.* **2009**, *80*, 224106.
- (91) Huang, Q.; Foo, M. L.; Lynn, J. W.; Zandbergen, H. W.; Lawes, G.; Wang, Y.; Toby, B. H.; Ramirez, A. P.; Ong, N. P.; Cava, R. J. *J. Phys.: Condens. Matter* **2004**, *16*, 5803.
- (92) Komaba, S.; Yabuuchi, N.; Kawamoto, Y. *Chem. Lett.* **2009**, *38*, 954.
- (93) Xia, X.; Dahn, J. R. *J. Electrochem. Soc.* **2012**, *159*, A647.
- (94) MacNeil, D. D.; Dahn, J. R. *J. Electrochem. Soc.* **2002**, *149*, A912.
- (95) Braconnier, J. J.; Delmas, C.; Hagenmuller, P. *Mater. Res. Bull.* **1982**, *17*, 993.
- (96) Komaba, S.; Takei, C.; Nakayama, T.; Ogata, A.; Yabuuchi, N. *Electrochem. Commun.* **2010**, *12*, 355.
- (97) Komaba, S.; Nakayama, T.; Ogata, A.; Shimizu, T.; Takei, C.; Takada, S.; Hokura, A.; Nakai, I. *ECS Trans.* **2009**, *16*, 43.
- (98) Yabuuchi, N.; Ikeuchi, I.; Kubota, K.; Komaba, S. *224th ECS Meeting Abstracts*, San Francisco, CA, 2013, MA2013-02, p 398.
- (99) Jones, C. D. W.; Rossen, E.; Dahn, J. R. *Solid State Ionics* **1994**, *68*, 65.
- (100) Yabuuchi, N.; Yamamoto, K.; Yoshii, K.; Nakai, I.; Nishizawa, T.; Omaru, A.; Toyooka, T.; Komaba, S. *J. Electrochem. Soc.* **2013**, *160*, A39.
- (101) Chen, C.-Y.; Matsumoto, K.; Nohira, T.; Hagiwara, R.; Fukunaga, A.; Sakai, S.; Nitta, K.; Inazawa, S. *J. Power Sources* **2013**, *237*, S2.
- (102) Xia, X.; Dahn, J. R. *Electrochem. Solid-State Lett.* **2011**, *15*, A1.
- (103) Fukunaga, A.; Nohira, T.; Kozawa, Y.; Hagiwara, R.; Sakai, S.; Nitta, K.; Inazawa, S. *J. Power Sources* **2012**, *209*, 52.
- (104) Rougier, A.; Gravereau, P.; Delmas, C. *J. Electrochem. Soc.* **1996**, *143*, 1168.
- (105) Rougier, A.; Delmas, C.; Chadwick, A. V. *Solid State Commun.* **1995**, *94*, 123.
- (106) Vassilaras, P.; Ma, X.; Li, X.; Ceder, G. *J. Electrochem. Soc.* **2013**, *160*, A207.
- (107) de Picciotto, L. A.; Thackeray, M. M.; David, W. I. F.; Bruce, P. G.; Goodenough, J. B. *Mater. Res. Bull.* **1984**, *19*, 1497.
- (108) Choi, N.-S.; Kim, J.-S.; Yin, R.-Z.; Kim, S.-S. *Mater. Chem. Phys.* **2009**, *116*, 603.
- (109) Armstrong, A. R.; Lyness, C.; Panchmatia, P. M.; Islam, M. S.; Bruce, P. G. *Nat. Mater.* **2011**, *10*, 223.
- (110) Davidson, I.; Greedan, J. E.; Vonsacken, U.; Michal, C. A.; Dahn, J. R. *Solid State Ionics* **1991**, *46*, 243.
- (111) Didier, C.; Guignard, M.; Denage, C.; Szajwaj, O.; Ito, S.; Saadoune, I.; Darriet, J.; Delmas, C. *Electrochem. Solid-State Lett.* **2011**, *14*, A75.
- (112) Hamani, D.; Ati, M.; Tarascon, J.-M.; Rozier, P. *Electrochem. Commun.* **2011**, *13*, 938.
- (113) Guignard, M.; Didier, C.; Darriet, J.; Bordet, P.; Elkaïm, E.; Delmas, C. *Nat. Mater.* **2013**, *12*, 74.
- (114) Didier, C.; Guignard, M.; Darriet, J.; Delmas, C. *Inorg. Chem.* **2012**, *51*, 11007.
- (115) Hewston, T. A.; Chamberland, B. L. *J. Phys. Chem. Solids* **1987**, *48*, 97.
- (116) Maazaz, A.; Delmas, C.; Hagenmuller, P. *J. Inclusion Phenom.* **1983**, *1*, 45.
- (117) Yabuuchi, N.; Yano, M.; Yoshida, H.; Kuze, S.; Komaba, S. *J. Electrochem. Soc.* **2013**, *160*, A3131.
- (118) Kim, D.; Lee, E.; Slater, M.; Lu, W.; Rood, S.; Johnson, C. S. *Electrochem. Commun.* **2012**, *18*, 66.
- (119) Vassilaras, P.; Toumar, A. J.; Ceder, G. *Electrochem. Commun.* **2014**, *38*, 79.
- (120) Wang, X.; Liu, G.; Iwao, T.; Okubo, M.; Yamada, A. *J. Phys. Chem. C* **2014**, *118*, 2970.
- (121) Kim, S.; Ma, X.; Ong, S. P.; Ceder, G. *Phys. Chem. Chem. Phys.* **2012**, *14*, 15571.
- (122) Menetrier, M.; Saadoune, I.; Levasseur, S.; Delmas, C. *J. Mater. Chem.* **1999**, *9*, 1135.
- (123) Ohzuku, T.; Ariyoshi, M.; Makimura, Y.; Yabuuchi, N.; Sawai, K. *Electrochemistry* **2005**, *73*, 2.
- (124) Kang, K. S.; Meng, Y. S.; Breger, J.; Grey, C. P.; Ceder, G. *Science* **2006**, *311*, 977.
- (125) Komaba, S.; Yabuuchi, N.; Nakayama, T.; Ogata, A.; Ishikawa, T.; Nakai, I. *Inorg. Chem.* **2012**, *51*, 6211.
- (126) Kalapsazova, M.; Stoyanova, R.; Zhecheva, E. *J. Solid State Electrochem.* **2014**, *1*.
- (127) Sathiya, M.; Hemalatha, K.; Ramesha, K.; Tarascon, J. M.; Prakash, A. S. *Chem. Mater.* **2012**, *24*, 1846.
- (128) Sun, Y.; Wang, Z.; Huang, X.; Chen, L. *J. Power Sources* **2005**, *146*, 678.
- (129) Okada, S.; Yamaki, J.-i. In *Lithium Ion Rechargeable Batteries*; Ozawa, K., Ed.; WILEY-VCH: Weinheim, 2009; p 57.
- (130) Yu, H.; Guo, S.; Zhu, Y.; Ishida, M.; Zhou, H. *Chem. Commun.* **2014**, *50*, 457.
- (131) Yoshida, H.; Yabuuchi, N.; Kubota, K.; Ikeuchi, I.; Garsuch, A.; Schulz-Dobrick, M.; Komaba, S. *Chem. Commun.* **2014**, *50*, 3677.
- (132) Cheng, J.-H.; Pan, C.-J.; Lee, J.-F.; Chen, J.-M.; Guignard, M.; Delmas, C.; Carlier, D.; Hwang, B.-J. *Chem. Mater.* **2013**, *26*, 1219.
- (133) Wang, X.; Tamaru, M.; Okubo, M.; Yamada, A. *J. Phys. Chem. C* **2013**, *117*, 15545.
- (134) Chagas, L. G.; Buchholz, D.; Wu, L.; Vortmann, B.; Passerini, S. *J. Power Sources* **2014**, *247*, 377.
- (135) Buchholz, D.; Chagas, L. G.; Winter, M.; Passerini, S. *Electrochim. Acta* **2013**, *110*, 208.
- (136) Yuan, D.; Hu, X.; Qian, J.; Pei, F.; Wu, F.; Mao, R.; Ai, X.; Yang, H.; Cao, Y. *Electrochim. Acta* **2014**, *116*, 300.
- (137) Kim, D.; Kang, S. H.; Slater, M.; Rood, S.; Vaughey, J. T.; Karan, N.; Balasubramanian, M.; Johnson, C. S. *Adv. Energy Mater.* **2011**, *1*, 333.
- (138) O'Keeffe, M.; Hyde, B. G. *Acta Crystallogr., Sect. B* **1978**, *34*, 3519.
- (139) Poizot, P.; Laruelle, S.; Grugeon, S.; Dupont, L.; Tarascon, J. M. *Nature* **2000**, *407*, 496.
- (140) Komaba, S.; Suzuki, K.; Kumagai, N. *Electrochemistry* **2002**, *70*, 506.
- (141) Komaba, S.; Mikumo, T.; Ogata, A. *Electrochem. Commun.* **2008**, *10*, 1276.
- (142) Komaba, S.; Mikumo, T.; Yabuuchi, N.; Ogata, A.; Yoshida, H.; Yamada, Y. *J. Electrochem. Soc.* **2010**, *157*, A60.

- (143) Koo, B.; Chattopadhyay, S.; Shibata, T.; Prakapenka, V. B.; Johnson, C. S.; Rajh, T.; Shevchenko, E. V. *Chem. Mater.* **2012**, *25*, 245.
- (144) Oh, S.-M.; Myung, S.-T.; Yoon, C. S.; Lu, J.; Hassoun, J.; Scrosati, B.; Amine, K.; Sun, Y.-K. *Nano Lett.* **2014**, *14*, 1620.
- (145) Hariharan, S.; Saravanan, K.; Ramar, V.; Balaya, P. *Phys. Chem. Chem. Phys.* **2013**, *15*, 2945.
- (146) Parant, J.-P.; Olazcuaga, R.; Devalette, M.; Fouassier, C.; Hagenmuller, P. *J. Solid State Chem.* **1971**, *3*, 1.
- (147) Doeff, M. M.; Peng, M. Y.; Ma, Y.; De Jonghe, L. C. *J. Electrochem. Soc.* **1994**, *141*, L145.
- (148) Doeff, M. M.; Richardson, T. J.; Kepley, L. *J. Electrochem. Soc.* **1996**, *143*, 2507.
- (149) Sauvage, F.; Laffont, L.; Tarascon, J. M.; Baudrin, E. *Inorg. Chem.* **2007**, *46*, 3289.
- (150) Kim, H.; Kim, D. J.; Seo, D.-H.; Yeom, M. S.; Kang, K.; Kim, D. K.; Jung, Y. *Chem. Mater.* **2012**, *24*, 1205.
- (151) Cao, Y.; Xiao, L.; Wang, W.; Choi, D.; Nie, Z.; Yu, J.; Saraf, L. V.; Yang, Z.; Liu, J. *Adv. Mater.* **2011**, *23*, 3155.
- (152) Su, D.; Ahn, H.-J.; Wang, G. *J. Mater. Chem. A* **2013**, *1*, 4845.
- (153) Jiao, F.; Bruce, P. G. *Adv. Mater.* **2007**, *19*, 657.
- (154) Tompsett, D. A.; Islam, M. S. *Chem. Mater.* **2013**, *25*, 2515.
- (155) Tarascon, J. M.; Guyomard, D. G.; Wilkens, B.; Mc Kinnon, W. R.; Barboux, P. *Solid State Ionics* **1992**, *57*, 113.
- (156) Yabuuchi, N.; Yano, M.; Kuze, S.; Komaba, S. *Electrochim. Acta* **2012**, *82*, 296.
- (157) Wadsley, A. *Acta Crystallogr.* **1953**, *6*, 433.
- (158) West, K.; Zachau-Christiansen, B.; Jacobsen, T.; Skaarup, S. *Solid State Ionics* **1988**, *28–30* (Part 2), 1128.
- (159) Tepavcevic, S.; Xiong, H.; Stamenkovic, V. R.; Zuo, X.; Balasubramanian, M.; Prakapenka, V. B.; Johnson, C. S.; Rajh, T. *ACS Nano* **2011**, *6*, 530.
- (160) West, K.; Zachau-Christiansen, B.; Jacobsen, T.; Atlung, S. *J. Electrochem. Soc.* **1985**, *132*, 3061.
- (161) Tarascon, J. M.; Hull, G. W. *Solid State Ionics* **1986**, *22*, 85.
- (162) Tarascon, J. M.; Hull, G. W.; Marsh, P.; Haar, T. *J. Solid State Chem.* **1987**, *66*, 204.
- (163) Park, J.; Kim, J.-S.; Park, J.-W.; Nam, T.-H.; Kim, K.-W.; Ahn, J.-H.; Wang, G.; Ahn, H.-J. *Electrochim. Acta* **2013**, *92*, 427.
- (164) Spahr, M. E.; Novák, P.; Haas, O.; Nesper, R. *J. Power Sources* **1995**, *54*, 346.
- (165) Tamaru, M.; Wang, X.; Okubo, M.; Yamada, A. *Electrochim. Commun.* **2013**, *33*, 23.
- (166) Padhi, A. K.; Nanjundaswamy, K. S.; Goodenough, J. B. *J. Electrochem. Soc.* **1997**, *144*, 1188.
- (167) Ravet, N.; Chouinard, Y.; Magnan, J. F.; Besner, S.; Gauthier, M.; Armand, M. *J. Power Sources* **2001**, *97–98*, 503.
- (168) Nishimura, S.-i.; Kobayashi, G.; Ohoyama, K.; Kanno, R.; Yashima, M.; Yamada, A. *Nat. Mater.* **2008**, *7*, 707.
- (169) Malik, R.; Burch, D.; Bazant, M.; Ceder, G. *Nano Lett.* **2010**, *10*, 4123.
- (170) Zaghib, K.; Trottier, J.; Hovington, P.; Brochu, F.; Guerfi, A.; Mauger, A.; Julien, C. M. *J. Power Sources* **2011**, *196*, 9612.
- (171) Le Page, Y.; Donnay, G. *Can. Mineral.* **1977**, *15*, 518.
- (172) Sun, A.; Beck, F. R.; Haynes, D.; Poston, J. A., Jr.; Narayanan, S. R.; Kumta, P. N.; Manivannan, A. *Mater. Sci. Eng., B* **2012**, *177*, 1729.
- (173) Moreau, P.; Guyomard, D.; Gaubicher, J.; Boucher, F. *Chem. Mater.* **2010**, *22*, 4126.
- (174) Avdeev, M.; Mohamed, Z.; Ling, C. D.; Lu, J.; Tamaru, M.; Yamada, A.; Barpanda, P. *Inorg. Chem.* **2013**, *52*, 8685.
- (175) Casas-Cabanas, M.; Roddatis, V. V.; Saurel, D.; Kubiak, P.; Carretero-Gonzalez, J.; Palomares, V.; Serras, P.; Rojo, T. *J. Mater. Chem.* **2012**, *22*, 17421.
- (176) Zhu, Y.; Xu, Y.; Liu, Y.; Luo, C.; Wang, C. *Nanoscale* **2013**, *5*, 780.
- (177) Lee, K. T.; Ramesh, T. N.; Nan, F.; Botton, G.; Nazar, L. F. *Chem. Mater.* **2011**, *23*, 3593.
- (178) Fang, H.; Pan, Z.; Li, L.; Yang, Y.; Yan, G.; Li, G.; Wei, S. *Electrochim. Commun.* **2008**, *10*, 1071.
- (179) Gardiner, G. R.; Islam, M. S. *Chem. Mater.* **2009**, *22*, 1242.
- (180) Asari, Y.; Suwa, Y.; Hamada, T. *Phys. Rev. B: Condens. Matter Mater. Phys.* **2011**, *84*, 134113.
- (181) Nishimura, S.-i.; Nakamura, M.; Natsui, R.; Yamada, A. *J. Am. Chem. Soc.* **2010**, *132*, 13596.
- (182) Zhou, H.; Upreti, S.; Chernova, N. A.; Hautier, G.; Ceder, G.; Whittingham, M. S. *Chem. Mater.* **2010**, *23*, 293.
- (183) Honma, T.; Togashi, T.; Ito, N.; Komatsu, T. *J. Ceram. Soc. Jpn.* **2012**, *120*, 344.
- (184) Barpanda, P.; Ye, T.; Nishimura, S.-i.; Chung, S.-C.; Yamada, Y.; Okubo, M.; Zhou, H.; Yamada, A. *Electrochim. Commun.* **2012**, *24*, 116.
- (185) Kim, H.; Shakoor, R. A.; Park, C.; Lim, S. Y.; Kim, J.-S.; Jo, Y. N.; Cho, W.; Miyasaka, K.; Kahraman, R.; Jung, Y.; Choi, J. W. *Adv. Funct. Mater.* **2013**, *23*, 1147.
- (186) Erragh, F.; Boukhari, A.; Elouadi, B.; Holt, E. *J. Crystallogr. Spectrosc. Res.* **1991**, *21*, 321.
- (187) Barpanda, P.; Ye, T.; Avdeev, M.; Chung, S.-C.; Yamada, A. *J. Mater. Chem. A* **2013**, *1*, 4194.
- (188) Ha, K.-H.; Woo, S. H.; Mok, D.; Choi, N.-S.; Park, Y.; Oh, S. M.; Kim, Y.; Kim, J.; Lee, J.; Nazar, L. F.; Lee, K. T. *Adv. Energy Mater.* **2013**, *3*, 770.
- (189) Barpanda, P.; Nishimura, S.-i.; Yamada, A. *Adv. Energy Mater.* **2012**, *2*, 841.
- (190) Kim, H.; Park, I.; Seo, D.-H.; Lee, S.; Kim, S.-W.; Kwon, W. J.; Park, Y.-U.; Kim, C. S.; Jeon, S.; Kang, K. *J. Am. Chem. Soc.* **2012**, *134*, 10369.
- (191) Sanz, F.; Parada, C.; Rojo, J. M.; Ruiz-Valero, C. *Chem. Mater.* **2001**, *13*, 1334.
- (192) Ellis, B. L.; Makahnouk, W. R. M.; Makimura, Y.; Toghill, K.; Nazar, L. F. *Nat. Mater.* **2007**, *6*, 749.
- (193) Recham, N.; Chotard, J. N.; Dupont, L.; Djellab, K.; Armand, M.; Tarascon, J. M. *J. Electrochem. Soc.* **2009**, *156*, A993.
- (194) Sanz, F.; Parada, C.; Ruiz-Valero, C. *J. Mater. Chem.* **2001**, *11*, 208.
- (195) Tripathi, R.; Wood, S. M.; Islam, M. S.; Nazar, L. F. *Energy Environ. Sci.* **2013**, *6*, 2257.
- (196) Yakubovich, O. V.; Karimova, O. V.; Melnikov, O. K. *Acta Crystallogr., Sect. C: Cryst. Struct. Commun.* **1997**, *53*, 395.
- (197) Kawabe, Y.; Yabuuchi, N.; Kajiyama, M.; Fukuhara, N.; Inamasu, T.; Okuyama, R.; Nakai, I.; Komaba, S. *Electrochim. Commun.* **2011**, *13*, 1225.
- (198) Kawabe, Y.; Yabuuchi, N.; Kajiyama, M.; Fukuhara, N.; Inamasu, T.; Okuyama, R.; Nakai, I.; Komaba, S. *Electrochemistry* **2012**, *80*, 80.
- (199) Chen, H.; Hao, Q.; Zivkovic, O.; Hautier, G.; Du, L.-S.; Tang, Y.; Hu, Y.-Y.; Ma, X.; Grey, C. P.; Ceder, G. *Chem. Mater.* **2013**, *25*, 2777.
- (200) Chen, H.; Hautier, G.; Ceder, G. *J. Am. Chem. Soc.* **2012**, *134*, 19619.
- (201) Barpanda, P.; Chotard, J.-N. I.; Recham, N.; Delacourt, C.; Ati, M.; Dupont, L.; Armand, M.; Tarascon, J.-M. *Inorg. Chem.* **2010**, *49*, 7401.
- (202) Tripathi, R.; Gardiner, G. R.; Islam, M. S.; Nazar, L. F. *Chem. Mater.* **2011**, *23*, 2278.
- (203) Barpanda, P.; Oyama, G.; Nishimura, S.; Chung, S. C.; Yamada, A. *Nat. Commun.* **2014**, *5*, No. 4358.
- (204) Goodenough, J. B.; Hong, H. Y. P.; Kafalas, J. A. *Mater. Res. Bull.* **1976**, *11*, 203.
- (205) Gaubicher, J.; Wurm, C.; Goward, G.; Masquelier, C.; Nazar, L. *Chem. Mater.* **2000**, *12*, 3240.
- (206) Gopalakrishnan, J.; Rangan, K. K. *Chem. Mater.* **1992**, *4*, 745.
- (207) Uebou, Y.; Kiyabu, T.; Okada, S.; Yamaki, J. *Rep. Inst. Adv. Mater. Study, Kyushu Univ.* **2002**, *16*, 1.
- (208) Plashnitsa, L. S.; Kobayashi, E.; Noguchi, Y.; Okada, S.; Yamaki, J.-i. *J. Electrochem. Soc.* **2010**, *157*, A536.
- (209) Jian, Z.; Zhao, L.; Pan, H.; Hu, Y.-S.; Li, H.; Chen, W.; Chen, L. *Electrochim. Commun.* **2012**, *14*, 86.

- (210) Saravanan, K.; Mason, C. W.; Rudola, A.; Wong, K. H.; Balaya, P. *Adv. Energy Mater.* **2013**, *3*, 444.
- (211) Jian, Z.; Yuan, C.; Han, W.; Lu, X.; Gu, L.; Xi, X.; Hu, Y.-S.; Li, H.; Chen, W.; Chen, D.; Ikuhara, Y.; Chen, L. *Adv. Funct. Mater.* **2014**, *24*, 4265.
- (212) Barker, J.; Saidi, M. Y.; Swoyer, J. L. *Electrochem. Solid-State Lett.* **2003**, *6*, A1.
- (213) Zhao, J. Q.; He, J. P.; Ding, X. C.; Zhou, J. H.; Ma, Y. O.; Wu, S. C.; Huang, R. M. *J. Power Sources* **2010**, *195*, 6854.
- (214) Liu, Z.-m.; Wang, X.-y.; Wang, Y.; Tang, A.-p.; Yang, S.-y.; He, L.-f. *Trans. Nonferrous Met. Soc. China* **2008**, *18*, 346.
- (215) Zhuo, H.; Wang, X.; Tang, A.; Liu, Z.; Gamboa, S.; Sebastian, P. *J. J. Power Sources* **2006**, *160*, 698.
- (216) Barker, J.; Gover, R. K. B.; Burns, P.; Bryan, A. *J. Electrochem. Solid-State Lett.* **2006**, *9*, A190.
- (217) Sauvage, F.; Quarez, E.; Tarascon, J. M.; Baudrin, E. *Solid State Sci.* **2006**, *8*, 1215.
- (218) Yakubovich, O. V.; Simonov, M. A.; Melnikov, O. K. *Kristallografiya* **1984**, *29*, 484.
- (219) Chihara, K.; Kitajou, A.; Gocheva, I. D.; Okada, S.; Yamaki, J.-i. *J. Power Sources* **2013**, *227*, 80.
- (220) Shakoor, R. A.; Seo, D.-H.; Kim, H.; Park, Y.-U.; Kim, J.; Kim, S.-W.; Gwon, H.; Lee, S.; Kang, K. *J. Mater. Chem.* **2012**, *22*, 20535.
- (221) Serras, P.; Palomares, V.; Goni, A.; Gil de Muro, I.; Kubiak, P.; Lezama, L.; Rojo, T. *J. Mater. Chem.* **2012**, *22*, 22301.
- (222) Park, Y.-U.; Seo, D.-H.; Kwon, H.-S.; Kim, B.; Kim, J.; Kim, H.; Kim, I.; Yoo, H.-I.; Kang, K. *J. Am. Chem. Soc.* **2013**, *135*, 13870.
- (223) Lim, S. Y.; Kim, H.; Chung, J.; Lee, J. H.; Kim, B. G.; Choi, J.-J.; Chung, K. Y.; Cho, W.; Kim, S.-J.; Goddard, W. A.; Jung, Y.; Choi, J. W. *Proc. Natl. Acad. Sci. U.S.A.* **2014**, *111*, 599.
- (224) Nose, M.; Nakayama, H.; Nobuhara, K.; Yamaguchi, H.; Nakanishi, S.; Iba, H. *J. Power Sources* **2013**, *234*, 175.
- (225) Nose, M.; Shiotani, S.; Nakayama, H.; Nobuhara, K.; Nakanishi, S.; Iba, H. *Electrochem. Commun.* **2013**, *34*, 266.
- (226) Nadir, A.; Delmas, C.; Salmon, R.; Hagenmuller, P. *Rev. Chim. Miner.* **1984**, *21*, 537.
- (227) Uebou, Y.; Okada, S.; Yamaki, J.-i. *J. Power Sources* **2003**, *115*, 119.
- (228) Arai, H.; Okada, S.; Sakurai, Y.; Yamaki, J.-i. *J. Power Sources* **1997**, *68*, 716.
- (229) Badway, F.; Cosandey, F.; Pereira, N.; Amatucci, G. G. *J. Electrochem. Soc.* **2003**, *150*, A1318.
- (230) Gocheva, I. D.; Nishijima, M.; Doi, T.; Okada, S.; Yamaki, J.; Nishida, T. *J. Power Sources* **2009**, *187*, 247.
- (231) Nishijima, M.; Gocheva, I. D.; Okada, S.; Doi, T.; Yamaki, J.-i.; Nishida, T. *J. Power Sources* **2009**, *190*, 558.
- (232) Yamada, Y.; Doi, T.; Tanaka, I.; Okada, S.; Yamaki, J.-i. *J. Power Sources* **2011**, *196*, 4837.
- (233) Wang, L.; Lu, Y.; Liu, J.; Xu, M.; Cheng, J.; Zhang, D.; Goodenough, J. B. *Angew. Chem., Int. Ed.* **2013**, *52*, 1964.
- (234) Lu, Y.; Wang, L.; Cheng, J.; Goodenough, J. B. *Chem. Commun.* **2012**, *48*, 6544.
- (235) Wu, X.; Deng, W.; Qian, J.; Cao, Y.; Ai, X.; Yang, H. *J. Mater. Chem. A* **2013**, *1*, 10130.
- (236) Matsuda, T.; Takachi, M.; Moritomo, Y. *Chem. Commun.* **2013**, *49*, 2750.
- (237) Mizuno, Y.; Okubo, M.; Hosono, E.; Kudo, T.; Zhou, H.; Ohishi, K. *J. Phys. Chem. C* **2013**, *117*, 10877.
- (238) Qian, J.; Zhou, M.; Cao, Y.; Ai, X.; Yang, H. *Adv. Energy Mater.* **2012**, *2*, 410.
- (239) Kim, T. B.; Choi, J. W.; Ryu, H. S.; Cho, G. B.; Kim, K. W.; Ahn, J. H.; Cho, K. K.; Ahn, H. *J. J. Power Sources* **2007**, *174*, 1275.
- (240) Peled, E. *J. Electrochem. Soc.* **1979**, *126*, 2047.
- (241) Wakihara, M.; Yamamoto, O. *Lithium Ion Batteries: Fundamentals and Performance*; WILEY-VCH Verlag GmbH: Weinheim, 2008.
- (242) Aurbach, D.; Markovsky, B.; Weissman, I.; Levi, E.; Ein-Eli, Y. *Electrochim. Acta* **1999**, *45*, 67.
- (243) Asher, R. C.; Wilson, S. A. *Nature* **1958**, *181*, 409.
- (244) Jache, B.; Adelhelm, P. *Angew. Chem.* **2014**, *126*, 10333.
- (245) Franklin, R. E. *Proc. R. Soc. London, Ser. A* **1951**, *209*, 196.
- (246) Jenkins, G. M.; Kawamura, K. *Nature* **1971**, *231*, 175.
- (247) Ban, L. L.; Crawford, D.; Marsh, H. *J. Appl. Crystallogr.* **1975**, *8*, 415.
- (248) Shiraishi, M. *Introduction to Carbon Materials*; The Carbon Society of Japan: Tokyo, 1984; p 33.
- (249) Dahn, J. R.; Xing, W.; Gao, Y. *Carbon* **1997**, *35*, 825.
- (250) Azuma, H.; Imoto, H.; Yamada, S.; Sekai, K. *J. Power Sources* **1999**, *81*, 1.
- (251) Conard, J.; Lauginie, P. *Tanso* **2000**, *2000*, 62.
- (252) Harris, P. J. F. *Philos. Mag.* **2004**, *84*, 3159.
- (253) Smith, M. A.; Foley, H. C.; Lobo, R. F. *Carbon* **2004**, *42*, 2041.
- (254) Kumar, A.; Lobo, R. F.; Wagner, N. J. *Carbon* **2005**, *43*, 3099.
- (255) Nagao, M.; Pitteloud, C.; Kamiyama, T.; Otomo, T.; Itoh, K.; Fukunaga, T.; Tatsumi, K.; Kanno, R. *J. Electrochem. Soc.* **2006**, *153*, A914.
- (256) Yata, S.; Kinoshita, H.; Komori, M.; Ando, N.; Kashiwamura, T.; Harada, T.; Tanaka, K.; Yamabe, T. *Synth. Met.* **1994**, *62*, 153.
- (257) Stevens, D. A.; Dahn, J. R. *J. Electrochem. Soc.* **2000**, *147*, 1271.
- (258) Sato, K.; Noguchi, M.; Demachi, A.; Oki, N.; Endo, M. *Science* **1994**, *264*, 556.
- (259) Mabuchi, A.; Tokumitsu, K.; Fujimoto, H.; Kasuh, T. *J. Electrochem. Soc.* **1995**, *142*, 1041.
- (260) Stevens, D. A.; Dahn, J. R. *J. Electrochem. Soc.* **2000**, *147*, 4428.
- (261) Mamun, S. M.; Herstedt, M.; Oikawa, K.; Gustafsson, T.; Otomo, T.; Furusaka, M.; Kamiyama, T.; Sakaue, H.; Edstrom, K. *Appl. Phys. A: Mater. Sci. Process.* **2002**, *74*, S1028.
- (262) Tatsumi, K.; Conard, J.; Nakahara, M.; Menu, S.; Lauginie, P.; Sawada, Y.; Ogumi, Z. *Chem. Commun.* **1997**, 687.
- (263) Guerin, K.; Menetrier, M.; Fevrier-Bouvier, A.; Flandrois, S.; Simon, B.; Biensan, P. *Solid State Ionics* **2000**, *127*, 187.
- (264) Gotoh, K.; Maeda, M.; Nagai, A.; Goto, A.; Tansho, M.; Hashi, K.; Shimizu, T.; Ishida, H. *J. Power Sources* **2006**, *162*, 1322.
- (265) Gotoh, K.; Ishikawa, T.; Shimadzu, S.; Yabuuchi, N.; Komaba, S.; Takeda, K.; Goto, A.; Deguchi, K.; Ohki, S.; Hashi, K.; Shimizu, T.; Ishida, H. *J. Power Sources* **2013**, *225*, 137.
- (266) Zhao, J.; Zhao, L. W.; Chihara, K.; Okada, S.; Yamaki, J.; Matsumoto, S.; Kuze, S.; Nakane, K. *J. Power Sources* **2013**, *244*, 752.
- (267) Chihara, K.; Chujo, N.; Kitajou, A.; Okada, S. *Electrochim. Acta* **2013**, *110*, 240.
- (268) Ponrouch, A.; Goñi, A. R.; Palacín, M. R. *Electrochim. Commun.* **2013**, *27*, 85.
- (269) Alcántara, R.; Lavela, P.; Ortiz, G. F.; Tirado, J. L. *Electrochim. Solid-State Lett.* **2005**, *8*, A222.
- (270) Ponrouch, A.; Marchante, E.; Courty, M.; Tarascon, J.-M.; Palacín, M. R. *Energy Environ. Sci.* **2012**, *5*, 8572.
- (271) Jeong, S.-K.; Inaba, M.; Mogi, R.; Iriyama, Y.; Abe, T.; Ogumi, Z. *Langmuir* **2001**, *17*, 8281.
- (272) Mogi, R.; Inaba, M.; Jeong, S.-K.; Iriyama, Y.; Abe, T.; Ogumi, Z. *J. Electrochim. Soc.* **2002**, *149*, A1578.
- (273) Nakai, H.; Kubota, T.; Kita, A.; Kawashima, A. *J. Electrochim. Soc.* **2011**, *158*, A798.
- (274) Borodin, O.; Behl, W.; Jow, T. R. *J. Phys. Chem. C* **2013**, *117*, 8661.
- (275) Aurbach, D.; Gamolsky, K.; Markovsky, B.; Gofer, Y.; Schmidt, M.; Heider, U. *Electrochim. Acta* **2002**, *47*, 1423.
- (276) Ota, H.; Sakata, Y.; Inoue, A.; Yamaguchi, S. *J. Electrochim. Soc.* **2004**, *151*, A1659.
- (277) Han, Z.-J.; Yabuuchi, N.; Shimomura, K.; Murase, M.; Yui, H.; Komaba, S. *Energy Environ. Sci.* **2012**, *5*, 9014.
- (278) Komaba, S.; Ishikawa, T.; Yabuuchi, N.; Murata, W.; Ito, A.; Ohsawa, Y. *ACS Appl. Mater. Interfaces* **2011**, *3*, 4165.
- (279) Monti, D.; Jónsson, E.; Palacín, M. R.; Johansson, P. *J. Power Sources* **2014**, *245*, 630.
- (280) Noor, S. A. M.; Howlett, P. C.; MacFarlane, D. R.; Forsyt, M. *Electrochim. Acta* **2013**, *114*, 766.
- (281) Egashira, M.; Tanaka, T.; Yoshimoto, N.; Morita, M. *Electrochemistry* **2012**, *80*, 755.

- (282) Fukunaga, A.; Nohira, T.; Hagiwara, R.; Numata, K.; Itani, E.; Sakai, S.; Nitta, K.; Inazawa, S. *J. Power Sources* **2014**, *246*, 387.
- (283) MacFarlane, D. R.; Tachikawa, N.; Forsyth, M.; Pringle, J. M.; Howlett, P. C.; Elliott, G. D.; Davis, J. H.; Watanabe, M.; Simon, P.; Angell, C. A. *Energy Environ. Sci.* **2014**, *7*, 232.
- (284) Crowe, R.; Badyal, J. P. S. *J. Chem. Soc., Chem. Commun.* **1991**, *958*.
- (285) Drofenik, J.; Gaberscek, M.; Dominko, R.; Poulsen, F. W.; Mogensen, M.; Pejovnik, S.; Jamnik, J. *Electrochim. Acta* **2003**, *48*, 883.
- (286) Li, J.; Lewis, R. B.; Dahn, J. R. *Electrochem. Solid-State Lett.* **2007**, *10*, A17.
- (287) Lee, J. H.; Paik, U.; Hackley, V. A.; Choi, Y. M. *J. Electrochem. Soc.* **2005**, *152*, A1763.
- (288) Yabuuchi, N.; Shimomura, K.; Shimbe, Y.; Ozeki, T.; Son, J.-Y.; Oji, H.; Katayama, Y.; Miura, T.; Komaba, S. *Adv. Energy Mater.* **2011**, *1*, 759.
- (289) Komaba, S.; Ozeki, T.; Yabuuchi, N.; Shimomura, K. *Electrochemistry* **2011**, *79*, 6.
- (290) Magasinski, A.; Zdyrko, B.; Kovalenko, I.; Hertzberg, B.; Burtovyy, R.; Huebner, C. F.; Fuller, T. F.; Luzinov, I.; Yushin, G. *ACS Appl. Mater. Interfaces* **2010**, *2*, 3004.
- (291) Kovalenko, I.; Zdyrko, B.; Magasinski, A.; Hertzberg, B.; Milicev, Z.; Burtovyy, R.; Luzinov, I.; Yushin, G. *Science* **2011**, *334*, 75.
- (292) Dahbi, M.; Nakano, T.; Yabuuchi, N.; Ishikawa, T.; Kubota, K.; Fukunishi, M.; Shibahara, S.; Son, J.-Y.; Cui, Y.-T.; Oji, H.; Komaba, S. *Electrochim. Commun.* **2014**, *44*, 66.
- (293) Moshkovich, M.; Gofer, Y.; Aurbach, D. *J. Electrochem. Soc.* **2001**, *148*, E155.
- (294) Peled, E.; Golodnitsky, D.; Ardel, G. *J. Electrochem. Soc.* **1997**, *144*, L208.
- (295) Gnanaraj, J. S.; Levi, M. D.; Levi, E.; Salitra, G.; Aurbach, D.; Fischer, J. E.; Claye, A. *J. Electrochem. Soc.* **2001**, *148*, A525.
- (296) Delmas, C.; Cherkaoui, F.; Nadiri, A.; Hagenmuller, P. *Mater. Res. Bull.* **1987**, *22*, 631.
- (297) Delmas, C.; Nadiri, A.; Soubeyroux, J. L. *Solid State Ionics* **1988**, *28–30* (Part 1), 419.
- (298) Zanini, M.; Shaw, J. L.; Tennenhouse, G. *J. J. Electrochem. Soc.* **1981**, *128*, 1647.
- (299) Wang, W.; Yu, C.; Liu, Y.; Hou, J.; Zhu, H.; Jiao, S. *RSC Adv.* **2013**, *3*, 1041.
- (300) Wang, W.; Yu, C.; Lin, Z.; Hou, J.; Zhu, H.; Jiao, S. *Nanoscale* **2013**, *5*, 594.
- (301) Zhao, L.; Pan, H. L.; Hu, Y. S.; Li, H.; Chen, L. Q. *Chin. Phys. B* **2012**, *21*, No. 028201.
- (302) Sun, Y.; Zhao, L.; Pan, H.; Lu, X.; Gu, L.; Hu, Y.-S.; Li, H.; Armand, M.; Ikuhara, Y.; Chen, L.; Huang, X. *Nat. Commun.* **2013**, *4*, 1870.
- (303) Yu, X.; Pan, H.; Wan, W.; Ma, C.; Bai, J.; Meng, Q.; Ehrlich, S. N.; Hu, Y.-S.; Yang, X.-Q. *Nano Lett.* **2013**, *13*, 4721.
- (304) Shirpour, M.; Cabana, J.; Doeff, M. *Energy Environ. Sci.* **2013**, *6*, 2538.
- (305) Rudola, A.; Saravanan, K.; Mason, C. W.; Balaya, P. *J. Mater. Chem. A* **2013**, *1*, 2653.
- (306) Rudola, A.; Saravanan, K.; Devaraj, S.; Gong, H.; Balaya, P. *Chem. Commun.* **2013**, *49*, 7451.
- (307) Aragon, M. J.; Vidal-Abarca, C.; Lavela, P.; Tirado, J. L. *J. Mater. Chem. A* **2013**, *1*, 13963.
- (308) Senguttuvan, P.; Rousse, G.; Seznec, V.; Tarascon, J.-M.; Palacin, M. R. *Chem. Mater.* **2011**, *23*, 4109.
- (309) Wu, W.; Mohamed, A.; Whitacre, J. F. *J. Electrochem. Soc.* **2013**, *160*, A497.
- (310) Park, S. I.; Gocheva, I.; Okada, S.; Yamaki, J.-i. *J. Electrochem. Soc.* **2011**, *158*, A1067.
- (311) Reddy, M. V.; Subba Rao, G. V.; Chowdari, B. V. R. *Chem. Rev.* **2013**, *113*, 5364.
- (312) Senguttuvan, P.; Rousse, G.; Vezin, H.; Tarascon, J. M.; Palacin, M. R. *Chem. Mater.* **2013**, *25*, 2391.
- (313) Chen, J. S.; Luan, D.; Li, C. M.; Boey, F. Y. C.; Qiao, S.; Lou, X. W. *Chem. Commun.* **2010**, *46*, 8252.
- (314) Chen, Z.; Belharouak, I.; Sun, Y. K.; Amine, K. *Adv. Funct. Mater.* **2013**, *23*, 959.
- (315) Myung, S. T.; Takahashi, N.; Komaba, S.; Yoon, C. S.; Sun, Y. K.; Amine, K.; Yashiro, H. *Adv. Funct. Mater.* **2011**, *21*, 3231.
- (316) Trinh, N. D.; Crosnier, O.; Schougaard, S. B.; Brousse, T. *ECS Trans.* **2011**, *35*, 91.
- (317) Yang, Z.; Choi, D.; Kerisit, S.; Rosso, K. M.; Wang, D.; Zhang, J.; Graff, G.; Liu, J. *J. Power Sources* **2009**, *192*, 588.
- (318) Ohzuku, T.; Takehara, Z.; Yoshizawa, S. *Electrochim. Acta* **1979**, *24*, 219.
- (319) Lunell, S.; Stashans, A.; Ojamäe, L.; Lindström, H.; Hagfeldt, A. *J. Am. Chem. Soc.* **1997**, *119*, 7374.
- (320) Xu, Y.; Lotfabad, E. M.; Wang, H. L.; Farbod, B.; Xu, Z. W.; Kohandehghan, A.; Mitlin, D. *Chem. Commun.* **2013**, *49*, 8973.
- (321) Wu, L.; Buchholz, D.; Bresser, D.; Chagas, L. G.; Passerini, S. *J. Power Sources* **2014**, *251*, 379.
- (322) Xiong, H.; Slater, M. D.; Balasubramanian, M.; Johnson, C. S.; Rajh, T. *J. Phys. Chem. Lett.* **2011**, *2*, 2560.
- (323) Huang, J. P.; Yuan, D. D.; Zhang, H. Z.; Cao, Y. L.; Li, G. R.; Yang, H. X.; Gao, X. P. *RSC Adv.* **2013**, *3*, 12593.
- (324) Hu, Y. S.; Kienle, L.; Guo, Y. G.; Maier, J. *Adv. Mater.* **2006**, *18*, 1421.
- (325) Ohzuku, T.; Ueda, A.; Yamamoto, N. *J. Electrochem. Soc.* **1995**, *142*, 1431.
- (326) Ferg, E.; Gummow, R. J.; de Kock, A.; Thackeray, M. M. *J. Electrochem. Soc.* **1994**, *141*, L147.
- (327) Andersson, S.; Wadsley, A. D. *Acta Crystallogr.* **1961**, *14*, 1245.
- (328) Andersson, S.; Wadsley, A. D. *Acta Crystallogr.* **1962**, *15*, 194.
- (329) Batygin, V. G. *Russ. J. Inorg. Chem.* **1976**, *12*, 762.
- (330) Pan, H.; Lu, X.; Yu, X.; Hu, Y.-S.; Li, H.; Yang, X.-Q.; Chen, L. *Adv. Energy Mater.* **2013**, *3*, 1186.
- (331) Wang, Y. S.; Yu, X. Q.; Xu, S. Y.; Bai, J. M.; Xiao, R. J.; Hu, Y. S.; Li, H.; Yang, X. Q.; Chen, L. Q.; Huang, X. *J. Nat. Commun.* **2013**, *4*, 2365.
- (332) Senguttuvan, P.; Rousse, G.; Arroyo y de Dompablo, M. E.; Vezin, H.; Tarascon, J. M.; Palacín, M. R. *J. Am. Chem. Soc.* **2013**, *135*, 3897.
- (333) Kabbour, H.; Coillot, D.; Colmont, M.; Masquelier, C.; Mentré, O. *J. Am. Chem. Soc.* **2011**, *133*, 11900.
- (334) Wu, X. Y.; Cao, Y. L.; Ai, X. P.; Qian, J. F.; Yang, H. X. *Electrochim. Commun.* **2013**, *31*, 145.
- (335) Wu, L.; Hu, X.; Qian, J.; Pei, F.; Wu, F.; Mao, R.; Ai, X.; Yang, H.; Cao, Y. *J. Mater. Chem. A* **2013**, *1*, 7181.
- (336) Darwiche, A.; Sougrati, M. T.; Fraisse, B.; Stievano, L.; Monconduit, L. *Electrochim. Commun.* **2013**, *32*, 18.
- (337) Wang, J. W.; Liu, X. H.; Mao, S. X.; Huang, J. Y. *Nano Lett.* **2012**, *12*, 5897.
- (338) Schacklette, L. W.; Taiguang, R. J.; Mcrae, M.; Toth, J. E.; Gould, S. EP0347952 A2; Allied Signal Inc. (US): 1989.
- (339) Kim, Y.; Park, Y.; Choi, A.; Choi, N.-S.; Kim, J.; Lee, J.; Ryu, J. H.; Oh, S. M.; Lee, K. T. *Adv. Mater.* **2013**, *25*, 3045.
- (340) Baggetto, L.; Keum, J. K.; Browning, J. F.; Veith, G. M. *Electrochim. Commun.* **2013**, *34*, 41.
- (341) Obrovac, M. N.; Christensen, L.; Le, D. B.; Dahn, J. R. *J. Electrochem. Soc.* **2007**, *154*, A849.
- (342) Jeong, G.; Kim, Y.-U.; Kim, H.; Kim, Y.-J.; Sohn, H.-J. *Energy Environ. Sci.* **2011**, *4*, 1986.
- (343) Li, H.; Huang, X.; Chen, L.; Wu, Z.; Liang, Y. *Electrochim. Solid-State Lett.* **1999**, *2*, 547.
- (344) Beaulieu, L. Y.; Hewitt, K. C.; Turner, R. L.; Bonakdarpour, A.; Abdo, A. A.; Christensen, L.; Eberman, K. W.; Krause, L. J.; Dahn, J. R. *J. Electrochem. Soc.* **2003**, *150*, A149.
- (345) Morito, H.; Yamada, T.; Ikeda, T.; Yamane, H. *J. Alloys Compd.* **2009**, *480*, 723.
- (346) Ellis, L. D.; Wilkes, B. N.; Hatchard, T. D.; Obrovac, M. N. *J. Electrochem. Soc.* **2014**, *161*, A416.
- (347) Komaba, S.; Matsura, Y.; Ishikawa, T.; Yabuuchi, N.; Murata, W.; Kuze, S. *Electrochim. Commun.* **2012**, *21*, 65.

- (348) Chevrier, V. L.; Ceder, G. *J. Electrochem. Soc.* **2011**, *158*, A1011.
- (349) Yabuuchi, N.; Matsuura, Y.; Ishikawa, T.; Kuze, S.; Son, J.-Y.; Cui, Y.-T.; Oji, H.; Komaba, S. *ChemElectroChem.* **2014**, *1*, 580.
- (350) Qian, J.; Wu, X.; Cao, Y.; Ai, X.; Yang, H. *Angew. Chem.* **2013**, *125*, 4731.
- (351) Baggetto, L.; Ganesh, P.; Meisner, R. P.; Unocic, R. R.; Jumas, J.-C.; Bridges, C. A.; Veith, G. M. *J. Power Sources* **2013**, *234*, 48.
- (352) Yamamoto, T.; Nohira, T.; Hagiwara, R.; Fukunaga, A.; Sakai, S.; Nitta, K.; Inazawa, S. *J. Power Sources* **2013**, *237*, 98.
- (353) Ellis, L. D.; Hatchard, T. D.; Obrovac, M. N. *J. Electrochem. Soc.* **2012**, *159*, A1801.
- (354) Qian, J.; Chen, Y.; Wu, L.; Cao, Y.; Ai, X.; Yang, H. *Chem. Commun.* **2012**, *48*, 7070.
- (355) Darwiche, A.; Marino, C.; Sougrati, M. T.; Fraisse, B.; Stievano, L.; Monconduit, L. *J. Am. Chem. Soc.* **2012**, *134*, 20805.
- (356) Xiao, L. F.; Cao, Y. L.; Xiao, J.; Wang, W.; Kovarik, L.; Nie, Z. M.; Liu, J. *Chem. Commun.* **2012**, *48*, 3321.
- (357) Matsuura, Y.; Ishikawa, T.; Yabuuchi, N.; Kuze, S.; Komaba, S. *The 53rd Battery Symposium in Japan*, Fukuoka, 2012; p 1E26.
- (358) Pauling, L.; Simonetta, M. *J. Chem. Phys.* **1952**, *20*, 29.
- (359) Keyes, R. W. *Phys. Rev.* **1953**, *92*, 580.
- (360) Nagao, M.; Hayashi, A.; Tatsumisago, M. *J. Power Sources* **2011**, *196*, 6902.
- (361) Sun, L.-Q.; Li, M.-J.; Sun, K.; Yu, S.-H.; Wang, R.-S.; Xie, H.-M. *J. Phys. Chem. C* **2012**, *116*, 14772.
- (362) Park, C. M.; Sohn, H. J. *Adv. Mater.* **2007**, *19*, 2465.
- (363) Marino, C.; Debenedetti, A.; Fraisse, B.; Favier, F.; Monconduit, L. *Electrochem. Commun.* **2011**, *13*, 346.
- (364) Dahbi, M.; Yabuuchi, N.; Kubota, K.; Tokiwa, K.; Komaba, S. *Phys. Chem. Chem. Phys.* **2014**, *16*, 15007.
- (365) Fullenwarth, J.; Darwiche, A.; Soares, A.; Donnadieu, B.; Monconduit, L. *J. Mater. Chem. A* **2014**, *2*, 2050.
- (366) Datta, M. K.; Epur, R.; Saha, P.; Kadakia, K.; Park, S. K.; Kumta, P. N. *J. Power Sources* **2013**, *225*, 316.
- (367) Park, Y.; Shin, D.-S.; Woo, S. H.; Choi, N. S.; Shin, K. H.; Oh, S. M.; Lee, K. T.; Hong, S. Y. *Adv. Mater.* **2012**, *24*, 3562.
- (368) Ryu, H. S.; Kim, J. S.; Park, J. S.; Park, J. W.; Kim, K. W.; Ahn, J. H.; Nam, T. H.; Wang, G. X.; Ahn, H. J. *J. Electrochem. Soc.* **2013**, *160*, A338.
- (369) Alcantara, R.; Jaraba, M.; Lavela, P.; Tirado, J. L. *Chem. Mater.* **2002**, *14*, 2847.
- (370) Su, D. W.; Wang, C. Y.; Ahn, H.; Wang, G. X. *Phys. Chem. Chem. Phys.* **2013**, *15*, 12543.
- (371) Sun, Q.; Ren, Q. Q.; Li, H.; Fu, Z. W. *Electrochim. Commun.* **2011**, *13*, 1462.
- (372) Ryu, H. S.; Kim, J. S.; Park, J.; Park, J. Y.; Cho, G. B.; Liu, X.; Ahn, I. S.; Kim, K. W.; Ahn, J. H.; Ahn, J. P.; Martin, S. W.; Wang, G.; Ahn, H. J. *J. Power Sources* **2013**, *244*, 764.
- (373) Klein, F.; Jache, B.; Bhide, A.; Adelhelm, P. *Phys. Chem. Chem. Phys.* **2013**, *15*, 15876.
- (374) Yue, J. L.; Sun, Q.; Fu, Z. W. *Chem. Commun.* **2013**, *49*, 5868.
- (375) Hariharan, S.; Saravanan, K.; Balaya, P. *Electrochim. Commun.* **2013**, *31*, 5.
- (376) Song, Z.; Zhou, H. *Energy Environ. Sci.* **2013**, *6*, 2280.
- (377) Nigrey, P. J.; MacInnes, D.; Nairns, D. P.; MacDiarmid, A. G.; Heeger, A. J. *J. Electrochem. Soc.* **1981**, *128*, 1651.
- (378) Zhao, R.; Zhu, L.; Cao, Y.; Ai, X.; Yang, H. X. *Electrochim. Commun.* **2012**, *21*, 36.
- (379) Deng, W.; Liang, X.; Wu, X.; Qian, J.; Cao, Y.; Ai, X.; Feng, J.; Yang, H. *Sci. Rep.* **2013**, *3*, 2671.
- (380) Sakaushi, K.; Hosono, E.; Nickerl, G.; Gemming, T.; Zhou, H.; Kaskel, S.; Eckert, J. *Nat. Commun.* **2013**, *4*, 1485.
- (381) Chen, H.; Armand, M.; Demaillly, G.; Dolhem, F.; Poizot, P.; Tarascon, J.-M. *ChemSusChem* **2008**, *1*, 348.
- (382) Luo, C.; Zhu, Y.; Xu, Y.; Liu, Y.; Gao, T.; Wang, J.; Wang, C. J. *Power Sources* **2014**, *250*, 372.
- (383) Yao, M.; Kuratani, K.; Kojima, T.; Takeichi, N.; Senoh, H.; Kiyobayashi, T. *Sci. Rep.* **2014**, *4*, 3650.
- (384) Armand, M.; Grugeon, S.; Vezin, H.; Laruelle, S.; Ribiere, P.; Poizot, P.; Tarascon, J. M. *Nat. Mater.* **2009**, *8*, 120.
- (385) Zhao, L.; Zhao, J.; Hu, Y.-S.; Li, H.; Zhou, Z.; Armand, M.; Chen, L. *Adv. Energy Mater.* **2012**, *2*, 962.
- (386) Abouimrane, A.; Weng, W.; Eltayeb, H.; Cui, Y.; Niklas, J.; Poluektov, O.; Amine, K. *Energy Environ. Sci.* **2012**, *5*, 9632.
- (387) Nakayama, H.; Nose, M.; Nobuhara, K.; Nakanishi, S.; Iba, H. *224th ECS Meeting Abstracts*, San Francisco, CA, 2013; MA2013-02, p 495.
- (388) Wang, S.; Wang, L.; Zhu, Z.; Hu, Z.; Zhao, Q.; Chen, J. *Angew. Chem.* **2014**, *126*, 6002.
- (389) Castillo-Martínez, E.; Carretero-González, J.; Armand, M. *Angew. Chem., Int. Ed.* **2014**, *53*, 5341.
- (390) Jian, Z.; Han, W.; Lu, X.; Yang, H.; Hu, Y.-S.; Zhou, J.; Zhou, Z.; Li, J.; Chen, W.; Chen, D.; Chen, L. *Adv. Energy Mater.* **2013**, *3*, 156.
- (391) Hartmann, P.; Bender, C. L.; Vračar, M.; Dürr, A. K.; Garsuch, A.; Janek, J.; Adelhelm, P. *Nat. Mater.* **2013**, *12*, 228.
- (392) Whitacre, J. F.; Wiley, T.; Shanbhag, S.; Wenzhuo, Y.; Mohamed, A.; Chun, S. E.; Weber, E.; Blackwood, D.; Lynch-Bell, E.; Gulakowski, J.; Smith, C.; Humphreys, D. *J. Power Sources* **2012**, *213*, 255.
- (393) Pasta, M.; Wessells, C. D.; Huggins, R. A.; Cui, Y. *Nat. Commun.* **2012**, *3*, 1149.
- (394) Li, Z.; Young, D.; Xiang, K.; Carter, W. C.; Chiang, Y.-M. *Adv. Energy Mater.* **2013**, *3*, 290.
- (395) Ushirogata, K.; Sodeyama, K.; Okuno, Y.; Tateyama, Y. *J. Am. Chem. Soc.* **2013**, *135*, 11967.
- (396) Chen, C. Y.; Matsumoto, K.; Nohira, T.; Hagiwara, R.; Oriksa, Y.; Uchimoto, Y. *J. Power Sources* **2014**, *246*, 783.
- (397) Hayashi, A.; Noi, K.; Sakuda, A.; Tatsumisago, M. *Nat. Commun.* **2012**, *3*, 856.
- (398) Noguchi, Y.; Kobayashi, E.; Plashnitsa, L. S.; Okada, S.; Yamaki, J.-i. *Electrochim. Acta* **2013**, *101*, 59.